Chapter 5
Functional Structure of the Peritoneum as a Dialyzing Membrane

L. Gotloib

Not everything that can be counted counts; and not everything that counts can be counted.

Albert Einstein

More than a century ago, Robinson [1], after summarizing more than two centuries of research, defined the diverse natural functions of the peritoneum as follows: a) to regulate fluid for nutrient and mechanical purposes: b) to facilitate motion; c) to minimize friction, and d) to conduct vessels and nerves to the viscera.

Several medical and scientific developments that occurred during the 20th century originated a new approach for the peritoneum being used as a dialysing membrane for long-term life support [2–6]. These same developments created the need for a deeper understanding of peritoneal structure and function.

The peritoneum is a serous membrane embryologically derived from mesenchyma and composed of thin layers of connective tissue covered by a sheet of mesothelium [7]. When the membrane is folded, forming the omentum and the mesentery, both luminal surfaces are covered by mesothelium.

The *anatomical* peritoneal surface area for the human adult is considered to range between 2.08 [8] and 1.72 m^2 [9], with a ratio of area/body weight of 0.284. The intestinal mesothelium, together with that of mesentery, makes up to 49% of the total mesothelial area [10]. For infants having a body weight of 2,700–2,900 g, the total peritoneal surface was found to oscillate between 0.106 [10] and 0.151 m^2 [8], with an area to body weight ratio that fluctuates between 0.383 [10] and 0.522. In infants the contribution of intestine and mesentery to the total surface area is 67.5% [10].

However, from the functional point of view, vis-à-vis peritoneal dialysis, it may well be that the peritoneal area of contact with the dialysis solutions were substantially lower than the anatomical one. This concept, postulated by Krediet et al., was defined as the effective surface area [11]. This hypothesis finds strong support in the elegant study performed by Chagnac et al. [12] showing that the peritoneal surface actively involved in the dialytic process, estimated in six CAPD patients, was 0.55∼0.04 m^2, about one third of the area measured in anatomical studies. Interestingly, other investigators reached similar conclusions in experiments performed in rats [13].

Peritoneal thickness is not uniform and varies according to the area examined. Measurements are quite problematic in parietal and diaphragmatic peritoneum due to the considerable amount of connective tissue, and at times fat, intervening between the peritoneum itself and the underlying tissue (Fig. 5.1). The submesothelial connective tissue layer of visceral peritoneum is firmly bound to the fibrous tissue of the viscus. Therefore, the mesentery, having mesothelial lining on both surfaces and including its trabecular connective framework, appears to be the most appropriate peritoneal portion for estimation of membrane thickness which, in the rabbit, ranges between 30 and 38 μm [14, 15] (Figs. 5.2 and 5.3).

Normal Mesothelium

Electron microscopic studies performed on mouse embryo disclosed that the mesothelium is derived from mesenchymal cells that become flattened, form their own basement membrane, and develop tight junctions as well as desmosomes [16] (Fig. 5.4, inset). Both pinocytotic vesicles and rough endoplasmic reticulum were present. Yolk sac of human embryos at the 5th–7th week of gestation also exhibit flattened mesothelial cells lying on a hyaline, homogeneous basement membrane [17, 18].

L. Gotloib (✉)
Ha'Emek Medical Center, Department of Nephrology, Afula, Israel
e-mail: gotloib@012.net.il

R. Khanna, R.T. Krediet (eds.), *Nolph and Gokal's Textbook of Peritoneal Dialysis*,
DOI 10.1007/978-0-387-78939-2_5, © Springer Science+Business Media, LLC 2009

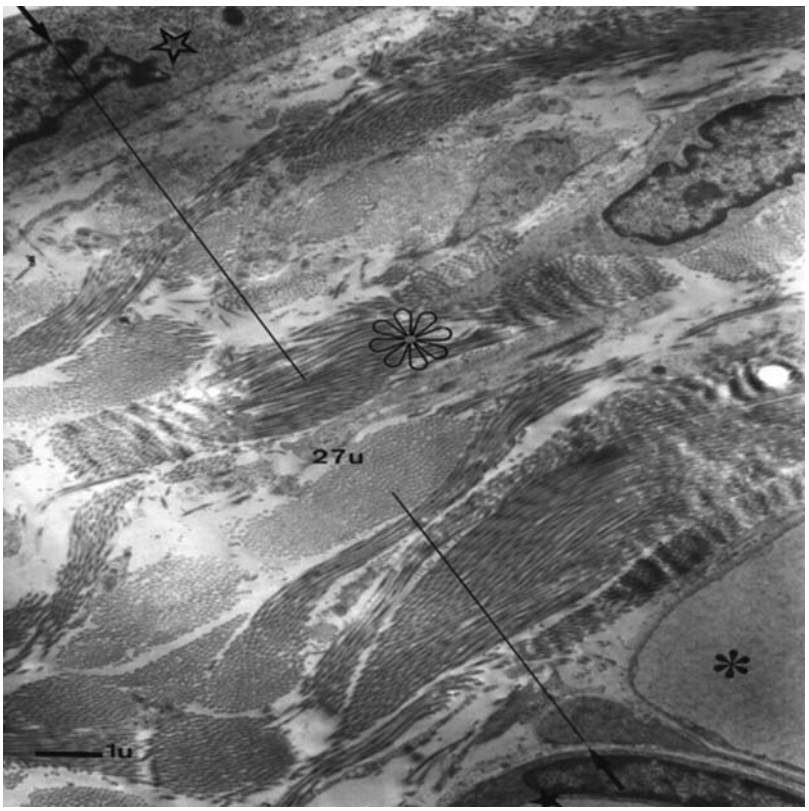

Fig. 5.1 Sample of diaphragmatic rabbit peritoneum. The distance (straight line) between the peritoneal space (upper arrow) and the lumen of the blood capillary (black star) is around 27 μm. The actual pathway through the collagen fibers (open asterisk) is longer (open star: mesothelial cell; black asterisk: fenestrated capillary (× 14,250))

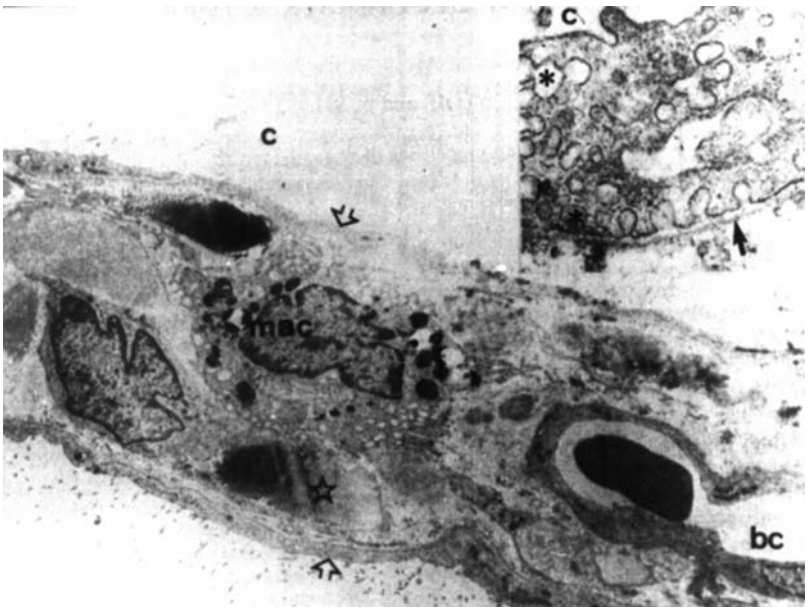

Fig. 5.2 Section of normal rabbit mesentery showing the mesothelial layer (open arrows) covering both aspects of the mesenteric surface area facing the abdominal cavity (c). The interstitium contains a continuous blood capillaty (bc), bundles of collagen (open star), as well as a macrophage (mac). Numerous microvilli can be seen at the lower mesothelial surface (original magnification × 4,750).

Upper right inset. Parietal peritoneum of normal mice. Note the presence of numerous pinocytotic vesicles (*) which, on the left side of the electron micrograph, form a chain between the luminal aspect of the mesothelial cell facing the abdominal cavity (c) and the abluminal one, lying on the continuous basement membrane (arrow) (× 41,500)

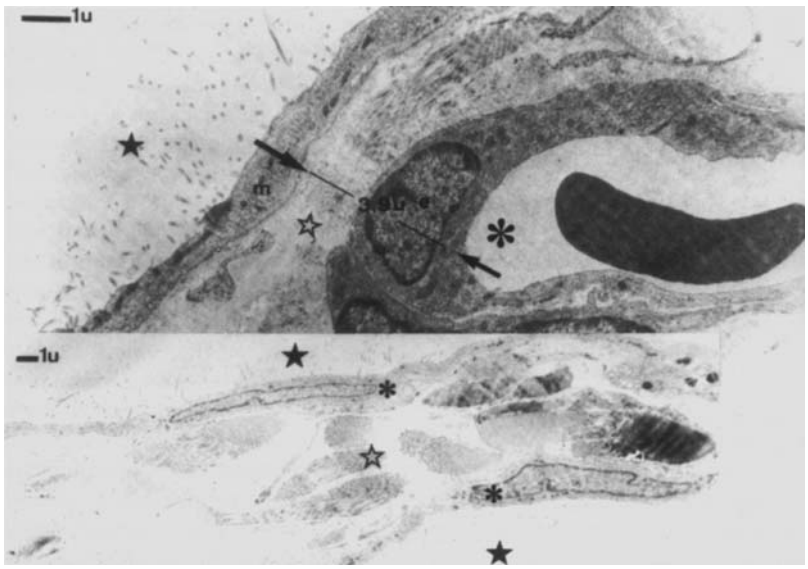

Fig. 5.3 The main photograph shows a sample of rabbit mesenteric peritoneum where the distance (straight line) between the peritoneal space (upper black star) and the microvascular lumen (*) is 3.9 µm (open star: interstitial connective tissue) (× 14,250).

Lower inset. Section of a 42.1 µm length avascular rabbit mesenteric peritoneum sample (black star: peritoneal space; asterisk: mesothelial cell; open star: interstitial connective tissue) (× 4,750)

The cell plasmalemma, when stained specifically, shows the typical trilaminar structure observed in all biological cell membranes [19]. The normal mesothelium occasionally shows macrophages implanted on the luminal peritoneal surface instead of mesothelial cells (Fig. 5.5).

The luminal aspect of the mesothelial cell plasmalemma has numerous cytoplasmic extensions: the microvilli (Figs. 5.2, 5.3, and 5.4), whose existence was originally reported by Kolossow [20] and many years later confirmed by electron microscopy on the serosa covering the rat oviduct [21, 22]. Even though microvilli are more frequently observed in visceral than in parietal peritoneum [23, 24], their distribution is variable and fluctuates from very numerous to completely absent [24, 25]. It should be taken into account, however, that microvilli are extremely sensitive to minor injury or even to dryness, and can therefore be lost from the cell surface if removal and handling of samples are not done with extremely careful techniques. On the other hand, loss of microvilli, as described in continuous ambulatory peritoneal dialysis (CAPD)patients [26] (Fig. 5.6), represent an early sign of impending apoptosis [27–29] that can be easily identified in mesothelial cell imprints (Fig. 5.7).

Light microscopy applied to the observation of resting mesothelium imprints [30] shows a continuous monolayer made up mostly of polygonal mononuclear cells (Fig. 5.8), showing, in mice visceral peritoneum, a density of about 300,000 cells/cm^2 [31]. The number of mesothelial cells per unit area seems higher on the visceral than on the parietal peritoneal surface. Of those cells, 1–2% are binucleated (Fig. 5.8, lower left inset), whereas cells showing three nuclei can be observed (Fig. 5.8).

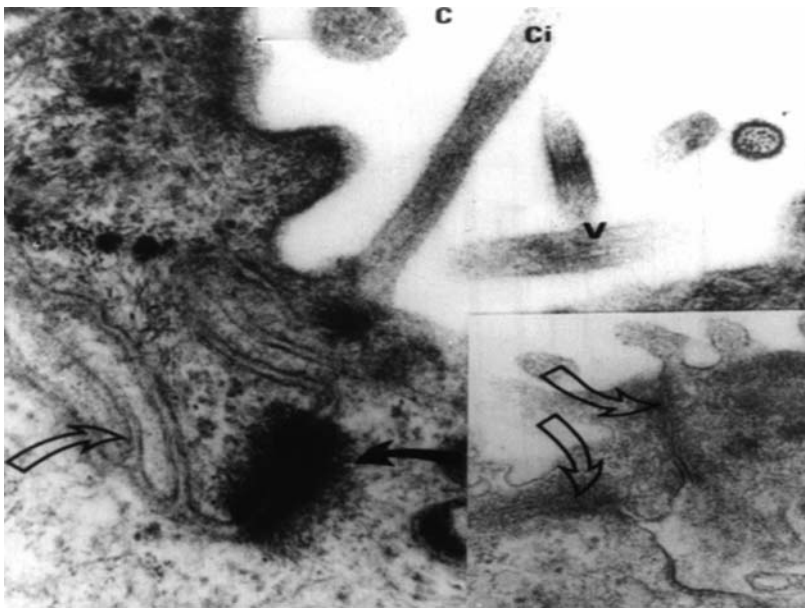

Fig. 5.4 Biopsy of parietal peritoneum taken from a chronic uremic patient on maintenance peritoneal dialysis. Note the presence of an oligocilium (Ci) showing the deviated axial microtubule (open arrow) and the attached basal body (black arrow). Their function is unknown (C: abdominal cavity; V: microvilli) (× 42,900).

Inset. (Lower right). Rabbit mesentery: the open arrows show tight junctions between adjoining mesothelial cells (× 62,500)

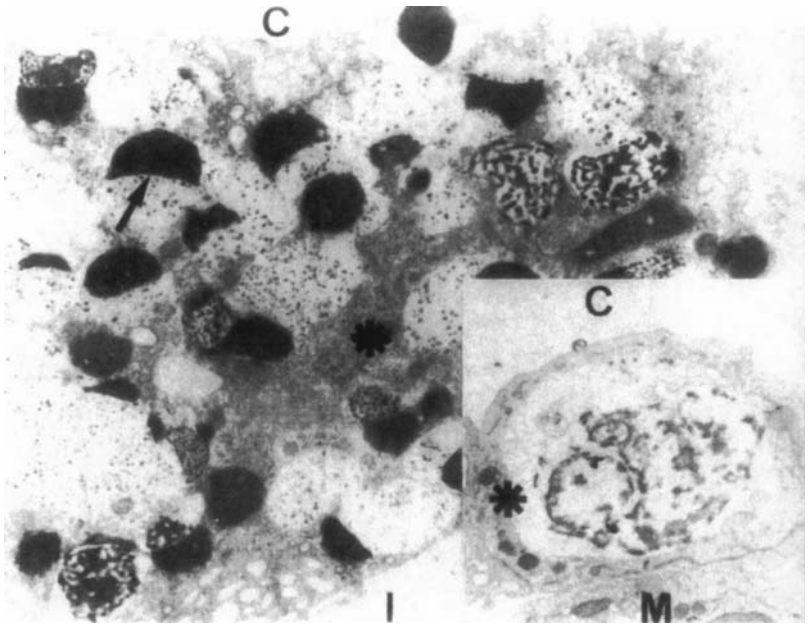

Fig. 5.5 Mesentery of normal rabbit. A macrophage (*) is covering a denuded area of peritoneum (C: abdominal cavity; black arrow: lysosome; I: interstitium). Original magnification × 27,500.

Inset. (Lower right). Mouse mesenteric mesothelium: a signet-ring macrophage (*) is covering a recently implanted mesothelial cell (M) (original magnification × 15,400)

Under normal circumstances the cell population of the monolayer is not stained by vital dyes such as Trypan Blue (Fig. 5.9). This is an indication of their viability. In perpendicular cuts observed under light microscopy, the resting normal mesothelium appears as a continuous layer formed by flattened cells that are apparently elongated, as a result of the angle of section (Fig. 5.10). The mesothelial sheet lies on a layer of connective interstitial tissue (Fig. 5.10), the thickness of which varies in the different portions of the peritoneum (Figs 5.1 and 5.3). The relevance of this point on peritoneal permeability will be discussed later.

Thickness of mesothelial cells in the rabbit ranges between 0.6 and 2 μm [14, 15] (Fig. 5.11).

The human omentum has not yet been studied in great depth. However, some ultrastructural investigations performed in mice and rats [22, 32] seem to indicate that there is little variation between species [33] and that, in mice, omental mesothelial cells can transiently increase their population of microvilli up to seven-fold, suggesting that their concentration in any given area could reflect functional adaptation rather than static structural variation [34].

The presence of pinocytotic vesicles in microvilli has been both reported [21, 23, 35] and denied [34].

Experimental studies done in mice and rats [35–37] using cationic tracers such as ruthenium red (MW 551 da) and cationized ferritin (MW 445 da) revealed the existence of anionic fixed charges on the luminal surface of the microvilli

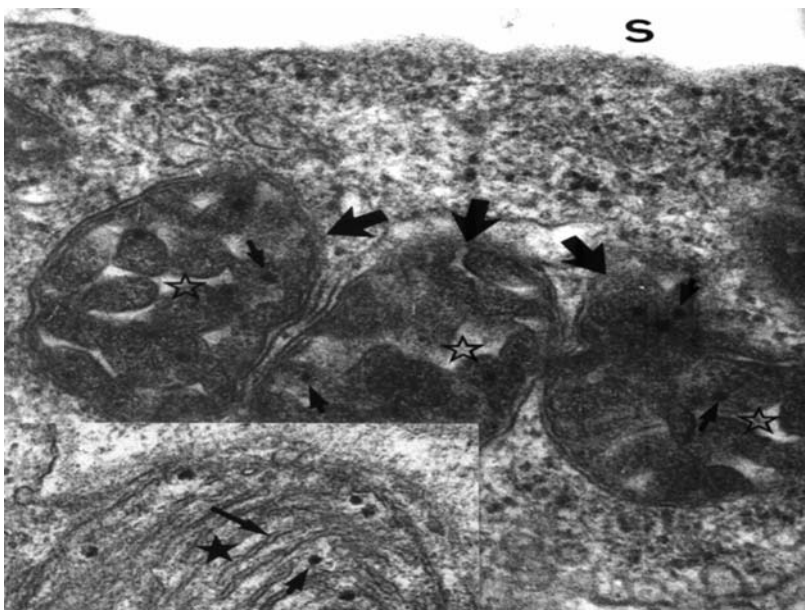

Fig. 5.6 Section of a mesothelial cell seen in a biopsy of parietal peritoneum taken from a patient on CAPD. Mitochondria (open stars) assumed a condensed configuration with increased density of the matrix, blurring of cristae as well as fusions and adhesions of the inner membrane (thick arrows). The matrical granules are still visible (short arrows). These signs of cell injury, in addition to the absence of microvilli, are early signs of impending apoptosis (S: peritoneal space) (× 54,600).

Inset. Intact mitochondrion (short star) showing normal cristae (long arrow) and matrical granules (short arrow) (× 64,550)

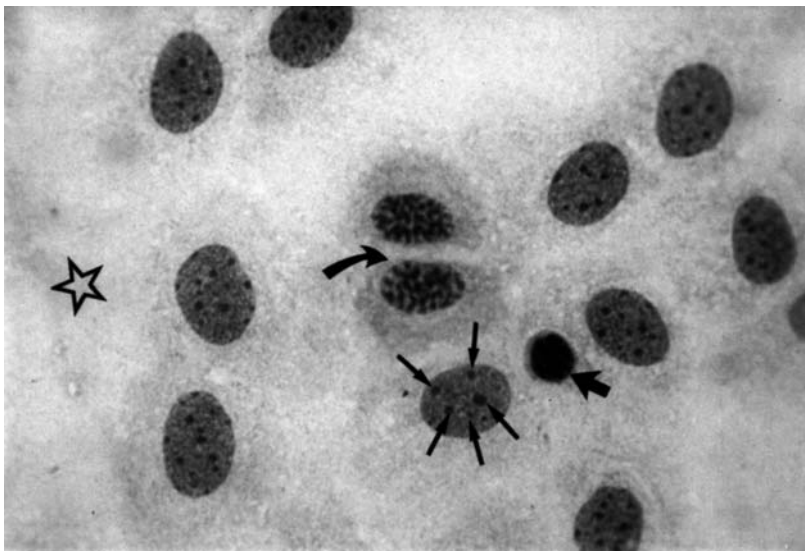

Fig. 5.7 Sample from a mouse injected for 30 consecutive days with 4.25% glucose-enriched dialysis solution. The material was taken 7 days after interruption of the exposure to the dialysis solution (7 days of recovery). This photograph shows the two most critical moments in the life cycle of a mesothelial cell: mitosis (curved arrow), and apoptosis (short thick arrow). Open star shows an area of peritoneum where the mesothelial monolayer is absent (desertic peritoneum). Note the substantially reduced density distribution of cells (small arrows: nucleoii) (hematoxylin-eosin; × 1,000)

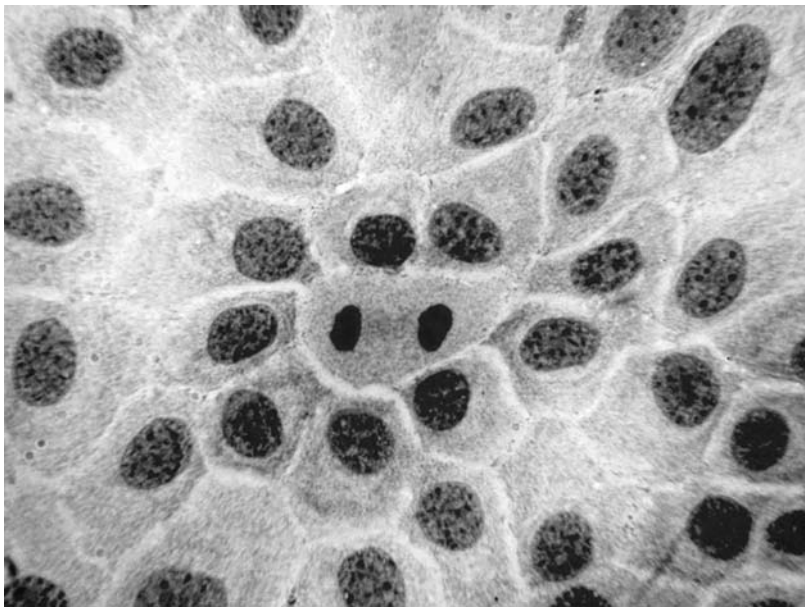

Fig. 5.8 Normal density distribution of mesothelial cells observed in intact, unexposed animals. Unstimulated mesothelium shows a quite low proportion of cells undergoing mitosis at any given time. (Center of microphotograph: cell in mitosis.) (× 1,000)

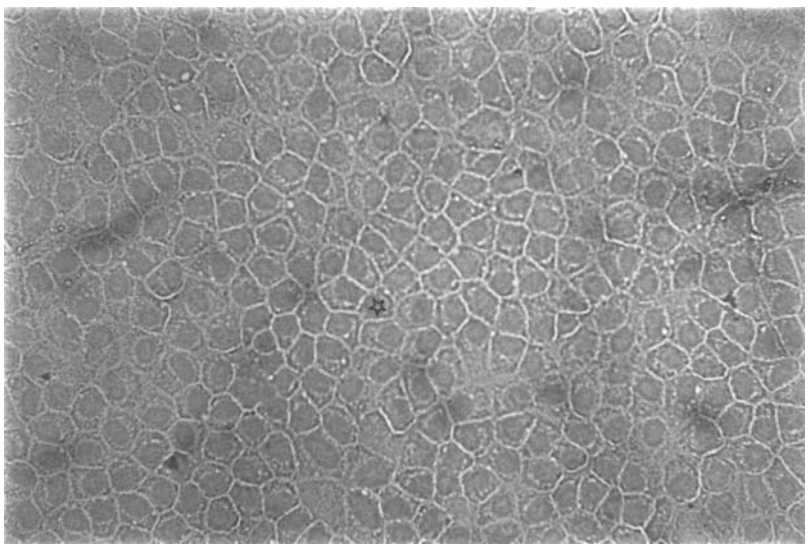

Fig. 5.9 Cell viability evaluated on visceral mesothelium by Trypan-blue exclusion in an intact unexposed mouse. The stain did not permeate the cell membrane (open star: mesothelial cell) (× 400)

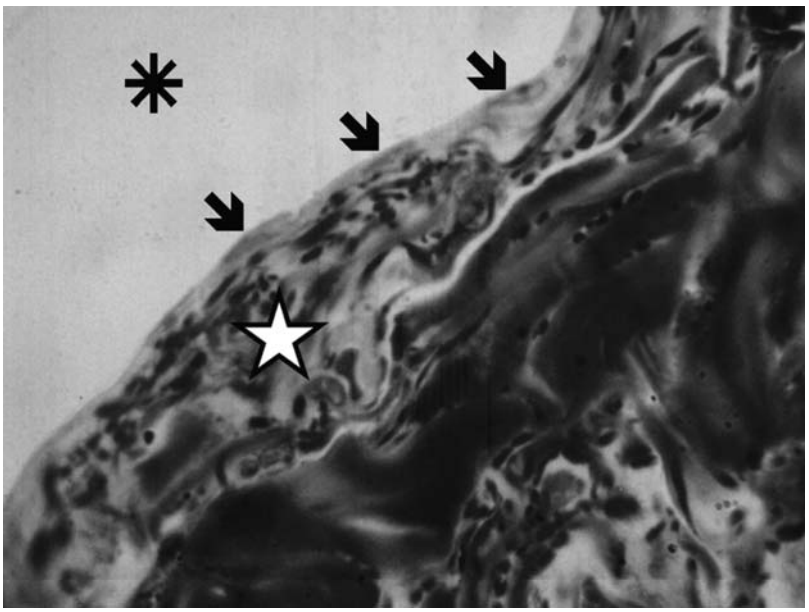

Fig. 5.10 Biopsy of parietal peritoneum taken from a uremic patient at the time of implanting the first dialysis catheter. Arrows point at nuclei of mesothelial cells. Open star was placed on the submesothelial interstitial tissue, the thickness of which ranges between 37 and 62 μm (*: peritoneal cavity) (toluidin blue; × 400)

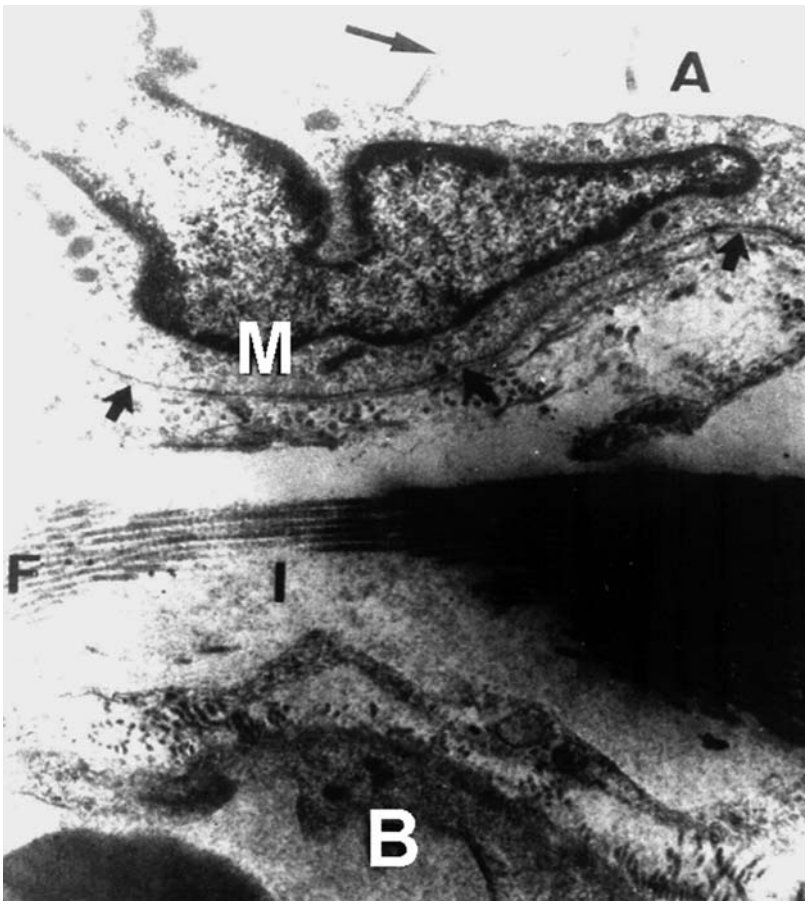

Fig. 5.11 Rabbit mesentery: normal resting mesothelial cell (M) lying on a continuous basement membrane (short arrows) (A: abdominal cavity; long arrow: microvilli; I: interstitium; F: collagen fibers; B: blood capillary; E: erythrocyte) (original magnification × 27,500)

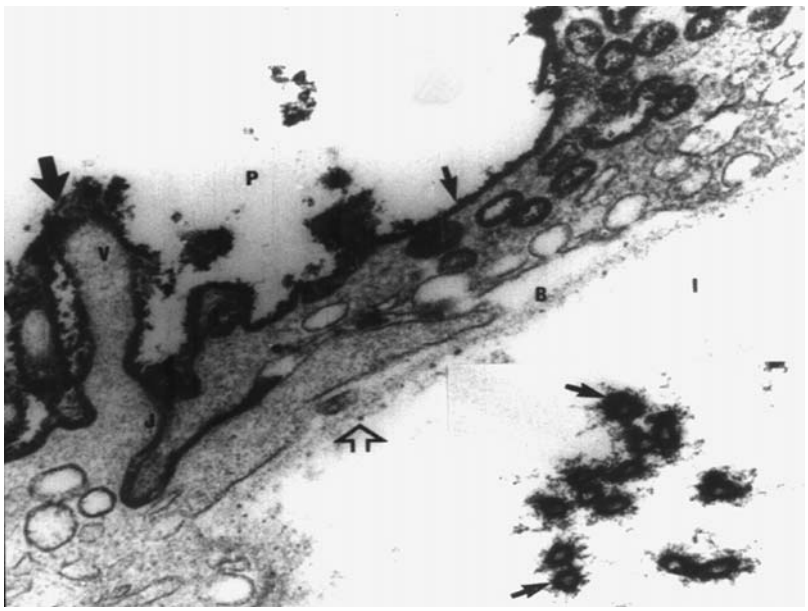

Fig. 5.12 Section of rat mesentery showing microvilli (V) with heavily ruthenium-red decorated glycocalyx (large arrow), also evident on the mesothelial cell plasmalemma (small arrow). The cationic dye also stains a long portion of the intercellular junction (J). The basement membrane (B) shows quite regularly distributed anionic sites (open arrow) (P: abdominal cavity; I: interstitium). Original magnification × 50,720.

Inset. Rat mesentery: transversal section of microvilli showing the fibrilar ruthenium red-stained glycocalyx (arrows) (× 50,720)

cytoplasmic membrane (Fig. 5.12, inset). This cell membrane coating, or glycocalyx, composed of fine fibers that are continuous with the membrane itself [38], furnishes the microvilli surface with electronegative charge, which most probably plays a significant role in the transperitoneal transfer of anionic macromolecules such as plasma proteins [36, 39], as well as in that of charged small molecules, as suggested by Curry and Michel [40] in their fiber matrix model of capillary permeability. This surface charge is substantially reduced in cells undergoing apoptosis [41]. The relevance of these charges upon peritoneal permeability will be discussed later.

Length of microvilli in rodents ranges between 0.42 and 2.7 μm, and their average diameter is 0.1 μm [14, 21, 23, 32]. We have observed a similar range in adult humans. However, mesothelial cells of human embryos (5th–7th week of gestation) showed microvilli up to 3.5 μm long [17].

It has been estimated that microvilli present in the striated border of intestinal epithelium increase the surface area of the intestine by a factor of 20 [42]. Consequently, it has been speculated that mesothelial microvilli could increase the actual peritoneal surface up to 40 m^2 [43].

Plasmalemma of mesothelial cells, like that of microvilli, shows electronegatively charged glycocalyx (Fig. 5.12) [35–37, 44].

Plasmalemmal vesicles, or caveolae, originally described by Lewis [45] in macrophages of rat omentum, are conspicuously present in mesothelial cells at both the basal and luminal borders, as well as in the paranuclear cytoplasm [21–23, 32, 46–48] (Fig. 5.2, inset). Their average diameter is approximately 0.717 μm [14]. At times, pinocytotic vesicles appear clustered together and communicating with each other (Fig. 5.2, inset). Occasionally they appear forming transcellular channels similar to those described in endothelial cells of blood capillaries [49, 50] (Fig. 5.13, inset), apparently communicating both aspects, luminal and abluminal, of the mesothelial cell. These channels can be formed by a chain of several vesicles (Fig. 5.13, inset) or just by two adjoining vesicles. Often pinocytotic vesicles appear to open through the plasma membrane into the luminal or abluminal aspect of the cell (Fig. 5.2, inset; Fig. 5.12), as well as into the intercellular space (Fig. 5.12), exhibiting a neck and a mouth whose respective average diameters are 0.176 and 0.028 μm [14]. With respect to the density distribution of these caveolae, it has been suggested that the parietal mesothelium is less well endowed than the visceral [47].

Palade [51] first proposed that a large part of the macromolecular transport across capillary walls could be attributed to exchange of pinocytotic vesicles between the internal and external surfaces of endothelial cells. This concept was repeatedly applied to the mesothelium. Several electron-dense tracers such as native ferritin [48], iron dextran [14, 32], and melanin [22] were found randomly distributed within pinocytotic vesicles of mesothelial cells after being injected intraperitoneally. Casley-Smith and Chin [47] calculated that the median transit time of vesicles through mesothelial cells ranges between 3 and 5 s, and that approximately 40% of the released vesicles reach the cytoplasmic membrane on the opposite side of the cell. It was even observed that metabolic inhibitors such as dinitrophenol, poisons (cyanide), or slow cooling to 0°C did not completely preclude the uptake of electrondense macromolecules by pinocytosis [48, 52]. This information, supporting Palade's prediction [51] that vesicles could be the structural

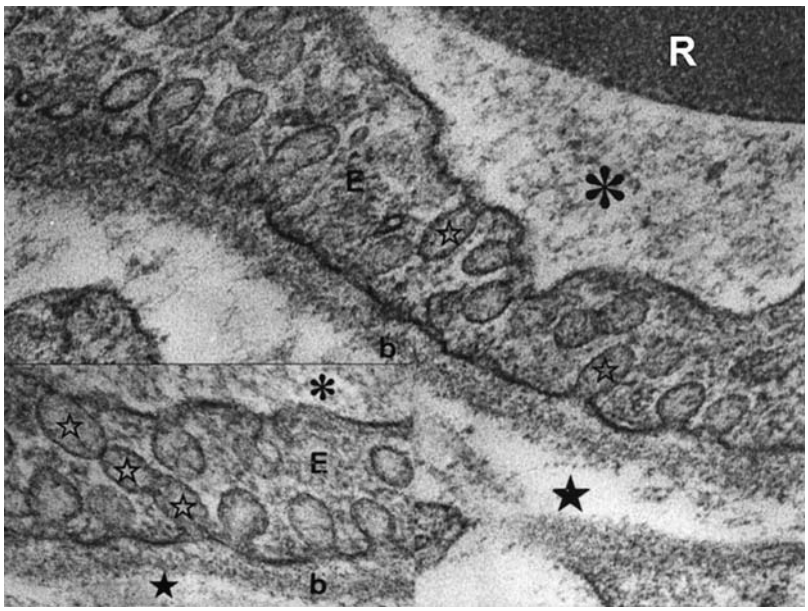

Fig. 5.13 Continuous blood capillary of rat mesenteric peritoneum. Plasmalemmal vesicles (open stars) are open to both aspects of the endothelial cell (E) (R: red blood cell; *: microvascular lumen; b: subendothelial basement membrane; black star: interstitial space) (× 87,000).

Inset. Another capillary from the same sample, showing a transcellular channel made up by a chain of three plasmalemmal vesicles (open stars), connecting both aspects of the endothelial cell (E) (*: microvascular lumen; b: subendothelial basement membrane; black star: subendothelial interstitial space) (× 87,000)

equivalent of the large pore [53], was challenged by stereological analysis of plasmalemmal vesicles. This study apparently showed that vesicles represent merely invaginations of the plasmalemma from both sides of the capillary wall in frog mesentery [54]. It was suggested that this organization of the vesicular system is incompatible with the concept that macromolecules could be transferred across cells by vesicular transport. The methodology followed in this study has been reviewed and criticized, and its conclusions have been refuted [55].

Furthermore, a huge body of scientifically based evidence indicates that endocytosis, transcytosis, as well as potocytosis (an endocytic pathway that utilizes phosphatylinositol anchored membrane proteins and plasmalemmal vesicles or caveolae to concentrate and internalize small molecules) are basic mechanisms used by cells to carry in, out, and through the cytoplasm a variety of substances [56]. The following part of our description applies to both mesothelium and endothelium.

Work done basically during the past decade shed new light on the intimal structure of pinocytotic vesicles. Even though their morphometric parameters are more or less homogeneous, differences in nature, function, and biochemical structure identified at least two kinds of vesicles showing distinctive characteristics.

Caveolae or plasmalemmal vesicles are membrane domains that represent a subcompartment of the plasma membrane [57], characteristic of all vascular endothelium [58]. In capillary endothelial cells, morphological studies indicate that caveolae are effectors of transcytosis of certain macromolecules across the microvascular endothelium: native as well as modified albumins [59–67], low-density lipoprotein (LDL) [68–71], protein hormones [72, 73], AGE [74], as well as orosomucoid [75], a 41 kDa glycoprotein that qualifies as a probe for the postulated large pore [76–78]. Furthermore, endocytosis and transcytosis of albumin–gold complexes have been observed in mice peritoneal mesothelium [79] (Fig. 5.14, inset; Fig. 5.15, inset).

Schnitzer and Oh have demonstrated that transendothelial transport of native albumin through caveolae in both experimental situations (in vivo as well as in the in vitro set-up) is dependent on the interactions of the probe with the endothelial cell surface protein albondin, a 60 kDa albumin binding protein formerly called gp60 [63]. Other binding proteins, gp30 and gp18, appear to mediate the attachment, endocytosis, and degradation of modified albumin. These vesicular carriers require key intracellular components that are sensitive to alkylation with N-ethylmaleimide. Indeed, this substance has been shown to substantially inhibit native albumin (MW: 67 kDa, $r = 36$ Å) and ferritin (MW $\sim$ 500 kDa, $r = 100$–110 Å) uptake, both transcytosed by caveolae [80]. Additional experiments have shown that transcytosis and capillary permeability of insulin and albumin are selectively inhibited by filipin, a complex of polyene antibiotics obtained from *Streptomyces filipenensis*, but does not affect endocytosis mediated by the clathrin-coated vesicles [81]. This concept that identifies two different vesicular pathways is completed with the recent discovery of caveolin, the major structural caveolar protein [82]. This substance is a 22 kDa integral protein that represents a subcompartment of the plasma membrane [57, 83]. Basically, it is a component of the coating covering the luminal aspect of caveolae [84] that, when specifically stained by immunocytochemical methods, serves as a useful marker to draw the diagnostic line between caveolae and other pinocytotic related structures, e.g., coated vesicles [85–87].

Coated pits and coated vesicles (Fig. 5.14, left and right insets) remain the most extensively characterized transport vesicles. They are involved in the intracellular transport of membrane proteins between a variety of membrane

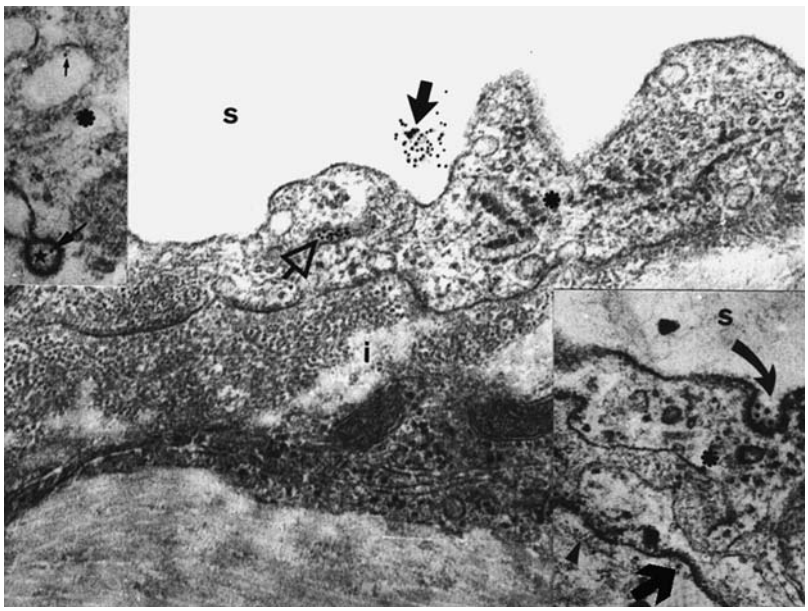

Fig. 5.14 Diaphragmatic peritoneum of a mouse taken 10 min after intra-arterial perfusion with gold-labeled albumin. Some particles (black arrow) can be seen in the peritoneal space (s). The mesothelial cell (*) shows a multivesicular body (open arrow) containing particles of the tracer (I: interstitial space) (× 41,500).

Upper left inset. Cytoplasmic compartment of a mesothelial cell (*) showing albu min–gold complexes decorating the membrane luminal aspect of a pynocytotic vesicle (small arrow), as well as that of coated vesicle (big arrow) (× 64,550).

Lower right inset. Particles of the tracer decorating the luminal glycocalyx of a coated pit (curved arrow) of a mesothelial cell (*), seen in the same sample. The tracer is also present in the abluminal aspect of the mesothelial cell (straight arrow), between the plasmalemma and the submesothelial basement membrane (arrowhead) (× 64,550)

components, mediate endocytosis of transmembrane receptors, and transport newly synthesized lysosomal hydrolases from the trans-Golgi network to lysosomes [88]. The luminal coat contains at least six polypeptides, in addition to the above-mentioned 180 kDa polypeptide clathrin [89, 90]. This type of vesicle is also involved in receptor-mediated endocytosis. Cell surface mediators operate endocytosis clusters into clathrin-coated pits, which pinch off to form vesicles that transport the receptors and their ligand [91]. The complex process of invagination, constriction and budding of clathrin-coated vesicles employs the coordinated actions of several proteins. The best characterized of them is the expanding family of dynamin guanosine triphosphate phosphatases (GTPase), essential for receptor-mediated endocytosis [92, 93]. This enzyme appears to be assembled around the necks of clathrin-coated pits, and assists in

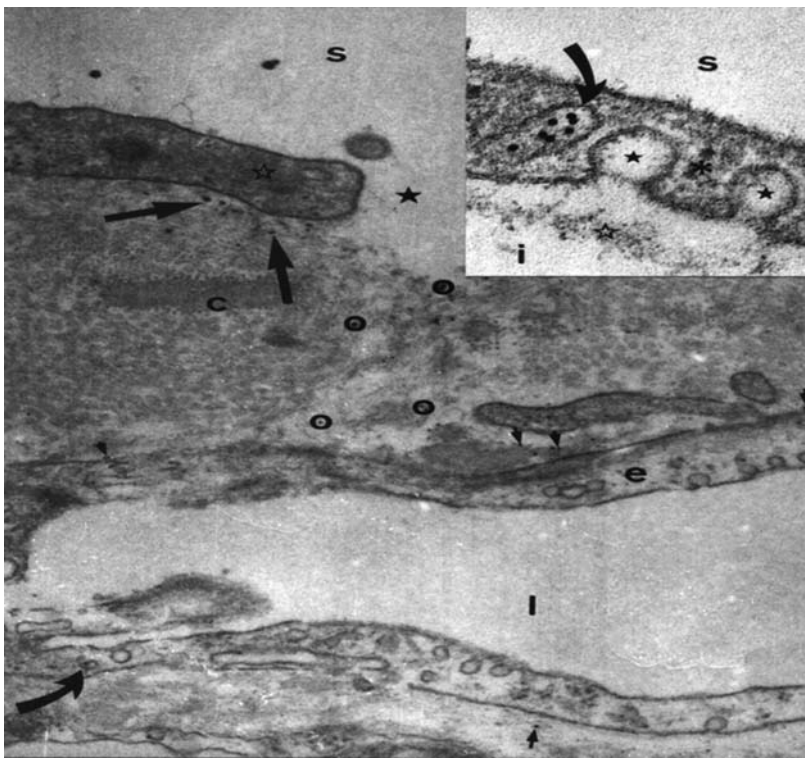

Fig. 5.15 Diaphragmatic peritoneum of a mouse, taken 10 min after intraperitoneal injection of albumin–gold complexes. The black star points at stomata communicating the peritoneal space(s), and the submesothelial connective tissue (c). Albu min–gold complexes (large straight arrow) are present immediately under the mesothelial cell (open star), between collagen fibers (open circles), as well as in the submesothelial interstitial space, near the lymphatic lacuna (short straight arrows). The curved arrow points at a particle of the tracer included in an endothelial pinocytotic vesicle (I: lymphatic lacuna; c: interstitial space) (× 30,740).

Inset. Mouse diaphragmatic mesothelium taken 10 min after intraperitoneal injection of albumin–gold complexes. Arrow indicates an endosome containing particles of the tracer (S: peritoneal space; *: mesothelial cell cytoplasm; black star: plasmalemmal vesicles; open star: submesothelial basement membrane; I: interstitial space) (× 64,550).

Used with permission from [79]

pinching vesicles from the plasma membrane [93]. Recently published information suggests that dynamins mediate both clathrin-dependent endocytosis and the internalization of caveolae in microvascular endothelial cells [94, 95].

Some 70 years ago [96], it was suggested that junctions between capillary endothelial cells should be considered the main pathway for exchanges across the microvascular wall. This concept was later extended to the peritoneal blood microvessels and mesothelium, and extensively analyzed within the frame of the two [77, 78], and lately, the three [97] pore size model of capillary and/or peritoneal permeability. (Assumed pores size: large pore: > 150 Å; small pore: up to 40–45 Å; ultra-small pore: 2–5 Å.) To date, physiological studies and mathematical models have failed to convincingly identify the morphological equivalents of the hypothetical cylindrical water-filled pores [76]. On the other hand, however, this short review of the topic testifies that, at least for protein traffic, the vesicular carried hypothesis has been largely proven and accepted in the last few years [80]. Basically, that caveolae and transcellular channels function as a continuous operating conveyor belt, fusing with each other [49, 50, 98, 99], and moving through the cell [98, 99]. The source of energy fuelling vesicular movement remains one of the many questions still open [98–104].

Furthermore, the demonstrated presence of glucose transporters in mesothelial cells [105] furnish further support regarding the active role of the monolayer in solute's transport from and to the peritoneal cavity. Specialized transporter proteins, which are the products of two closely related genes, UT-A (Sic 14a2) and UT-B (Sic 14a1), modulate the movement of urea across cell membranes. Up to date, five UT-A isoforms have been identified in most tissues [106]. It may be speculated that UT-A transporters are also present in the mesothelium. This hypothesis deserves to be explored.

Additionally, recently published evidence demonstrated not only the presence of aquaporin channels in mesothelial cells, but also that their expression can be modulated by both osmotic and non-osmotic stimulation [107]. The relevance of these channels for peritoneal permeability will be analyzed in the section dealing with peritoneal microvasculature. Their presence in mesothelial cells is one more indication giving support to Henle's prediction that the essential anatomy and physiology of the peritoneum are located in its "endothelia" [108].

Simionescu et al. [109] showed the existence of differentiated microdomains on the luminal surface of capillary endothelium where they found a distinct and preferential distribution of electronegative fixed charges, also called anionic sites. Cationic tracers, which did not bind to caveolae or to transcellular channels, decorated the luminal glycocalyx, coated pits, and coated vesicles [98, 103, 109]. Recent studies applying cationic tracers such as ruthenium red and cationized ferritin in rat and mouse peritoneum also showed a preferential distribution of negative charges at the level of the mesothelial cells luminal surface [36, 37, 44] (Figs. 5.12 and 5.16). Density of these surface plasmalemmal charges is substantially reduced in cells undergoing apoptosis [41].

Mesothelial cell boundaries are tortuous, with adjacent cells often tending to overlap (Fig. 5.4, inset; Fig. 5.12). Tight junctions close the luminal side of the intercellular boundaries [14, 21, 32] (Figs. 5.4 and 5.12). When studied in the horizontal plane by using the freeze-fracture technique, these junctional contact areas were defined as cell extensions and finger-like processes, overlapping into the adjacent cell body. Cell processes were wedge-shaped and numerous, and the cell periphery appeared serrated [110]. Desmosomes have also been observed near the cellular

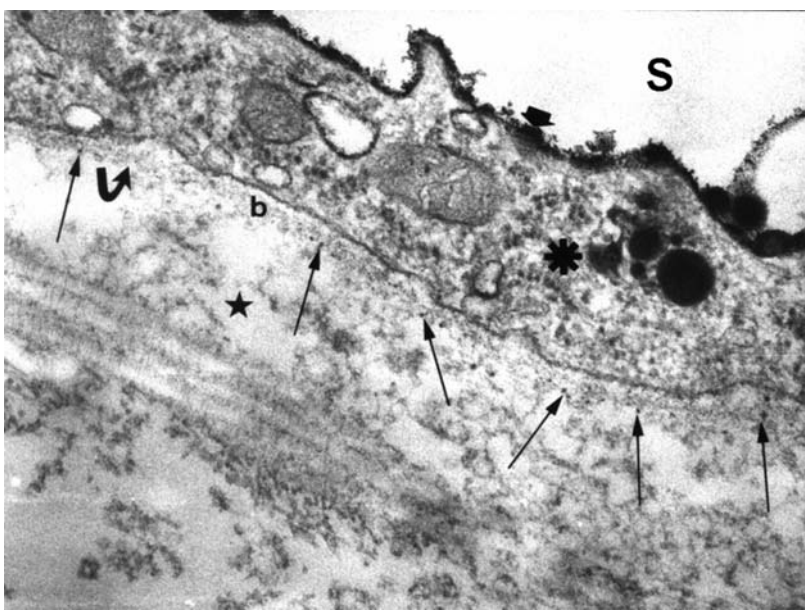

Fig. 5.16 Mesenteric mesothelial cell of a diabetic rat (*). The animal was perfused with ruthenium-red 6 months after induction of the disease, with streptozotocin (glucose blood levels were higher than 500 mg/dL; glycated hemoglobin: $16.38 \pm 0.57\%$). Glycocalyx covering the cavitary aspect of the mesothelial cell is heavily decorated by the cationic tracer (thick arrow). The submesothelial basement membrane (b) shows few dispersed anionic sites (long arrows), as well as areas where they are completely absent (curved arrow) (s: peritoneal cavity; black star: interstitial space) ($\times$ 41,500)

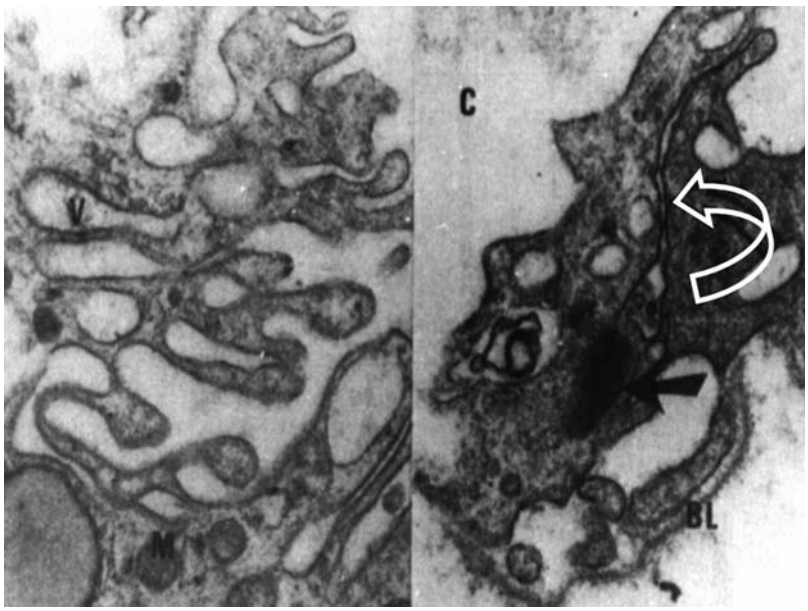

Fig. 5.17 Biopsy of parietal peritoneum taken from a 67-years-old chronic uremic patient, who was on IPD for a period of almost 2 years. A young mesothelial cell shows numerous vacuoles (V) giving a worm-like appearance, which is why this structure is called micropinocytosis vermiformis. The abluminal aspect of the mesothelial cell is lying on a hyaline basement membrane (open arrow) (C: abdominal cavity; M: mitochondrion) (× 26,000).

Right inset. Another area of the same biopsy. This electron micrograph shows the vacuolized cytoplasm of two adjacent mesothelial cells developing a new intercellular junction (open arrow). Note the presence of a typical desmosome (black arrow). The basement membrane (BL) is still discontinuous (original magnification × 30,740)

luminal front [14, 23, 25, 32] (Fig. 5.17) and so have gap junctions [25]. The abluminal portions of cell interfaces usually show an open intercellular infundibulum. Completely open intercellular interphases have not been observed in normal, resting mesothelium [14, 21, 32]. Even desquamated mesothelial cells showing severe degenerative changes can keep their junctional system almost intact (Fig. 5.18). These junctional morphological features are, however, different from those observed between mesothelial cells covering the diaphragmatic lymphatic lacunae, which are more cuboidal and prominent than mesothelial cells observed in other areas of the peritoneal surface.

The existence of stomata (open intermesothelial communications between the abdominal cavity and the submesothelial diaphragmatic lymphatics), predicted by William Hewson [1] 100 years before being discovered by Von Recklinghausen [111], have been the subject of a long and rich controversy along the years. Accepted by some [112–114] and denied by others [115–117], it was not until the advent of electron microscopy that their existence was demonstrated [44, 118, 119]. Scanning electron microscopy disclosed the patent intermesothelial junctions forming gaps whose average diameter ranged between 4 and 12 μm [118, 119] and circumscribed by cuboidal mesothelial cells. These gaps open into submesothelial lymphatics [44] and have not been observed in diaphragmatic mesothelium covering nonlacunar areas [119]. Additional studies have shown the passage of particles from the abdominal cavity into the submesothelial diaphragmatic lymphatics [114, 120]. These studies also confirm the results of experiments

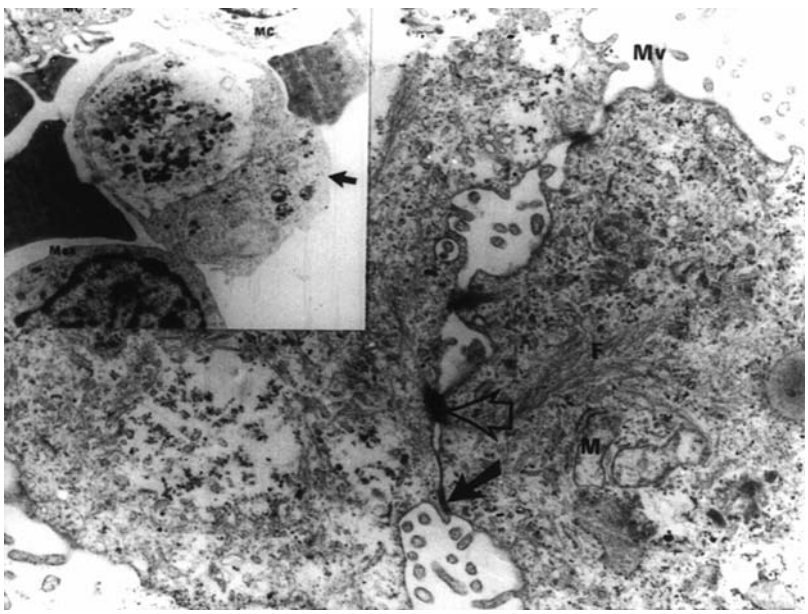

Fig. 5.18 Effluent dialysate obtained from a noninfected patient on peritoneal dialysis. Two desquamated mesothelial cells show severe degenerative changes: swollen mitochondria (M) with broken membranes, sheaves of filaments (F), and swollen cytoplasm. Part of the tight junction is still present (black arrow), as well as a desmosome (open arrow) (M: microvilli) (original magnification × 15,400).

Upper left inset. Effluent dialysate obtained from the same patient. Note the presence of a signet-ring macrophage (arrow), as well as part of two floating mesothelial cells (Mc) (mac: macrophage) (original magnification × 8,600)

performed by Allen [113], who demonstrated the passage of frog erythrocytes through stomata of the mouse diaphragmatic peritoneum, and their appearance within submesothelial lymphatics. This pathway paved the way for intraperitoneal blood transfusions that have been successfully performed in fetuses [121, 122], human adults [123], rats, mice, dogs, and lambs [124, 125]. On the other hand, intraperitoneal malignant cells [126] and bacteria [127] also leave the abdominal cavity on their way to the central venous circulation, through diaphragmatic stomata. The same pathway applies for absorption of albumin–gold complexes injected into the peritoneal cavity (Fig. 5.15) [79]. These structures can be found only between mesothelial cells overlying lacunae.

At the sites of stomata and their channels, mesothelial and lymphatic endothelial cells contain actin-like filaments [128] assumed to induce cell contraction, opening the stomatal pathway for the passage of macromolecules and cells. Cationized ferritin has been observed decorating the glycocalyx of mesothelial and lymphatic endothelial cells located along the stomata, as well as the coated pits and coated vesicles of both types of cells [44, 129]. It should be noted that the presence of stomata has been recently detected in mouse mesenteric mesothelium [130], in omental, ovaric, and pelvic peritoneum, as well as in that covering the anterior liver surface and the anterior abdominal wall [131, 132]. Therefore, it may be assumed that all these extradiaphragmatic openings contribute to the absorptive capacity of the entire peritoneal membrane. Albumin–gold complexes appear to be absorbed also from the peritoneal space through stomata [79] (Fig. 5.15), even though the capability of this pathway for the uptake of the probe did not seem to be much higher than that shown by nonstomatal mesothelial infundibular junctions that contained only 1% of the injected tracer.

Stomata have been ascribed the role of a preferential pathway for the output of fluids, cells, particles, and bacteria from the abdominal cavity [133]. However, the luminal surface of mesothelial cells (which limits the gaps), after staining with cationized ferritin, displayed dense labeling of their cytoplasmic plasmalemma as well as coated pits and coated vesicles. The same cationic tracer also decorated the lymphatic endothelial plasmalemma, which circumscribed the stomatal openings [44]. If this is so, the passage of solutes through stomata is most likely dependent not only on molecular weight, size, and shape, but also on electric charge [44].

Studies in rat and mouse perfused with ruthenium red revealed that intermesothelial cell junctions were, in general, stained just at the level of their infundibulum, even though the dye now and then decorated the junctional complex, staining approximately 50% of its length [37] (Fig. 5.12).

Nuclei are generally located in the central region of mesothelial cells, showing an elongated, oval, or reniform appearance with occasional irregularities in their outlines and sometimes protrusions and indentations (Fig. 5.11). The chromatin is fine, evenly distributed and forms a dense rim around the nuclear membrane (Fig. 5.11). In normal unexposed mesothelium, around 2% of cells are binucleated [31] (Fig. 5.8). Nucleoli have been reported both as present and absent [21, 32]. However, studies performed in imprints [31] showed that they are present and that their number ranges between 6 and 8 (Fig. 5.7). Rough endoplasmic reticulum and ribosomes are dispersed in the cytoplasm. Mitochondria and the Golgi complex are evident mainly in perinuclear areas (Fig. 5.6). Although seldom observed, isolated cilia may emerge from the luminal aspect of mesothelial cells, showing in their cytoplasmic part the axial microtubule as well as the attached basal body (Fig. 5.4). More frequently observed in splenic mesothelium [134], their functional significance is still unknown [135].

The submesothelial basement membrane, originally described by Todd and Bowman [136], and later reported as hyaline, homogeneous, one-layered, and continuous [112, 128], with an average thickness of approximately 40 nm for mouse and rabbit peritoneum [14, 22], normally appears lying under the mesothelial layer of visceral, parietal, and diaphragmatic peritoneum [137] (Figs. 5.11 and 5.17). As an exception, the functional significance of which is still unknown, the omental mesothelium of mice and humans lacks basement membrane [22, 138].

Submesothelial basement membrane of visceral, parietal, and diaphragmatic peritoneum of rat and mouse, perfused with the cationic tracer ruthenium red, consistently showed anionic charges periodically distributed along the lamina rara externa and interna, most of the time, forming double rows [36, 37] (Fig. 5.12).

The reported average diameter of ruthenium red–stained particles in the basement membrane was 2.7 nm, whereas the average distance measured between the one-row oriented basal lamina dye particles ranged between 65 and 90 nm, not far from the interval value of 60 nm observed using the same tracer in rats [139] and human kidney glomeruli [140].

The fact that these charges are, as stated above, distributed along both aspects of the basement membrane implies that the charge-free interval is actually smaller than the mean distance calculated for each membrane layer. The electric field of each particle of ruthenium is around 8–10 nm, and charge discrimination for negative tracers is effective for substances with a molecular radius around 1 nm, corresponding approximately to a globular molecule showing a molecular weight of 2 kDa [141]. In this sense it should be taken into account that the radius of macromolecular anionic albumin is 3.6 nm, whereas its molecular weight is 67 kDa.

It should be noted that the density distribution of these anionic fixed charges of the basement membrane almost disappears during the acute inflammatory reaction secondary to septic peritonitis [142] (Fig. 5.19), and is substantially reduced in rats, soon after 4 months of streptozotocin-induced, uncontrolled diabetes [143] (Fig. 5.16).

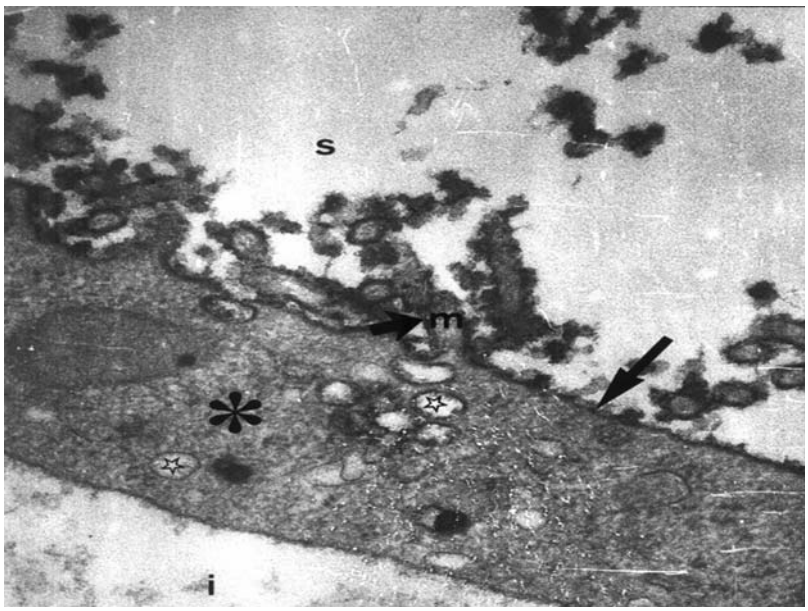

Fig. 5.19 Rat mesenteric mesothelium. The animal was perfused with ruthenium-red, 24 h after experimental induction of *E. coli* peritonitis. Plasmalemmal vesicles or caveolae (open stars) can be seen in the cytoplasm of the mesothelial cell (*). The submesothelial basement membrane is absent, as well as the normally present anionic sites. The luminal aspect of microvilli (m) and that of the cellular membrane are decorated by the cationic tracer (short and long arrows, respectively) (S: peritoneal space; I: edematous interstitial space) (× 41,500)

The relevance of the electronegative charge of the mesothelial monolayer upon the peritoneal permeability to anionic plasma proteins will be discussed in the section dealing with microvascular permeability.

Reduplicated submesothelial basement membrane has been observed in diabetic and nondiabetic chronic uremic patients treated by maintenance peritoneal dialysis [144, 145] (Fig. 5.20). It has been shown that perivascular basement membrane thickness increases with age [146, 147] as well as in the direction of head to foot [147, 148]. This same ultrastructural alteration has been observed in diabetics [147, 149]. It has been suggested that diabetes alone is not responsible for excessive accumulation of basement membrane associated with aging [150]. Therefore, it could be claimed that the reduplication of basement membrane observed in human mesothelium is a by-product of cell renewal regardless of the cause of cell death that triggers the process of repopulation [144, 151]. However, the fact that this phenomenon was also detected in the submesothelial basement membrane of diabetic rats suggests that a high glucose content in the extracellular fluid appears to be related to the mechanism(s) leading to these changes [143].

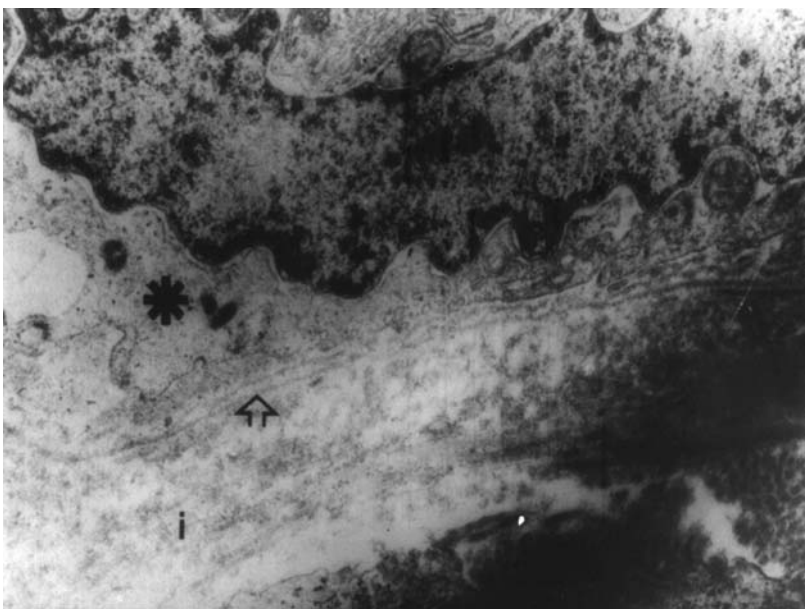

Fig. 5.20 Parietal peritoneum taken from a 67-year-old patient on IPD. The open arrow shows the reduplicated submesothelial basement membrane (*: mesothelial cell; i: submesothelial interstitium) (original magnification × 24,600)

Interstitium

Connective tissue, which originates from mesenchyma, is composed of cells and fibers embedded in an amorphous substance. The main connective tissue cell is the fibroblast and the main fiber is collagen [152].

The submesothelial connective tissue normally has a low cell population surrounded by high-molecular-weight intercellular material. Fibroblasts, mast cells in the proximity of blood microvessels (Fig. 5.21), occasional monocytes and macrophages (Fig. 5.2) are frequently observed.

Substantial amounts of quite compact bundles of collagen are usually interposed between the blood microvessels and the mesothelial layer (Figs. 5.1, 5.2, and 5.3). The collagen density distribution in the different regions of visceral peritoneum is quite variable [146].

The macromolecular common denomination of connective tissues is a broad molecular class of polyanions: the tissue polysaccharides. They form a gel-like structure with the collagen fibers [153], which, when stained with ruthenium red, shows the presence of anionic fixed charges [37].

Thickness of the interstitial layer is extremely variable in the different portions of the peritoneum. This heterogeneity can also be applied to the distances separating the submesothelial blood vessels from the peritoneal cavity, ranging between 1–2 μm to $\geq$ 30 μm (Fig. 5.1). It should be noted that restriction of molecular movement through the interstitial tissue and its progression from or to the microvasculature is affected not only by their molecular weight, shape, and electric charge, but also by the length of the pathway. According to Fick's law of diffusion, it is the difference in concentration per unit of distance (the concentration gradient) that determines the rate of movement of the solute. If we double the distance over which the same concentration difference occurred, the gradient and, therefore, the rate of transfer, would be cut in half. Therefore, the relevance of the interstitial compartment thickness in the transperitoneal transfer of solutes may well be critical [78, 154], and diffusion of solutes coming out from capillaries far from the abdominal cavity could be rendered useful only in long-dwell exchanges, like those performed in CAPD.

The question of the interstitium in terms of plasma to lymph traffic of macromolecules has been basically investigated in lung interstitial tissue [155], which, at physiological pH, has the properties of a negatively charged membrane [156]. Therefore, the polyanionic glycosaminoglycans (mainly hyaluronan) and glycoproteins located in the interstitial ground substance have the capability of influencing the interstitial distribution of volumes of plasma proteins coming out from the intravascular compartment, according to their molecular charge [157]. It has been suggested that these glycosaminoglycans restrict free diffusion through the interstitium [158] and can both reduce the interstitial distribution volume of anionic plasma proteins, and retard the plasma-lymph traffic of cationic macromolecules [155]. Anyway, the effect of protein charge on the interstitial hydraulic conductivity has been only partly clarified.

Fig. 5.21 Interstitial tissue of human parietal peritoneum. Bundles of collagen (c) and fibroblasts (f) are interposed between the blood microvessels (open stars) and the mesothelial cells (not included in the electron micrograph). Mast cells (*) are frequently observed near blood microvessels (original magnification × 42,900)

The extremely low and, at times, negative interstitial pressure (0 to –4 mm Hg) [159–161] represents, together with the capillary permselectivity and the lymphatic drainage, one of the three key factors modulating the plasma-to-lymph fluid traffic, therefore, preventing the formation of interstitial edema [162, 163]. Specifically, during peritoneal dialysis, studies by Flessner [164] have shown that transfer of small solutes through the tortuous interstitial pathways is primarily by diffusion, and that convection may contribute to overall transport in parietal tissue. As stated above, in normal conditions the interstitium has a hydrostatic pressure near 0 [159, 164]. During clinical peritoneal dialysis the intra-abdominal pressure ranges between 4 and 10 cm H_2O [165, 166], thus creating a pressure gradient that drives fluid as well as solutes out of the peritoneal cavity to the interstitium. Thus, fluid loss from the abdominal cavity to the periperitoneal interstitial space is directly proportional to intra-abdominal pressures higher than 2 cm H_2O [166].

Blood Microvessels

Capillaries of human and rodent parietal [167] and visceral peritoneum [43, 168] have been reported to be of the continuous type (Figs. 5.1, 5.3, 5.22–5.24), according to the classification of Majno [169]. However, the existence of fenestrated capillaries in human parietal and rabbit diaphragmatic peritoneum (Figs. 5.1 and 5.25), as well as in mouse mesentery [170–172] has been reported. The incidence of fenestrated capillaries in human parietal peritoneum (Fig. 5.22, inset) appears to be low (1.7% of the total number of capillaries) [172]. The reported density of fenestrated microvessels in mouse mesentery and rabbit diaphragmatic peritoneum ranged between 26 and 29% of the observed capillaries, whereas their presence in parietal peritoneum of nondialyzed uremic patients was only 1.7%. It should be noted, however, that the anterior abdominal wall of humans comprises less than 4% of the peritoneal surface area [10]. Diameter of fenestrae, which ranged between 60 and 90 nm, is well within the range of fenestrae observed in other capillary beds: 40–70 nm in renal peritubular capillaries [173], glomerular capillaries [169], and rabbit submandibular gland [174]. The reported density of fenestrae counted along the capillary circumference of mice mesenteric microvessels is 3.4 fenestrae/micron [175]. This value is quite close to that of 3 fenestrae/micron of capillary circumference observed in renal glomerular capillaries [169]. Density of fenestrae per square micron of endothelial surface is 45–60/μm^2 in renal peritubular capillaries [176] and 20/μm^2 in renal glomerular capillaries [169], whereas their frequency in mouse mesenteric capillaries is approximately 12/μm^2 [171].

The density distribution of submesothelial microvessels along the different portions of the peritoneum is variable. In the rabbit the mesentery appears to be the most vascularized peritoneal segment (contributing 71.1% of the total number of observed capillaries). The reported diaphragmatic and parietal contributions to the total microvascular bed examined were 17.9 and 10.9%, respectively [177].

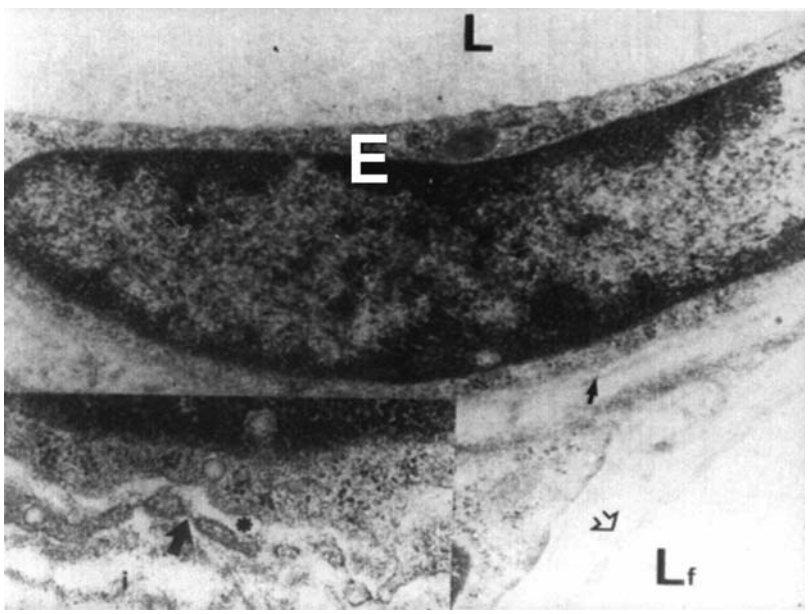

Fig. 5.22 Continuous capillary of a blood mesenteric rabbit capillary whose endothelial layer (E) is lying on the basement membrane (black arrow). (open arrow) (L: lumen of continuous capillary. (Original magnification × 47,400).

Lower left inset. Fenestrated capillary of human parietal peritoneum. The arrow points to a fenestral diaphragm (i: interstitium; *: lumen of fenestrated capillary) (original magnification × 42,900).

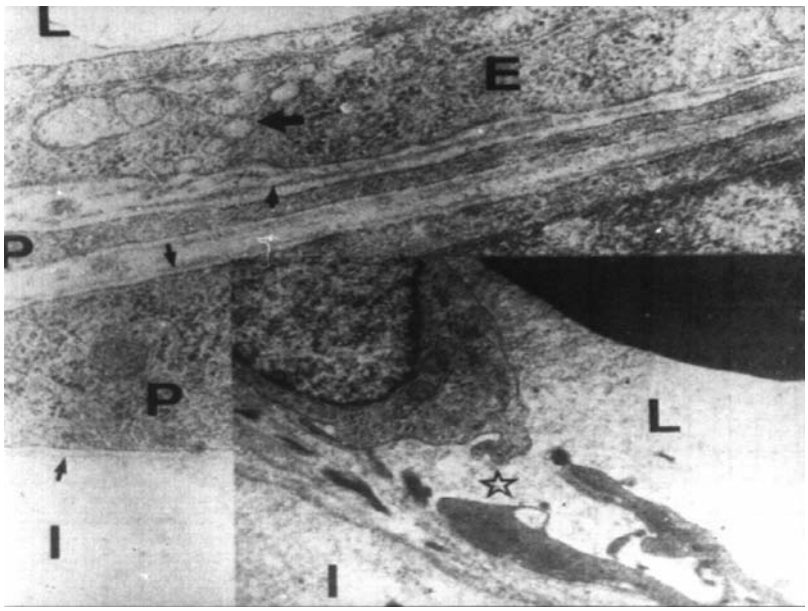

Fig. 5.23 Postcapillary venule of rabbit mesentery. The large arrow shows a transcellular channel (L: microvascular lumen; E: endothelial cell; short arrow: subendothelial basement membrane; P: pericyte; small arrows: subperithelial basement membrane; I: interstitium) (× 62,500).

Lower right inset. Human parietal peritoneum taken from a 21-year-old patient with *E. coli* peritonitis. The star shows an open interendothelial junction of a blood capillary. Note part of an erythrocyte in the upper right quadrant (L: capillary lumen; I: interstitium) (original magnification ×41,500)

In rabbit mesentery the main population of continuous blood microvessels is represented by:

1. True capillaries (without perithelial cells), the mean luminal diameter of which is 7.2 μm and whose mean wall thickness is 0.4 μm (Figs. 5.11, 5.22, 5.23, and 5.24).
2. Venous capillaries usually formed by the confluence of two or three capillaries. These show a thin endothelial layer, occasional peripheral perithelial cells, and have a mean luminal diameter of 9.2 μm.
3. Postcapillary venules whose luminal diameter ranges between 9.4 and 20.6 μm [43].

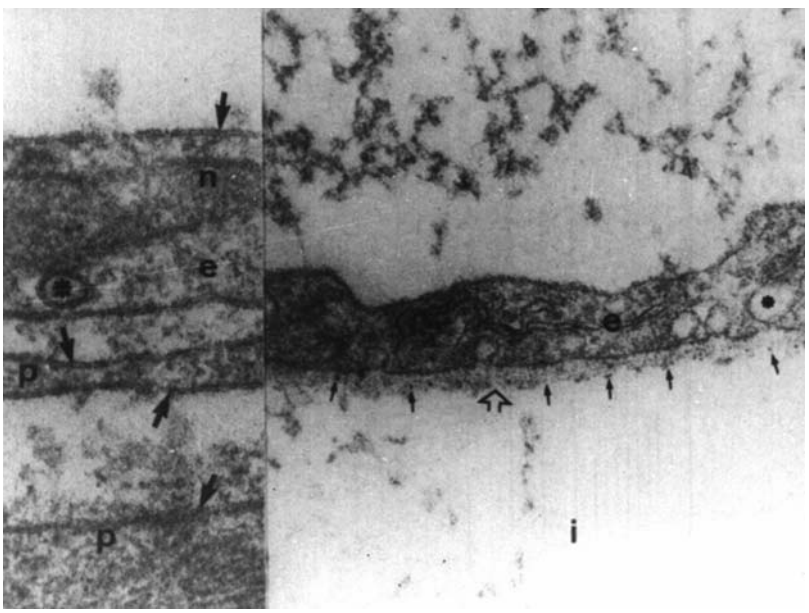

Fig. 5.24 The right part of the figure shows part of a blood capillary wall observed in a sample of diaphragmatic peritoneum obtained from a normal rat. The luminal aspect (upper cell border) of the endothelial cell (e) shows a fine reticular glycocalyx stained by ruthenium red which, on the other hand, does not decorate pynocytotic vesicles (*). The subendothelial basement membrane (open arrow) is continuous and shows quite regularly distributed ruthenium-red stained anionic sites (small arrows) along both the lamina rara externa and the lamina rara interna (original magnification × 50,720).

Inset. Left part of the figure. Part of a postcapillary venule observed in mesentery of rat, 5 days after induction of peritonitis. The trilaminar structure of the endothelial (e) and perithelial cell plasmalemma is clearly observed (arrows), as well as that of the limiting membrane of the pinocytotic vesicle (*). Glycocalyx, basement membrane and anionic sites are absent (n: nucleus of endothelial cell) (original magnification × 84,530)

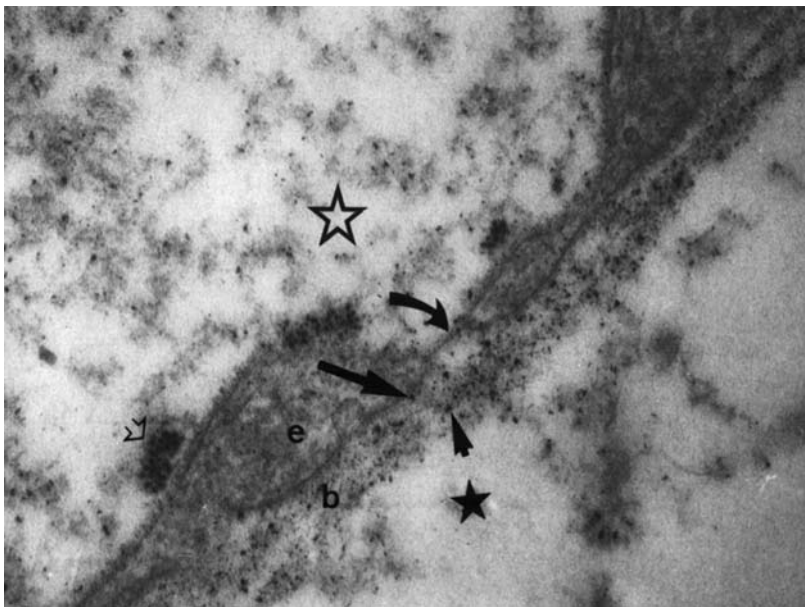

Fig. 5.25 Fenestrated capillary of mouse mesenteric peritoneum. The animal was perfused with cationized ferritin. Particles of the tracer decorate the luminal (long straight arrow) and the abluminal (short black arrow) aspects of the basement membrane (b) laying under the endothelial cells (e). A fenestral diaphragm is also decorated on its luminal aspect by particles of cationized ferritin (curved arrow). Clumps of the tracer appear located on the luminal endothelial cell plasmalemma (open arrow) (open star: microvascular lumen; black star: subendothelial interstitial space) (× 41,500)

With increasing luminal diameter there is a proportional increase in wall thickness due to the presence of more perithelial cells encircling the endothelial layer [178] (Fig. 5.23). The average ratio of luminal diameter to wall thickness is approximately 10/1 [178]. All aforementioned exchange vessels present at their luminal aspect a limiting area that separates the endothelial cell from the circulating blood and is formed by the plasmalemma with its trilaminar structure [19] (Fig. 5.24) and the glycocalyx (Fig. 5.24). The latter, originally described by Luft [38] in other vascular beds, has also been observed at the luminal aspect of peritoneal microvessels [39, 179] The presence of sialoconjugates, proteoglycans, and acidic glycoproteins organized as a fibrous network provides the plasmalemmal glycocalyx with electronegative charge [180] (Fig. 5.26).

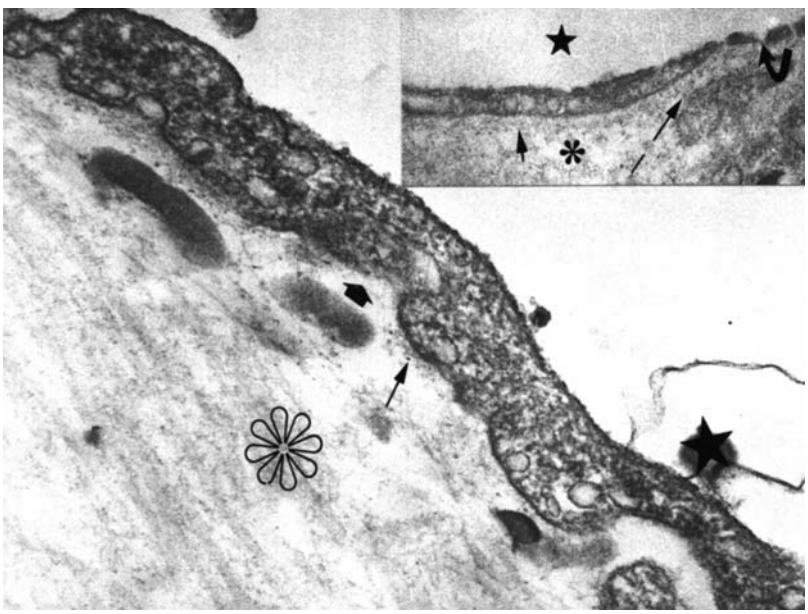

Fig. 5.26 Continuous capillary of rat mesentery. The sample of tissue was recovered 24 h after induction of abdominal sepsis. Distribution of subendothelial anionic sites is irregular; at times they are totally absent (thick arrow), whereas in other portions of the basement membrane they can be seen, but showing an extremely low density (small thin arrow). The luminal aspect of the endothelial cell shows a black rim decorated by ruthenium red, indicating the still-present negative charges of the endothelial glycocalyx (star: microvascular lumen; *: edematous interstitial tissue) (ruthenium red; × 41,500).

Inset. Mesenteric fenestrated capillary taken from the same animal. Occasional anionic sites (long arrow) can be seen along the basement membrane. Most of its length is free from ruthenium-red decorated negative charges (short arrow) (*: structureless interstitial space; star: capillary lumen; curved arrow: fenestra) (ruthenium-red; × 30,740)

There is evidence that anionic plasma proteins (albumin and IgG) are adsorbed to the glycocalyx of microvascular endothelial cells [181]. The fiber-matrix model of capillary permeability envisages the glycocalyx as a meshwork of glycoprotein fibers that, after adsorbing circulating proteins, would tighten its mesh, thereby rendering the underlying endothelium less accessible to water and other water-soluble molecules [40]. Furthermore, it has been shown that the adsorption of circulating anionic plasma proteins to the glycocalyx renders the underlying endothelium relatively impermeable to large, electron-dense, anionic tracers such as native ferritin (MW $\sim$ 450 kDa) [181].

The mean endothelial cell width of rabbit mesenteric capillaries is 0.4 μm, unless the cytoplasm bulges up to more than 1 μm at the site of the nucleus (compare Figs. 5.3 and 5.22 with Fig. 5.24). The cytoplasm includes the usual cell organelles: mitochondria, rough endoplasmic reticulum and free ribosomes [14, 169].

The mitochondrial content of vascular endothelial cells in frog mesentery decreases gradually from arterioles towards venous capillaries and subsequently increases toward venules [182].

The Golgi complex displays variable degrees of development in biopsies taken from different patients. This same variability was observed when comparing different peritoneal microvascular endothelial cells present in a single sample.

The cytoplasmic matrix of endothelial cells shows long filaments, parallel to the longitudinal cellular axis. Their diameter ranges between 20 and 100 Å [169], and at times they appear in bundles. These intermediate-size filaments seem to be a common component of the cytoplasmic matrix of vascular endothelial cells showing, however, a lower density distribution than that observed in other cell types [135].

Nuclei are generally oval, elongated (Fig. 5.22), or occasionally kidney-shaped with focal surface irregularities (Fig. 5.11). Their mean short-axis width in rabbit mesentery is 0.957 ± 0.417 μm [14].

Plasmalemmal vesicles, which can be found in most cell types, are particularly common in capillary endothelia [183], where they occupy approximately 7% of the cell volume [101] (Fig. 5.23). Their outer diameter is approximately 700 Å (it ranges between 500 and 900 Å) [14, 36, 50] and they have a round or oval shape surrounded by a three-layered membrane of 80 Å thickness (Fig. 5.24, inset).

According to their location in the cytoplasmic matrix, vesicles can be classified into three groups: a) vesicles attached to the plasmalemma limiting the blood front of the endothelial cell; b) free vesicles within the cytoplasmic matrix; and c) attached vesicles, but this time to the tissue front of the endothelial cell plasmalemma [50] (Fig. 5.23). The density population of plasmalemmal vesicles varies considerably from one vascular segment to another, even within the same microvascular territory [49, 50]. In the mouse diaphragm, arterioles show 200 vesicles/μm^2, true capillaries 900 μm^2, venular segments of capillaries 1,200 μm^2, and postcapillary venules 600 μm^2 [49].

Most vesicles that open to the extracellular medium have necks whose diameter can be as small as 100 Å [50]. Transendothelial channels formed by a chain of vesicles opening simultaneously on both fronts of the endothelium have been described in capillaries of mouse diaphragmatic muscle [49] as well as in postcapillary venules of rabbit and rat mesentery (Figs. 5.23 and 5.27) [14]. The relative frequency of transendothelial channels has been found to be higher in true capillaries than in arterioles and venules, with the highest density in the venular segment of capillaries [103]. Microvessels of frog mesentery showed a density distribution of three transendothelial channels for every

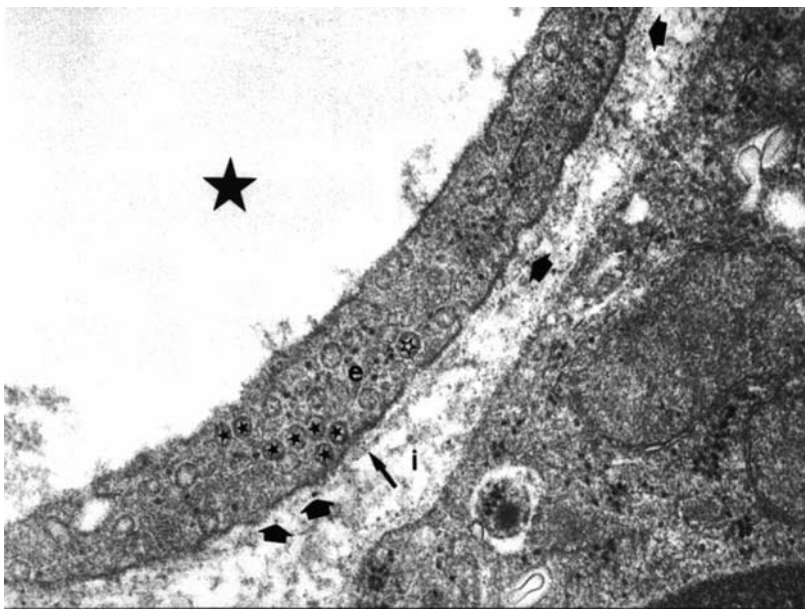

Fig. 5.27 Mesenteric capillary of a rat 6 months after induction of diabetes with streptozotocin (glucose blood levels were higher than 500 mg/dL; glycated hemoglobin $16.38 \pm 0.57\%$). The animal was perfused with ruthenium red. The basement membrane (long arrow), lying under the endothelial cell (e), shows few and occasional anionic sites (thick arrows) (large black star: capillary lumen; open star: pinocytotic vesicle; small black stars: transendothelial channel; i: interstitial space) ($\times$ 41,500)

400 vascular profiles examined [182]. Just as in observations made on mesothelial cells, plasmalemmal vesicles and transendothelial channels do not bind cationic electron-dense tracers that, on the other hand, decorate the luminal aspect of coated pits and coated vesicles [98, 109] in the peritoneal microvasculature [37].

The functional significance of plasmalemmal vesicles or caveolae, vesicles, transendothelial channels, coated pits, and coated vesicles has been discussed in the section on normal mesothelium.

As stated above, in fenestrated capillaries, endothelial cells are pierced by fenestrae closed by a diaphram [184] (Fig. 5.22, inset; Figs. 5.25 and 5.28). Fenestrae are not static structures. It has been shown that their prevalence can be increased under the effect of vitamin A metabolites [185], the influence of sexual hormones [168], thrombocytopenia [186], and by the acute inflammatory reaction [169]. In this sense a microvascular bed (capillaries and postcapillary venules), supplied with a continuous endothelium, can rapidly develop endothelial fenestrations under the influence of vascular endothelial growth factor (VEGF), a 34–42 kDa cytokine, released by different cell types (eosinophils, neutrophils, and others) during the acute inflammatory reaction [187–190]. This effect has been demonstrated in vivo [191, 192], after acute and chronic exposure of different microvascular beds.

High concentrations of negative fixed charges (heparin and heparan sulfate) have been found on the blood front of fenestral diaphragms in several microvascular beds [98, 109, 184, 193–196]. They are expected to discriminate against anionic macromolecules, essentially anionic plasma protein. Similarly, mesenteric fenestrated capillaries of mice perfused with the cationic tracer ferritin showed densely packed anionic fixed charges on the endothelial cell glycocalyx, on the luminal aspect of fenestral diaphragms, as well as along both sides of the subendothelial basement membrane [175] (Fig. 5.25).

What is the role of fenestrae and intercellular junctions in the still ill-defined mechanisms related to capillary permeability? For more than 25 years the fenestral pathway was ascribed a major role in the permeability capabilities of fenestrated capillaries [197]. Some investigators suggested that, while open fenestrae could represent the ultrastructural equivalent of the large pore [77], fenestrae, closed by diaphragms (Fig. 5.25), could also provide a diffusive pathway for water- and lipid-soluble substances [198]. However, fenestral openings of 60–90 nm diameter are too large to be considered the structural equivalent of the hypothetical large pores, the radii of which range between 11 and 35 nm [77, 199]. Furthermore, the density of these pores, estimated at one every 20 μm^2 [50], is substantially lower than the density of fenestrae per square micron observed in microvascular beds.

At least from a theoretical point of view, the presence of anionic fixed charges at the level of fenestral diaphragms, as well as in the subendothelial basement membrane (Fig. 5.25), is a strong argument against the transfenestral passage of macromolecular anionic proteins [139, 200]. Indeed, previously reported physiological studies have demonstrated the selectivity and restriction of the fenestrated microvascular wall to the passage of electronegatively charged

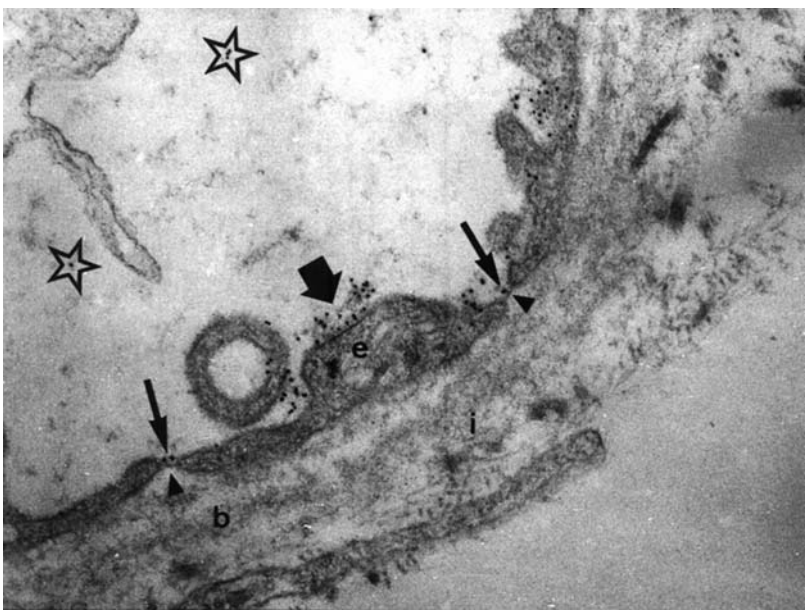

Fig. 5.28 Fenestrated capillary of mouse mesentery taken 30 min after intra-arterial perfusion of the tissue with albumin–gold complexes. Particles of the tracer can be seen in the microvascular lumen (open stars), on the glycocalyx of the endothelial plasmalemma (short thick arrow), as well as on the luminal aspect (long arrows) of fenestral diaphragms (arrowheads). The tracer did not reach the subendothelial interstitial space (i) (b: subendothelial basement membrane) (× 50,720)

macromolecules [201–203]. Moreover, the permeability of fenestrated capillaries to anionic macromolecules is not higher than that of capillaries of the continuous type [204]. In this context Fig. 5.28 offers a descriptive account of the problem, observed in our laboratory (Gotloib L, unpublished observations). Rat mesentery was perfused (in vivo) through the arterial tree with negatively charged albumin–gold complexes for a period of 30 min. As can be seen, substantial amounts of albumin–gold particles appear contacting the luminal aspect of the endothelial cell plasmalemma, as well as free into the capillary lumen. Particles of the tracer can be observed in close apposition to the luminal front of fenestral diaphragms. However, albumin–gold particles were not seen in the subendothelial space, even 30 min after perfusion. These observations support the hypothesis that fenestrae are not permeable to anionic plasma proteins. Consequently, it appears that fenestral openings are unrelated to the theoretically predicted large pore system [197, 200, 204, 205]. On the other hand, fenestrated endothelia have higher hydraulic conductivity, and are more permeable to small ions and molecules than continuous endothelia [206].

Capillary endothelial cells are linked to each other by tight junctions (zonula occludens), originally described by Farquhar and Palade [207–209] (Fig. 5.29). Communicating or gap junctions have been observed in arteriolar endothelium [208]. Postcapillary venules have loosely organized junctions with discontinuous ridges and grooves of which 25–30% appear to be open with a gap of 20–60 Å [50]. The presence of gap junctions has also been documented [14].

Cytoplasmic plasmalemma bordering both sides of junctions also shows anionic fixed charges [37]. Their functional significance in relation to the passage of charged molecules will be discussed later.

Research performed during the past 10–15 years revealed that interendothelial tight junctions appear as a set of long, parallel, linear fibrils that circumscribe the cell, with short fibrillar fragments interconnecting the main parallel array. The number of fibers correlates with junctional permeability: the more densely packed the fibrillar mesh, the lower the junctional permeability [210]. Therefore, the tight junction is not a simple fusion between the outer plasmalemmal leaflets of neighboring cells [211]; rather, it consists of protein molecules such as occludins and cadherins in tight junctions, desmoleins and desmocolins in desmosomes, and connexins in gap juctions [212, 213].

Occludin is an integral membrane protein, exclusively localized at tight junctions in both epithelial and endothelial cells [212], and is directly involved in sealing the cleft, creating the primary barrier to the diffusion of solutes through the paracellular pathway as well as regulating, according to the modulation of occludin expression, the permeability properties of different microvascular beds [214]. Occludin is bound on the endothelial cytoplasmic surface to ZO-1, a 220 kDa membrane-associated protein likely to have both structural and signaling roles [215, 216].

Vascular endothelial cadherin, in turn, is an endothelial-specific cadherin that regulates cell to cell junction organization in this cell type, and provides strength and cohesion to the junction [217]. Cadherins are also implicated

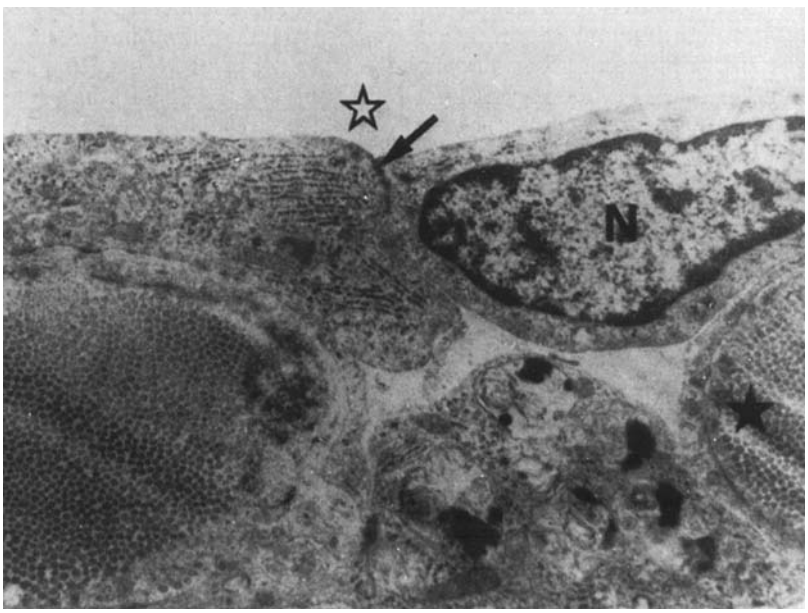

Fig. 5.29 Blood capillary of rabbit mesentery. The black arrow points at a tight junction formed by two adjoining endothelial cells. A macrophage can be observed lying under the endothelial cells interposed between two bundles of collagen (black stars) (open star: capillary lumen; N: nucleus of endothelial cell) (original magnification × 85,000)

in junctional permeability, basically under the effect of inflammatory mediators such as tumor necrosis factor and histamine, which have been shown to induce a redistribution of these adhesion molecules to nonjunctional regions and junctional disassembly [218, 219].

The role of tight junctions in the permeability capabilities of the microvasculature, during the situation of normal physiology, has been a topic for intensive research and controversy through the years. Whereas some groups considered the intercellular cleft as the main pathway for water, as well as for small and large solutes and electrolytes [220, 221], other groups developed the concept that tight junctions create a regulated paracellular barrier to the movement of water, solutes, and immune cells between the microvascular compartment and the interstitial space, enabling the endothelial monolayer to create compositionally different fluid compartments [210, 222–224]. Recently published information indicates that the presence of tight junctions does not imply a foolproof seal of the intercellular cleft. Instead, this structure contains discrete ion-selective pathways through the extracellular portion of the junction, regulated, at least in part, by the activity of the cytoskeleton [210, 225]. As stated above, the transmembrane protein occludin is an excellent candidate for the sealing protein. Understanding the mechanisms involved in junction permeability will require both a more detailed molecular characterization of tight junction proteins and the regulation by the endothelial cells of their attachment to the perijunctional cytoskeleton [222]. As stated by Renkin [204] in 1977, identification of the tight junction with the diffusional pathway for macromolecular plasma proteins, in a situation of normal physiology, still remains questionable. Their role in capillary permeability is still debated.

As for blood cells, recent investigations showed that neutrophils preferentially migrate by crossing at tricellular corners, rather than passing through tight junctions that lie between two adjacent endothelial cells [226].

The basement membrane of true capillaries is normally a thin sheet at the interface between the abluminal aspect of the endothelial cell and the connective tissue (Figs. 5.13 and 5.22). In postcapillary venules it is interposed between the endothelial and the periendothelial cell (Fig. 5.23). Generally uniform for a given structure, its thickness varies among the different parts of the body. True capillaries of normal rabbit mesentery have a mean basal membrane thickness of 0.234 ± 0.095 μm [14]. As described for the submesothelial basement membrane, that of human capillaries also exhibits a significantly increasing thickness in the direction of head to foot [147]. It has been suggested that these regional variations are secondary to differences in venous hydrostatic pressure effective on the capillary bed [147]. Diabetic and nondiabetic patients on long-term peritoneal dialysis, showing reduplicated submesothelial basement membrane, had similar alterations on the capillary basement membrane of parietal peritoneum [144]. These changes were also observed in postcapillary venules and small arterioles of parietal peritoneum taken from diabetic uremics on CAPD (Figs. 5.30 and 5.31), as well as in skin capillaries (Fig. 5.32). Additionally, reduplication of mesenteric subendothelial capillary basement membrane has been recently reported in streptozotocin-induced diabetic rats, as early as after 4 months of uncontrolled hyperglycemia [144], whereas thickening was seen in the same animals 6 months after induction of the disease. These structural alterations of diabetic basement membranes seem to be derived from a substantial increased presence of collagen IV [149, 227–231] which, according to in vitro studies, appears to derive from extended exposure of cells to high concentrations of glucose [232, 233].

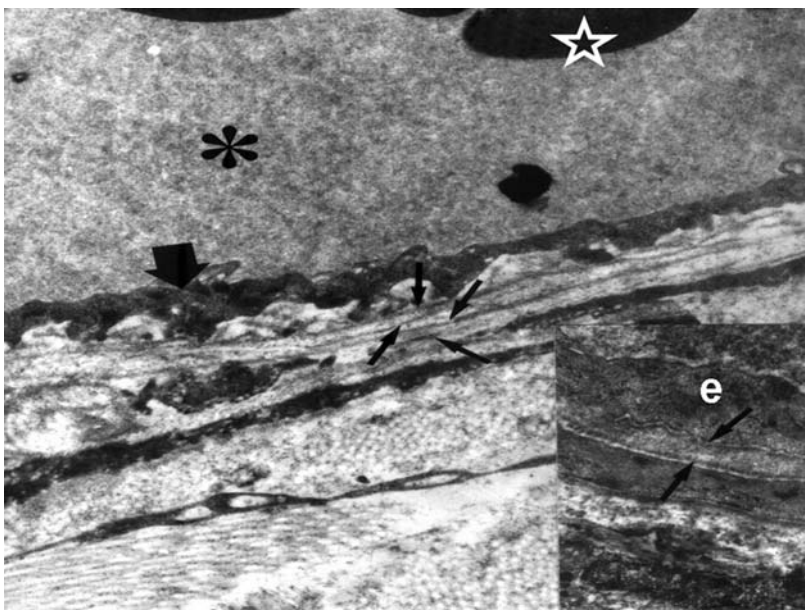

Fig. 5.30 Subendothelial reduplicated basement membrane (small arrows) observed in a small venule of parietal peritoneum taken from a diabetic patient on CAPD (open star: red blood cells; *: vascular lumen; thick arrow: endothelial cell) (× 15,400).

Inset. One arteriole from the same biopsy shows splitting of the subendothelial basement membrane (arrows) (e: endothelial cell) (× 12,600)

Fig. 5.31 Blood capillary of parietal peritoneum taken from a 69-year-old uraemic patient on IPD for almost 3 years. The endothelial cell (e) is lying on a reduplicated basement membrane (arrow) (i: interstitium) (× 24,600)

In rats, both thickening and layering of microvascular basement membrane can also develop as a consequence of aging [151, 234], but not before completing the first year of life [234].

So far, it may be speculated that reduplication or layering of submesothelial and peritoneal microvascular basement membranes in nondiabetics on CAPD could result from their continuous and long exposure to high glucose concentrations.

Subendothelial basement membranes of both continuous and fenestrated capillaries (Figs. 5.24 and 5.25), have regularly distributed anionic fixed charges along both aspects of the membrane [39, 175]. Their density distribution in continuous capillaries ranges between 31 and 34 μm of basement membrane [39, 143]. These values, shown in the section devoted to the mesothelial basement membrane, are not far from those detected in other microvascular basement membranes.

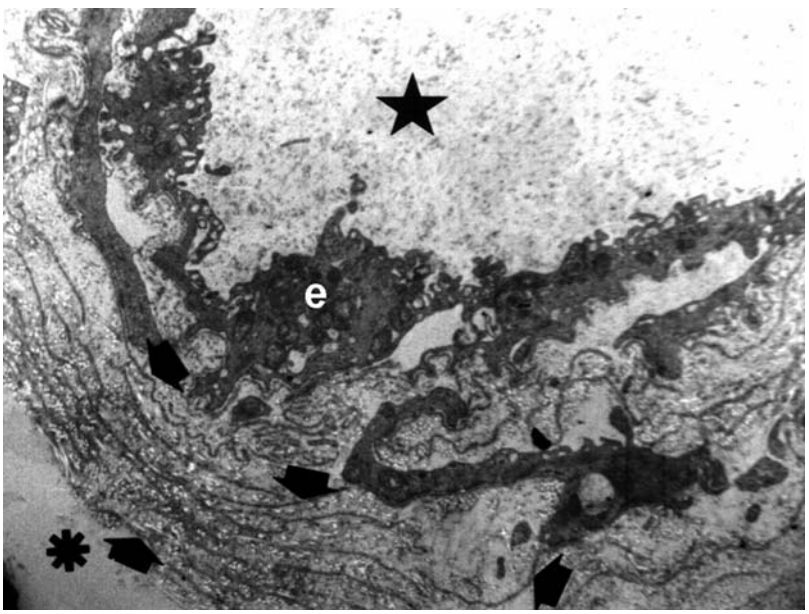

Fig. 5.32 Blood capillary observed in a skin biopsy taken from the same diabetic chronic uraemic patient, whose parietal peritoneum was shown in Fig. 5.31. Arrows point at the multiple layers of basement membrane (star: microvascular lumen; e: endothelial cell; *: interstitial space) (× 5,850)

The chemical composition of the fixed electronegative charges linked to the subendothelial basement membrane has been explored in several microvascular beds. Studies have shown that their main structural components are glycosaminoglycans such as heparan sulfate and chondroitin sulfate [109, 235–237]. This is at variance with the biochemical and histochemical observations made on the glycocalyx cell surface charges, the main component of which is sialic acid and sialo conjugate. This pattern has been detected in microvascular endothelium [238–242], pleural, pericardial, and peritoneal mesothelial cells [243], as well as in macrophages [244], erythrocytes [245], and platelets [246].

What is the functional significance of these electronegative charges? A strong body of literature supports the concept that the permselectivity of capillary walls to anionic macromolecules is basically dependent on molecular charge, besides size and shape [139, 141, 167, 205, 236, 247–253]. Investigations performed in in vivo, whole organ studies [155], in isolated perfused frog capillaries [254], and in isolated rat hindquarters [248] have demonstrated their presence evaluating permeability of different endogenous proteins in a variety of microvascular beds. Indeed, similar results were observed in patients on CAPD comparing dialysate to plasma concentrations of amino acids, having almost the same molecular weight but quite different charge [255], as well as in rat peritoneum, using charged dextrans [256]. The fact that endogenous proteins of graded size are heterogeneous with respect to their molecular charge [257] lead to some conflicting results [258]. The key to this problem was found investigating clinical and experimental situations, where the permselectivity was substantially reduced or neutralized, enabling the observer to evaluate changes in permeability, derived from the absence of the normally present fixed electronegative charges. In the clinical set-up, type I diabetes [259], congenital [260, 261], and acquired nephrotic syndrome [262, 263] have been shown to expose the association of depleted glomerular negative charges and loss of the permselectivity of the capillary wall, leading to massive proteinuria. Experimental interventions performed in laboratory animals confirmed, in turn, the aforementioned findings. Enzymatic removal of sulfated (heparan sulfate) or nonsulfated (hyaluronic acid) glycosaminoglycans from the glomerular basement membrane resulted in a substantially increased permeability to bovine serum albumin [264]. Rats with streptozotocin-induced diabetic nephropathy showed reduced glycosaminoglycan contents in the glomerular basement membrane [265], decreased presence of their heparan sulfate-associated anionic sites [266], as well as significantly increased proteinuria [143]. Further observations made in the streptozotocin diabetic rat have shown a substantial reduction in the submesothelial and capillary subendothelial density distribution of anionic fixed charges (from 31 ± 2 to 12 ± 2 ruthenium red-decorated anionic sites/μm of basement membrane) and, at the same time, a significant increase of albumin losses in the peritoneal dialysis effluent, indicating a marked decrease of the permselective capabilities of the charged components of the peritoneal membrane (Fig. 5.16) [143]. Similar observations were made in intact rats after neutralization of the peritoneal negative charges with protamine sulfate [267].

The acute inflammatory reaction is the most spectacular experimental set-up to demonstrate the permeability changes derived from an acute reduction of the microvascular negative charge. This situation has been classically defined by the development of acute low hydrostatic pressure, high capillary permeability, and albumin-rich interstitial edema [163, 268]. In this sense the generalized acute inflammatory reaction derived from abdominal sepsis promotes a major erosion of the density distribution of the anionic fixed charges in several microvascular beds, diaphragmatic and mesenteric peritoneum (showing values as low as six anionic sites/micron of basement membrane) [269], myocardium [270], skeletal muscle, pancreas, renal peritubular capillaries [271], as well as in the submesothelial basement membrane of rat diaphragmatic and mesenteric peritoneum [142] (Figs. 5.19 and 5.26). Additional studies in the same experimental model of abdominal sepsis in rats demonstrated abnormally increased albumin content in mesenteric, diaphragmatic, and pancreatic interstitial fluid [272]. This drastic loss of the permselectivity of the capillary wall derives from a massive liberation and reduced inactivation of a host of mediators of inflammation triggered by acute inflammation [273–275], including tumor necrosis factor alpha, interleukins, platelet-activating factor, leukotrienes, thromboxane A2, activators of the complement cascade, kinins, transforming growth factor B, vascular endothelial growth factor, as well as many others already known, or still waiting to be identified [185, 276–279].

The role of intercellular junctions in macromolecular leakage during acute inflammation is still controversial. Some groups pointed to the endothelial tight junction as the main pathway for extravasation of macromolecular plasma protein. It was postulated that inflammatory mediators such as histamine, serotonin, bradykinin and leukotriene E4 induced junctional openings (Fig. 5.23, inset), by means of endothelial cells contraction [280–283] or by a loss of occludin and cadherin from the junctional complex [284, 285]. Unpublished observations from our laboratory (Gotloib L.) made in intact rats, as well as in rats with *E. coli* peritonitis, by means of intra-arterial injection of albumin–gold complexes, showed that most particles of the tracer cross the endothelial barrier transcellularly, via plasmalemmal vesicles. In both experimental situations, intact and infected rats, the tracer was not seen beyond the junctional infundibulum (Figs. 5.33 and 5.34); just the opposite: the tracer was present in plasmalemmal vesicles (Fig. 5.34, inset), and reached the subendothelial space in areas far from intercellular junctions (Figs. 5.33 and 5.34). This concept of transcellular transport of albumin through the capillary wall, also during acute inflammation, is

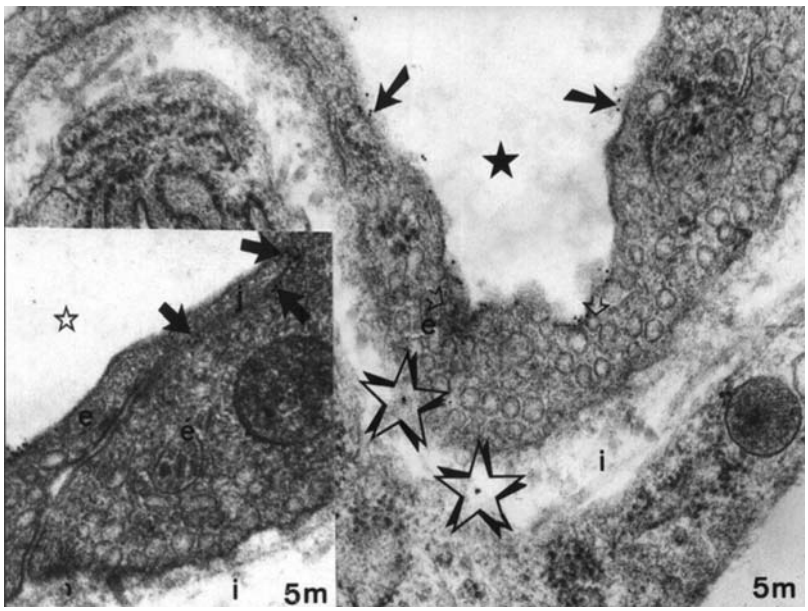

Fig. 5.33 Blood continuous capillary of mouse diaphragmatic peritoneum. The material was taken 5 min after intra-arterial perfusion of the tissue with albumin–gold. Particles of the tracer decorate the luminal aspect (black arrows) of the endothelial cell, as well as that of pynocytotic vesicles (open arrows). Note the presence of albumin–gold complexes (open stars) in the subendothelial interstitial space (i), in an area free of intercellular junctions (× 41,500).

Inset. Another aspect of the same sample shows particles of the tracer (arrows) in the luminal side of the intercellular junction, whereas the interstitial space (i) is devoid of albumin–gold complexes (open star: microvascular lumen; b: subendothelial basement membrane; e and é: adjacent endothelial cells) (× 41,500)

supported by recently published evidence postulating a significant role for plasmalemmal vesicles and even for fenestrations induced by vascular endothelial growth factor [286–288].

Water transport across endothelium of continuous capillaries was classically thought to occur almost completely via the paracellular pathway through intercellular junctions. Transcellular transport was considered to be nil.

However, the relevance of the transcellular pathway also for water has recently been brought to the forefront by the immunohistochemical identification of aquaporin-1 channels in peritoneal microvascular endothelium [289, 290], as well as in rat peritoneal mesothelium [107]. Expression of this transmembrane water channel protein in the endothelial cell surface of continuous capillaries appeared to be basically localized in plasmalemmal vesicles, and its concentration is quantitatively comparable to that seen in erythrocyte plasma membrane [291]. The presence of aquaporin-1 in microvascular endothelium provides a molecular explanation for the water permeability of some capillary beds [292], as well as a low-energy cost pathway [293] for almost 70% of the transmembrane transport of water [289]. Furthermore, this evidence confirms the predicted concept that, also during peritoneal dialysis, not less than 50% of the transperitoneal water flow occurs through postulated ultra-small transcellular pores [97] that appear to be metabolically driven pathways rather than just holes located in the microvascular wall.

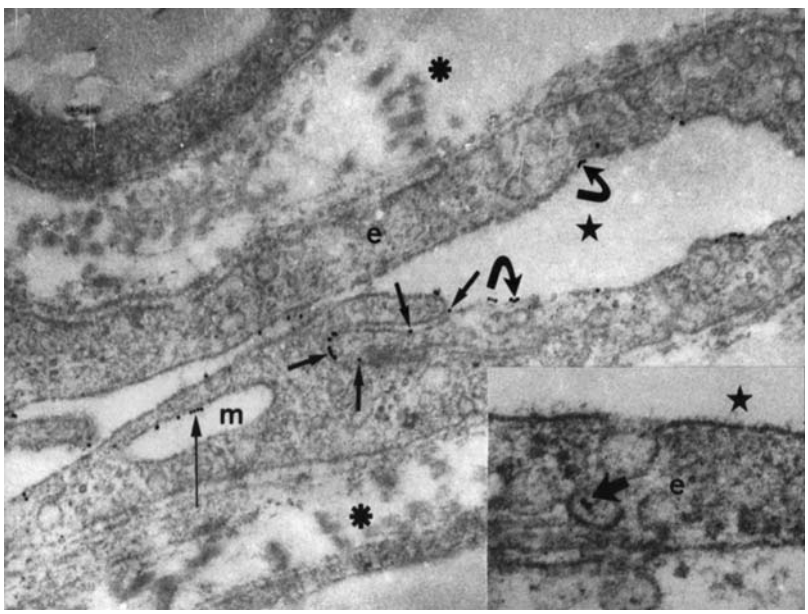

Fig. 5.34 Mesenteric capillary of a rat with experimentally induced *E. coli* peritonitis. Intraarterial perfusion with albumin–gold was performed 24 h after provoking the disease. Particles of the tracer can be seen adsorbed to the luminal aspect of the endothelial cell membrane (curved arrows), as well as within the infundibulum of the interendothelial cell junction (short arrows). Some particles of the tracer (long thin arrow) are also present in a cytoplasmic multivesicular body (m) (*: interstitial space; e: endothelial cell; black star: capillary lumen) (× 41,500).

Inset: Another aspect of the sample taken from the same animal. Albumin–gold complexes are also present in a pinocytotic vesicle (arrow) (star: capillary lumen; e: endothelial cell) (× 84,530)

Summarizing the information obtained from ultrastructural and physiological studies, it can be stated that the microvascular endothelial cell should be considered a highly active structure, serving not only as a permeability barrier and an effective thromboresistant surface, but also as the location of important synthetic and other metabolic activities [182, 209].

Continuous capillaries are more permeable to larger molecules than are fenestrated capillaries [199]. Coated pits and coated vesicles are involved in receptor-mediated endocytosis, whereas the uncharged pinocytotic vesicles and transcellular channels are involved in the transfer of proteins and fluid-phase pinocytosis. The transcellular pathway plays a relevant role in the transmembrane transport of water and macromolecular plasma proteins. Additionally, all the resistances described by Predescu et al. [75] along the pathway leading from the microvascular lumen to the abdominal cavity, are negatively charged [37, 39].

Lymphatics

The lymphatic system serves to drain, from the interstitial compartment, a range of materials such as water, proteins, colloid materials and cells [294], all elements included in the interstitial fluid. Under normal conditions fluid crosses the microvascular endothelial membrane at a rate whose magnitude depends on the Starling forces acting at each aspect of the capillary membrane, as well as on the permeability properties of the endothelial microvascular monolayer. The local autoregulation of interstitial volume is provided by automatic adjustment of the transcapillary Starling forces and lymphatic drainage [161]. Therefore, an alteration in the aforementioned forces results in interstitial accumulation of fluid that will eventually be removed by the lymphatic flow that, in situations of high capillary permeability edema occurring during acute inflammation, can increase by a factor of ten [295]. In the abdominal cavity, lymphatics have a relevant role in the prevention of ascites [296].

Work during the last 20 years has revealed relevant evidence characterizing lymphatic structure and organization. The first stage of lymph collection occurs through a system of interstitial nonendothelial channels, or low-resistance pathways known as pre-initial lymphatics [297, 298], which have been seen in the cat and the rabbit mesentery [299].

This most peripheral part of the lymph vessel system is a completely open net of tissue channels which drain, at least in the cat mesentery, mainly along the paravascular area of the venous microvasculature, into a network of 0.5 mm long, irregularly shaped endothelial tubes, approximately 20–30 μm width [300]. By the time these tubes are completely filled they can reach a maximal diameter of up to 75 μm [301]. A single endothelial layer (Fig. 5.35, inset) forms these endothelial tubes defined as initial lymphatics or lymphatic capillaries [299, 301, 302].

The subendothelial area is most of the time devoid from basement membrane, as well as from a smooth muscle layer present in larger lymphatic collectors [303]. The sporadically observed patches of basement membrane have, as in blood capillaries, anionic fixed charges that can be decorated by cationic tracers [304]. Due to the absence of muscular layer, lymphatic capillaries lack the capability for spontaneous contractility [305]. However, the fact that lymphatic

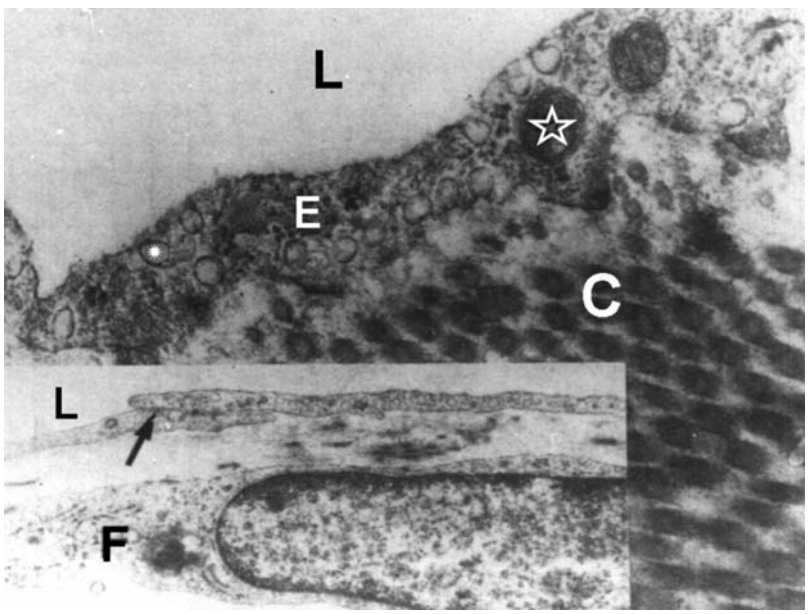

Fig. 5.35 Partial view of a lymphatic lacuna observed in a sample of rabbit diaphragmatic peritoneum. The thin endothelial cell (E) shows numerous pinocytotic vesicles (*) and occasional mitochondria (star). Note the absence of subendothelial basement membrane (L: lacunar lumen; C: collagen fibres) (original magnification × 85,000).

Lower left inset. Lymphatic capillary of rabbit diaphragmatic peritoneum. Two adjoining endothelial cells, forming a tight junction (arrow), appear lying on the interstitial tissue. Basement membrane, as well as anchoring filaments, are not observed (L: capillary lumen; F: fibroblasts) (original magnification × 62,500)

endothelial cells contain an abundant supply of fine actin-like filaments, 40–60 Å in diameter, arranged in bundles parallel to the long axis of the cell, led some investigators to postulate that these filaments could function as a contractile element of the lymphatic capillary wall [306, 307].

Anchoring filaments, having histochemical and ultrastructural characteristics similar to those observed in elastin-associated microfibrils, form a uniform population of fibrous elements, leading to the development of structural and functional continuity between the abluminal aspect of the lymphatic capillary endothelial cell and the elastic network of the adjacent connective tissue [308]. The main role of these anchoring filaments is the prevention of capillary collapse, when the interstitial pressure gains strength as a consequence of expanded fluid content of the interstitial compartment [309]. This simple element enables the lymphatic system to launch a mechanism of fluid drainage that accounts for 25% of the safety factors that can prevent formation of interstitial edema [308]. In this context it has been proposed that initial lymphatics directly sense and regulate the interstitial fluid volume [310].

The total surface area of pre-initial and initial lymphatics seems to be smaller than the total exchange area of blood microvessels [198]. Other studies on cat and rabbit mesentery showed the additional presence of flat, blind saccular structures up to 40 μm wide, with a wall made up of a simple layer of thin endothelial cells, devoid of basement membrane [198, 300].

Lymphatic endothelial cells are flat and elongated, showing an average thickness of 0.3 μm in non-nuclear areas [46, 306]. The luminal aspect of lymphatic endothelium, when exposed to cationic tracers such as cationized ferritin or ruthenium red, shows a high density of anionic fixed charges that, at times, can also be detected labeling the luminal aspect of the intercellular cleft (Fig. 5.36) [307, 44]. These charges prevent the adhesion of electronegatively charged blood cells to the endothelial luminal surface and may play a significant role in the movement of charged solutes from the interstitial compartment to the capillary lumen [44]. Furthermore, the absence of subendothelial and negatively charged basement membrane (Fig. 5.36) points at the asymmetry of the lymphatic capillary wall that is at variance with the electric symmetry characteristic of blood capillaries.

Nuclei of endothelial cells are flattened and, on electron microscopy, appear elongated. Their irregular outline shows a thin peripheral rim of dense chromatin. Plasmalemmal vesicles [46, 311] and transendothelial channels, similar to those described for blood microvessels, are commonly observed [307]. Plasmalemmal vesicles have been shown to participate in the transcellular movement of albumin–gold complexes, from the submesothelial interstitial space to the lumen of capillary lymphatics [79] (Fig. 5.37). Furthermore, the endocytotic pathway has been shown up by the presence of the same tracer into cytoplasmic endosomes (Fig. 5.38).

Several types of interendothelial junctions have been described. Approximately 2% of the whole junctional system consists of open junctions, showing gaps up to 100 nm width, that can, at times, be as wide as 1,000 nm [307, 312]. These openings serve as a way in for macromolecular solutes such as gold-labeled albumin (Fig. 5.38) or cationized ferritin (Fig. 5.39). At times two adjoining endothelial cells overlap each other, forming a kind of valvular junction that can be easily opened by an eventual increase of interstitial pressure (Fig. 5.36, inset). Junctional infundibuli show anionic fixed charges similar to those observed in the luminal endothelial glycocalyx (Fig. 5.36). Around 10% of junctions are

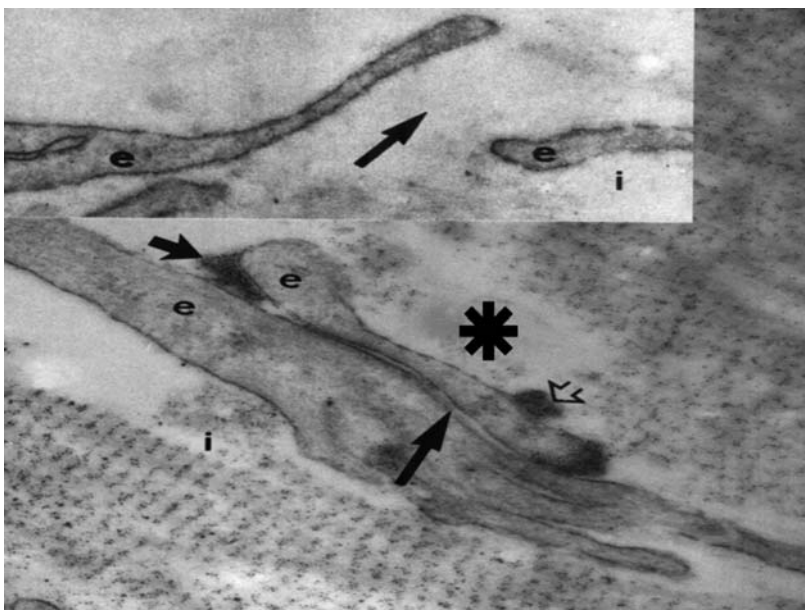

Fig. 5.36 Mesenteric lymphatic capillary of a mouse perfused with cationized ferritin. The long arrow points at the intercellular junction formed by two adjacent endothelial cells (e). The short black arrow indicates the presence of the electropositive tracer on the luminal aspect of the intercellular junction, whereas the open arrow shows particles of ferritin decorating the endothelial luminal plasmalemma. Note the absence of subendothelial basement membrane (*: microvascular lumen. i: subendothelial interstitial space) (× 41,500).

Inset. Mesenteric lymphatic capillary of an intact mouse. The arrow points at an open intercellular cleft formed by two adjacent endothelial cells (e). The junction serves as a valvular structure sensitive to the hydrostatic gradient between the interstitial space (i) and the microvascular lumen (open star) (× 41,500)

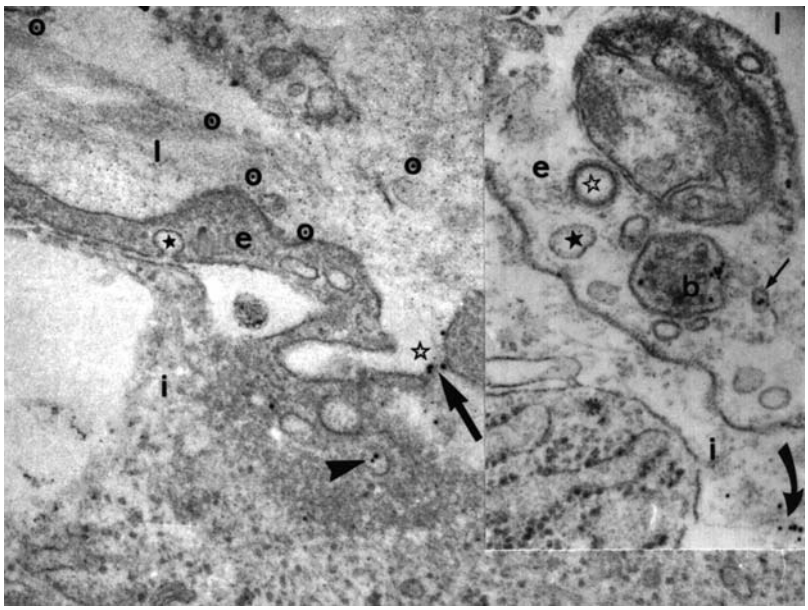

Fig. 5.37 Diaphragmatic submesothelial lymphatic capillary taken from a mouse 10 min after intraperitoneal injection of albumin–gold complexes.

Left inset. Albumin–gold complexes (long arrow) can be observed in their pathway through an open interendothelial cell junction (open star). More particles of the tracer are seen (open circles) within the luminal space (I) of the microvessel. Arrowhead points at albumin–gold included into a pinocytotic vesicle (i: subendothelial interstitial space; black star: plasmalemmal vesicle) (× 41,500).

Right inset. Lymphatic capillary endothelial cell (e). Albumin–gold complexes appear in an endosome (b) as well as in a pinocytotic vesicle (straight arrow). Curved arrow points at albumin–gold complexes present in the interstitium (i). Notice the absence of subendothelial basement membrane (black star: plasmalemmal vesicle; open star: coated vesicle) (× 64,450).

Used with permission from [79]

zonula adherens, whereas the rest are tight junctions [301, 313]. It has been proposed that, in addition to the organized prelymphatic system [314], a small percentage of open junctions (1–6%) can account for a substantial proportion of the lymphatic pathway for fluid as well as small and large molecule drainage [301].

The diaphragmatic lymphatic capillary net is organized as a plexus along the submesothelial surface [315], which drains, through an intercommunicating microvascular system, into a plexus on the pleural side of the diaphragm [133]. The distribution of the whole diaphragmatic network is irregular, and varies in different species.

A prominent feature of diaphragmatic lymphatics is the presence of flattened, elongated cisternae or lacunae, approximately 0.3–0.6 cm length, with a long axis that is parallel to the long axis of the muscle fibres [315–317] (Fig. 5.40). The monolayer endothelial lining of the lymphatic lacunae is thin and shows no tight junctions. Adjacent cells usually overlap, forming valve-like processes, leaving an open interface that can be as wide as 12 μm. The cytoplasm of endothelial cells, basement membrane, and anchoring filaments of lymphatic lacunae are similar to those structures described for lymphatic capillaries. While anionic sites have not been observed, the glycocalyx of cisternal endothelium, when exposed to ferritin, is heavily decorated by the cationized tracer, which also appears along the open intercellular clefts [44, 318].

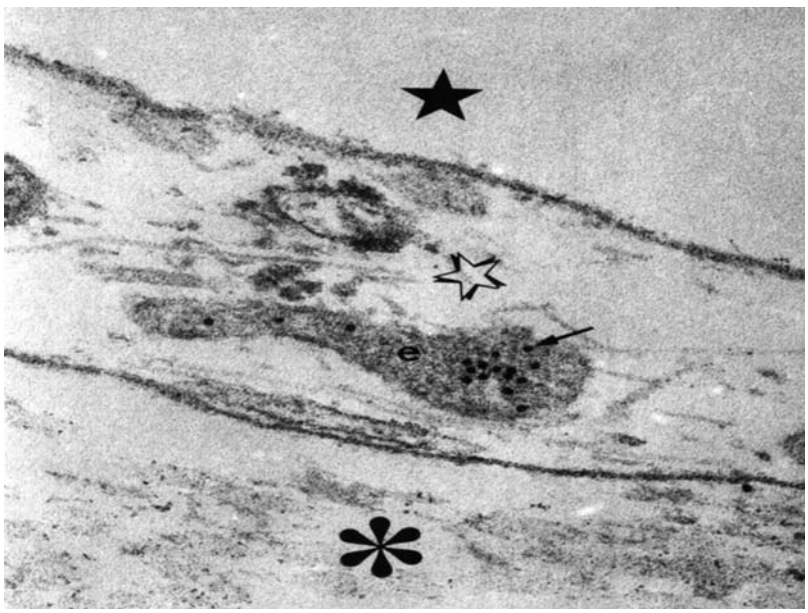

Fig. 5.38 Diaphragmatic lymphatic capillary of a rat. The sample was taken 15 min after starting intraarterial perfusion with albumin–gold complexes. Endosome (e) present in the cytoplasm of the endothelial cell (open star) shows particles of the tracer. This may well represent the endocytotic pathway for degradation of the complex. Note the absence of subendothelial basement membrane (black star: microvascular lumen; *: interstitial tissue) (× 87,000)

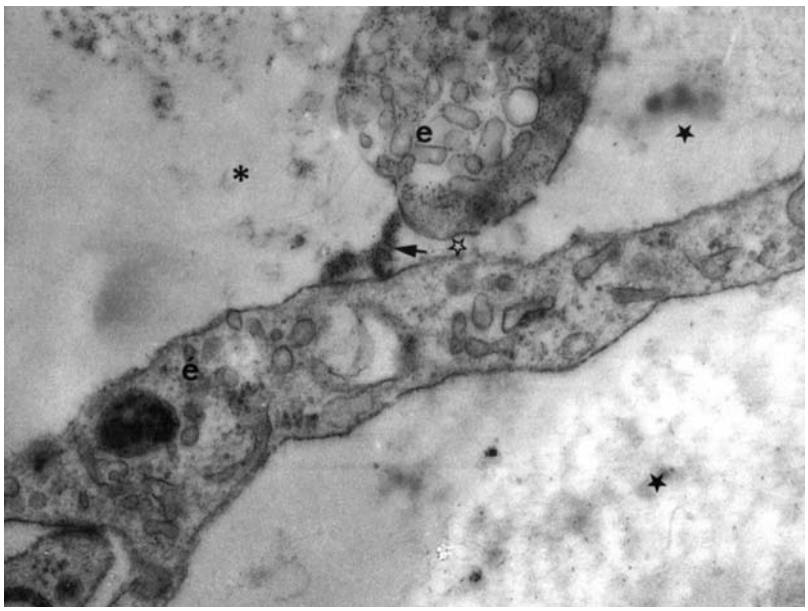

Fig. 5.39 Mesenteric lymphatic capillary obtained from a mouse intraperitoneally injected with cationized ferritin. Particles of the tracer (arrow) can be seen entering the microvascular lumen (*) through the open interendothelial cell junction (open star). Again, note the absence of subendothelial basement membrane and anionic sites (e and é: lymphatic endothelial cells; black stars: interstitial space) (× 41,500)

Diaphragmatic lymphatic lacunae, regularly connected by transverse anastomosis [114], and capillaries from the whole peritoneal lymphatic network, including the rich omental plexus [319], drain into a system of precollector, small-caliber lymph vessels that have a poorly developed smooth muscle layer underlying the endothelium. These vessels, which have semilunar valves [1, 320], drain, in turn, into the larger collecting vessels, whose diameter ranges between 40 and 200 μm [321]. The luminal aspect of the endothelial layer shows a sequence of valvular segments, with a semilunar bicuspidal valve at the distal end of each [133, 321]. The smooth muscle layer underlying the subendothelial basement membrane shows a spiral arrangement around the endothelial tube that becomes more pronounced towards the downstream end of the intervalvular segment [305, 322, 323]. Distances between adjacent valves range between 0.1 and 0.6 mm [323]. Thereby, the anatomical and functional unit (lymphangion) is established, consisting of one valve and the following intervalvular segment, which measures 2–3 mm in length [324]. This collecting segment, limited by two one-way valves and an intrinsic smooth muscle layer, compresses the lymphatic lumen driving the intravascular fluid centrally into the next compartment, making up an escalated system of drainage that has, in the proximal part of each lymphangion, a valve that prevents retrograde flow [305]. The presence of valves also enables this part of the system to reach differential intraluminal pressures around 1–2 cm of water [325].

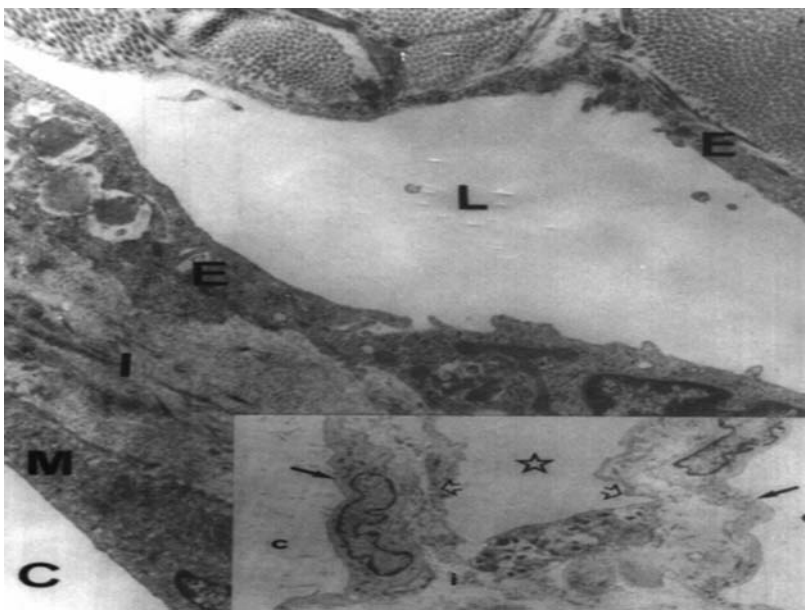

Fig. 5.40 Lymphatic lacuna of rabbit diaphragmatic peritoneum. The wide lacunar lumen (L) is surrounded by the lymphatic endothelium (E). Connective tissue (I) is interposed between the lacuna and the mesothelial cell layer (M) (C: abdominal cavity) (original magnification × 17,750).

Lower right inset. Lymphatic lacuna of rabbit mesentery. The open star shows the lacunar lumen surrounded by a thin endothelial layer (open arrows). Mesothelial cells (black arrows) are covering both aspects of the mesenteric peritoneal surface (i: interstitium. C: abdominal cavity) (original magnification × 4,750)

Capillary lymph that flows from the interstitium slowly moves downstream (average velocity for particles with diameter up to 5 μm = 1 μm/min) [303], drains into large collecting channels (40–200 μm diameter), and proceeds in the direction of the central venous circulation, propelled by peristaltic and rhythmic contractions of consecutive lymphangions [292, 303, 321, 326], with frequencies ranging between 4 and 12 contractions/minute [321, 326]. Within each lymphangion, hydrostatic pressure increases to a threshold of approximately 12 cm of water, after which the proximal valve is closed, and the downstream valve is opened. The cycle is repeated in the following segment. Contractility of lymphangions is modulated by a pacemaker site of spontaneous activity, apparently located, at least in bovine mesenteric lymphatics, in the vessel wall near the inlet valve of the unit. Activity propagates at a speed of 4 mm/s, and the ejection fraction was evaluated at 45–65% [327].

Contractions are generated by myogenic stimuli (hydrostatic pressure of 5–7 cm water) [327], and influenced by activation of α- and β-adrenoreceptors [328–330], histamine, leukotriene C4 and D4, platelet-activating factor [331, 332], PGF2 alpha, PGA2, PGB2 [333], bradykinin [334], and vasoactive intestinal peptide [335]. It should be noted that all the aforementioned vasoactive substances are mediators of inflammation present in high concentrations in blood and tissues during the localized or the generalized acute defense reaction [276].

Lymph flows from collectors to the thoracic duct and the right lymph duct, and finally drains into the subclavian veins. Lymphangions join larger collecting lymphatic vessels, forming a dichotomous tree that drains entire tissue regions. This arrangement has been described in the diaphragm as well as in mesentery [305, 325, 336].

Innervation of lymph vessels has been studied in the dog and cat mesentery, by means of silver stains [320]. It was shown that large lymphatic collectors have myelinated nerves that remain on the adventitial area, and nonmyelinated nerve fibers that penetrate into the region of valve attachment and are considered to be the motor supply to the smooth muscle. Bovine mesenteric lymphatics show adrenergic nerve fibers in the media, as well as in the adventitia. Human mesenteric lymph collector neurotransmitters are both adrenergic and cholinergic, the former being prevalent. Lymphatic capillaries are devoid of innervation [337].

Since Starling [338, 339], it has been accepted that, besides the removal of excess interstitial tissue, the lymphatic system has the special function of absorbing protein. Normally, blood capillaries leak protein, which will not re-enter the blood vessels unless delivered by the lymphatic system [340]. It is generally accepted that the rate of lymph formation is equal to the net capillary efflux under normal physiological conditions, in order for the interstitial fluid volume to remain constant [310]. However, the mechanisms involved in the formation of lymph, at the level of the most peripheral part of the lymphatic system, are still controversial. According to Allen and Vogt [341], who formulated the hydraulic theory, lymph formation is the end-result of hydraulic forces acting across initial lymphatics. Assuming that the interstitial hydrostatic pressure is zero, or even negative [159, 342], any rise will also increase the initial lymphatic flow, and edema will eventually develop if and when the lymphatic drainage capabilities are exceeded [343–345]. This concept of increased hydrostatic pressure as the main factor in the process of lymph formation was extrapolated to the lymphatic absorption from the peritoneal cavity [346, 347]. In this context it was postulated that, during peritoneal dialysis, the intra-abdominal pressures [348, 349] modulated lymphatic drainage from the abdominal cavity well within the range of values observed in dialyzed patients [166, 350]. This concept has been substantially challenged by a series of elegant studies performed by Flessner et al. [166, 351], who showed that a significant proportion of the intra-abdominal fluid is lost to the abdominal wall, the rate of which is also dependent on the intra-abdominal pressure. This fluid, after being incorporated to the tissues surrounding the abdominal cavity, will be drained through the lymphatic circulation [352]. The eventual influence of the intrathoracic negative pressure upon the lymphatic downstream circulation [353] may well be an additional component of the hydrostatic forces involved in lymph progression to the venous-blood compartment.

The osmotic theory of lymph formation [354] postulates the existence of a protein-concentrating mechanism at the level of the initial lymphatics, the main result of which would be that only 10–40% of the fluid initially entering within the lymphatic network would flow downstream, back to the blood compartment, and the remaining fluid would be filtered out from the lymphatics as a protein-free solution. This process would eventually cause a high protein concentration, and an oncotic gradient between the contents of the initial lymphatics and the surrounding interstitial fluid. Other investigators have proposed a vesicular theory of lymph formation, which holds that plasmalemmal vesicles provide the major route for transendothelial transport of protein, thereby creating the oncotic gradient needed for further fluid flow between adjacent cells or through transendothelial channels [355, 356]. This hypothesis is supported by recent studies that have shown active transendothelial transport of albumin in plasmalemmal vesicles [60, 357]. Figure 5.37 shows gold-labeled albumin transported by plasmalemmal vesicles of a mouse diaphragmatic lymphatic capillary.

On the other hand, it has been suggested that the postulated mechanisms may not necessarily be exclusive in the sense that some or all could function simultaneously. However, the relative influence of each one could vary in different areas of the initial lymphatic network [358].

The relevance of peritoneal lymphatics, as well as their impact upon ultrafiltration during peritoneal dialysis, is addressed in Chapter 6. Omental milky spots have, relatively recently, attracted the attention of investigators working in

the field of peritoneal dialysis. First described by Von Recklinghausen in pleura of rabbits [359], and later on in humans [360], these structures are part of the peritoneal lymphatic system [361]. Been described as submesothelial lymphoid structures essential for the maturation of resident peritoneal macrophages, they are actively involved in peritoneal defense reactions under a diversity of inflammatory conditions [362]. Macroscopically, milky spots appear as small (up to 1 mm diameter), white bodies, most commonly detected in perivascular areas of the greater omentum. Their structure, as seen under light microscopy, has been thoroughly reviewed by Di Paolo et al. [362, 363] in rats, rabbits as well as in patients on long-term peritoneal dialysis. In all the abovementioned species, they are located in the submesothelial tissue, showing blood capillaries surrounded by lymphocytes and macrophages and, at times, even lymphatic microvessels that can be identified within the frame of the same structure. The cell population of milky spots is made up by 400–600 cells, including macrophages (45–70%), lymphocytes (14–29%), and a low number of plasma cells (around 6%). Occasionally, megakariocytes and adipocytes can also be detected. Work done in experimental animals showed that number and size of milky spots, as well as their cell population, substantially increase after introduction of a peritoneal catheter, at the time of infection and inflammation, or after repeated exposure of the peritoneum to dialysis solutions containing 1.5 or 4.25% glucose [363]. Observations made in patients depicted changes not far from those seen in experimental animals, since both, size and cellularity of milky spots increased with the time-span of maintenance term peritoneal dialysis [363].

Peritoneal Innervation

The first report announcing the presence of nerves in the peritoneal interstitium was made by Haller in 1751 [364] and confirmed during the 19th century by Ranvier and Robin who, using osmic acid and silver nitrate, described nerve trunks, branches, and nerve endings accompanying arteries and veins. Robinson [1] described the peritoneum as being richly supplied with myelinated and nonmyelinated nerves (Fig. 5.41).

In rat mesentery, networks of adrenergic axons innervate the principal and small arteries and arterioles. Precapillary arterioles, collecting venules and small veins are not innervated, and are most likely under the influence of humoral vasoactive substances [365]. Lymphatic innervation was described in the previous section.

In 1741, Vater observed that the submesothelial connective tissue of cat mesentery contained oval corpuscles with a diameter of approximately 1–2 mm. In 1830, Paccini rediscovered and gave a systemic description of this corpuscle, known as the Vater–Paccini corpuscle [1]; it takes the form of a nonmyelinated nerve ending, which, in transverse section, appears as a sliced onion. In humans it has been observed in the peritoneum of mesentery and visceral ligaments, functioning as the main receptor for perception of pressure.

Fig. 5.41 Parietal peritoneum taken from a 67-year-old chronic uraemic patient on IPD, showing a transversal section of an unmyelinated nerve (star) (× 12,600).

Inset. Rabbit mesentery showing a myelinated nerve fiber (star: Schwann cell cytoplasma; arrow: myelin; A: axon) (original magnification × 47,400)

Cytology of the Peritoneal Fluid

The peritoneal fluid of laboratory animals has classically been a favored site for experiments dealing with the inflammatory response [366], as well as for those designed to analyse the biological reaction to infection [367].

More than 50 years ago, Josey and Webb realized that fluid shifts into and out of the peritoneal cavity could change the concentration of cells without affecting their absolute number [368–371]. The methodological answer to this question was given by Seeley and colleagues, who weighed peritoneal fluid and measured the cellular concentrations, and so were able to estimate the absolute number of cells [372]. Padawer and Gordon [370], after analyzing the cellular elements present in peritoneal fluid of eight different normal mammals, concluded that the most frequently observed cells were eosinophils, mast cells and mononuclears (including lymphocytic and macrophagic elements). Total cell numbers, as well as percentages of the different cells, varied greatly among the species examined. Neutrophils were never observed in normal animals. Total absolute counts were higher for females than for males, as well as for older animals compared with younger ones. In the individual animal, under normal conditions, the number of cells present within the abdominal cavity was constant [370].

Observation of peritoneal fluid obtained from healthy women showed that macrophages and mesothelial cells contributed more than 70% of the whole cell population, whereas lymphocytes and polymorphonuclears contributed to a lesser extent (18 and 7%, respectively) [373]. Other investigators observed that at the midphase of the menstrual cycle, macrophages, which comprised 82–98% of the peritoneal cells, showed morphological as well as biochemical heterogeneity and were seen to be involved in phagocytosis of erythrocytes [374] (Fig. 5.42). However, other studies showed up to four different types of cytological patterns in peritoneal fluid of women during the course of the menstrual cycle, in all of which mesothelial cells contributed substantially to the total cell counts. The paramenstrual type was in most cases hemorrhagic and highly cellular [375]. Ciliocytophtoria, anucleated remnants of ciliated mesothelial cells, can be occasionally observed in effluent dialysate, basically in young women. Inability to identify

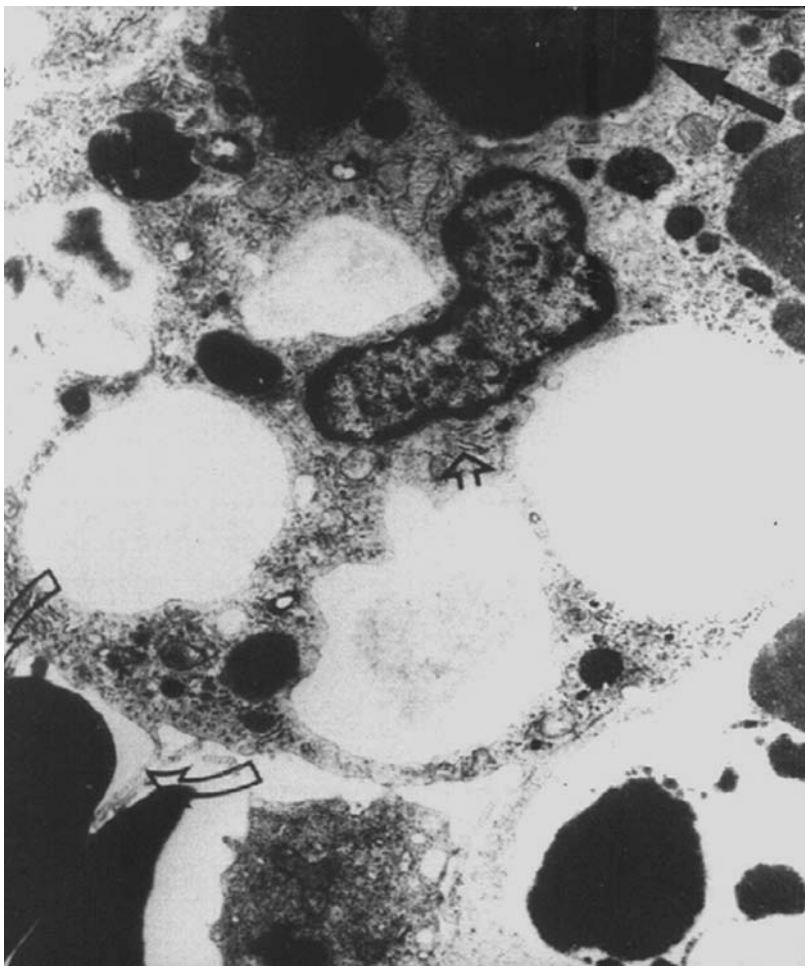

Fig. 5.42 Peritoneal effluent obtained from a chronic uraemic patient on peritoneal dialysis. The macrophages depicted in the figure show phagolysosomes digesting erythrocytes (black arrow). Note the presence of rough endoplasmic reticulum (short open arrow) near the nucleus (n). The former normally appears in macrophages when the cells are involved in phagocytic activity. The curved open arrows are pointing to cell processes engulfing red blood cells (× 8,600)

these structures can mislead the laboratory team as well as the physician to search for parasitic or fungal contamination [376].

The apparently puzzling effect of intraperitoneal saline inducing substantial influx of neutrophils into the abdominal cavity, which was observed long ago [367], was not confirmed when the experiments were carried out using sterile techniques. Bacterial lipopolysaccharides proved to be very effective in producing intraperitoneal exudate rich in cells [371]. This phenomenon was inhibited by prior intraperitoneal injection of cortisone [377].

In humans, sterile inflammatory effusions are characterized by a rich cellular content including neutrophils, lymphocytes, macrophages, mesothelial cells, eosinophils, and basophils, usually in that order of frequency [378]. The presence of macrophages, mesothelial cells, lymphocytes, eosinophils, and even plasma cells has been confirmed by electron microscope studies [379–381].

Peritoneal eosinophilia (eosinophils >10–50%) has been experimentally induced by intraperitoneal injection of iodine, chalk, nucleic acids, pilocarpine, hemoglobin or red blood cells, egg albumin, gold salts, mineral and vegetable oils, hydatidic fluid, and saline [378, 382]. On the other hand, intraperitoneal injection of bacteria and/or bacterial endotoxins induces a massive migration of neutrophils and monocytes into the peritoneal cavity [370, 383, 384].

The information presented above suggests that the cell content of effluent peritoneal dialysate is likely to be modified by so many factors that a concise description of a standardized cytological pattern becomes extremely difficult. There are, however, a few aspects of peritoneal effluent dialysate that have been defined: a) Patients on CAPD have total cell counts up to 50 cells/mL [383]. (b) The population of resident peritoneal cells observed in patients on long-term peritoneal dialysis is basically made up by macrophages (around 50% of the population), and lower

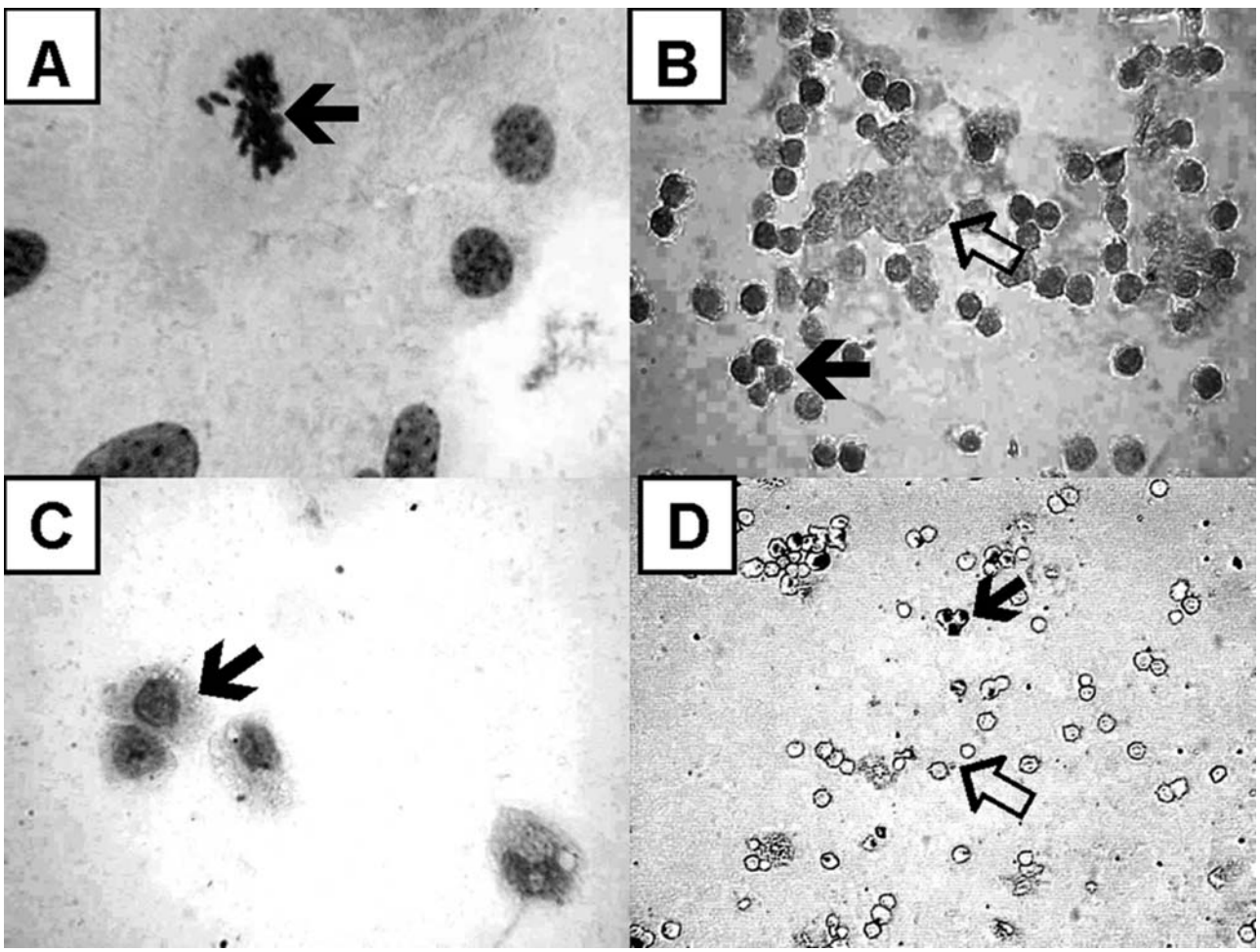

Fig. 5.43 Samples of the first dialysate effluent recovered from a new chronic uremic patient starting renal replacement therapy by means of PD. **(A)** Wandering mesothelial cell undergoing mitosis. (Black arrow: methaphase:). (Hematoxylin-eosin; × 1,000). **(B)** A high proportion of cells show positive immunostaining for PCNA (black arrow), indicating remarkable mitotic activity. (Open arrow: unstained free floating mesothelial cells). (PCNA immunostaining; × 400). **(C)** Occasionally, small groups of nonviable mesothelial cells can be detected (black arrow). (Trypan Blue staining; × 1,000). **(D)** Few mesothelial cells express β-galactosidase. (β-Galactosidase staining at pH 6; × 160)

prevalence of lymphocytes, mast cells, and mesothelial cells [385–388]. (c) During infection there is a substantial increase in total cell number [389], as well as in the proportion of neutrophils [385–388]. (d) Fluid eosinophilia is a basic component of the still ill-defined eosinophilic peritonitis [390–392].

Besides, the unphysiological situation of PD derives in substantial micro environmental changes that significantly affect the life cycle of the exposed and still attached monolayer. As a result, the population of cells recovered from dialysate effluent from a new patient is considerably different from that of patients on long-term PD. As shown in Fig. 5.43, cells detected in the first effluent of a new patient show remarkable mitotic activity (Figs 5.43a and 5.43b), a quite modest proportion of non viable cells (Fig. 5.43c) as well as a low prevalence of cells demonstrating positive expression to beta galactosidase, denoting the low prevalence of cells undergoing terminal replicative senescence (Fig. 5.43d). On the other hand, mesothelial cells isolated from effluent of patients on long-term PD (Fig. 5.44) show a quite different phenotype: they appear mostly as nonviable (Fig. 5.44a), the mitotic activity is nil (Fig. 5.44b), the vast majority are positively stained by beta galactosidase (Figs 5.44c and 5.45d), whereas a high proportion are undergoing apoptosis (Fig. 5.46). As it will be discussed later, this senescent phenotype of mesothelium was also detected in the monolayer of experimental animals exposed to high glucose concentration dialysis fluids. So, it may be hypothesized that careful and sequential observation of mesothelial cells recovered from patients' effluent, using the aforementioned staining technique, may well give quite representative information regarding the regenerative capabilities of the mesothelial monolayer still dressing the cavitary aspect of the peritoneal membrane of patients undergoing long-term PD.

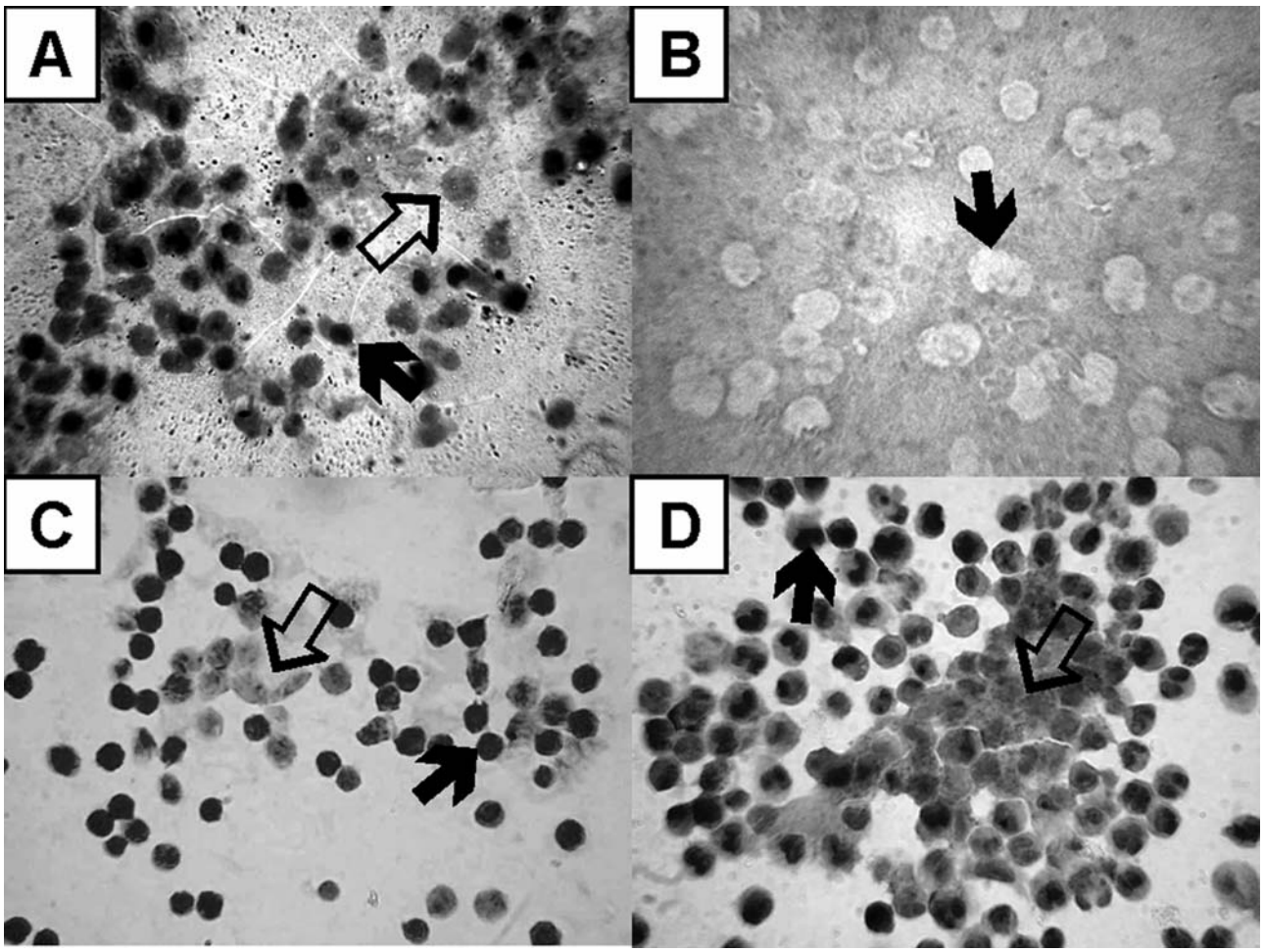

Fig. 5.44 Samples of fluid taken from effluent of a patient treated by means of CAPD for a period of seven months. **(A)** Most cells appear as nonviable, as indicated by positive staining with Trypan Blue (black arrow). (Open arrow: nonstained viable cells). (Trypan Blue; × 400). **(B)** There are no cells expressing PCNA positive immunostaining (black arrow), indicating that the mitotic activity is nil. (PCNA immunostaining; × 1,000). **(C)** Most cells show β-galactosidase expression (black arrow), pointing at the fact that they have reached a situation of terminal replicative senescence. (Open arrow: unstained cells). (β-Galactosidase expression at pH 6; × 400). **(D)** A substantial proportion of cells show P53 activity (black arrow), indicating that they are undergoing apoptosis. (Open arrow: unstained cells). (P53 immunostaining; × 400)

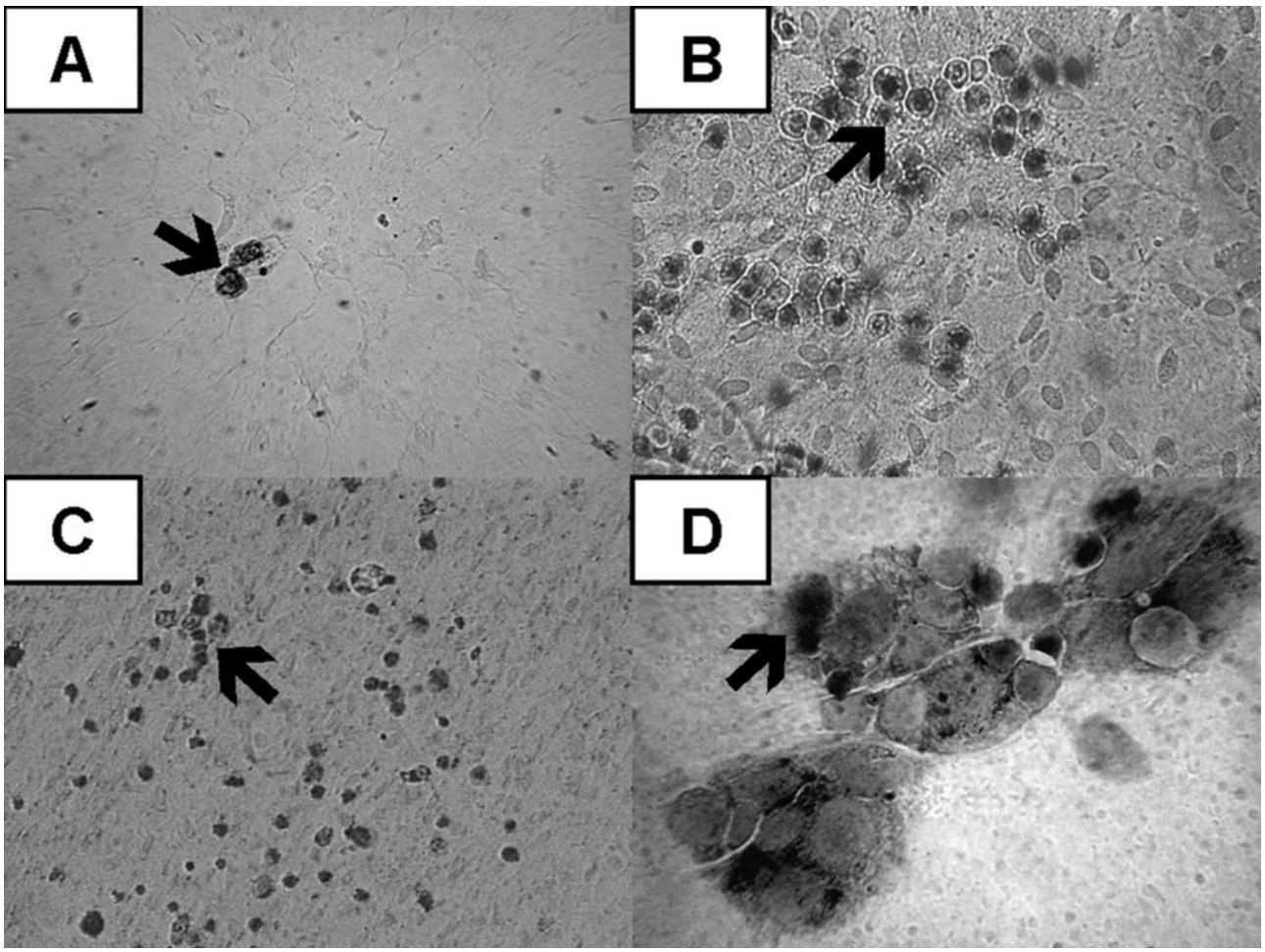

Fig. 5.45 (A) Sample of intact, unexposed mice mesothelium. Notice the low proportion of cells expressing β-galactosidase (arrow). (β-Galactosidase staining at pH 6; × 400). **(B)** Imprint recovered from a mouse after 30 days exposure to one daily intraperitoneal injection of 4.25% glucose, lactated dialysis solution. Arrow calls attention to the high prevalence of senescent cells, as indicated by positive staining to β-galactosidase. (β-Galactosidase staining at pH 6; × 400). **(C)** This imprint was recovered from a rat treated during 30 days with one daily intraperitoneal injection of 7.5% icodextrin. The prevalence of senescent cells is substantially higher than that detected in intact, unexposed animals. (β-Galactosidase staining at pH 6; × 160). **(D)** Mesothelial cells recovered from dialysate effluent of a patient on long term (7 months) peritoneal dialysis. Most cells express β-galactosidase activity. (β-Galactosidase staining at pH 6; × 1,000)

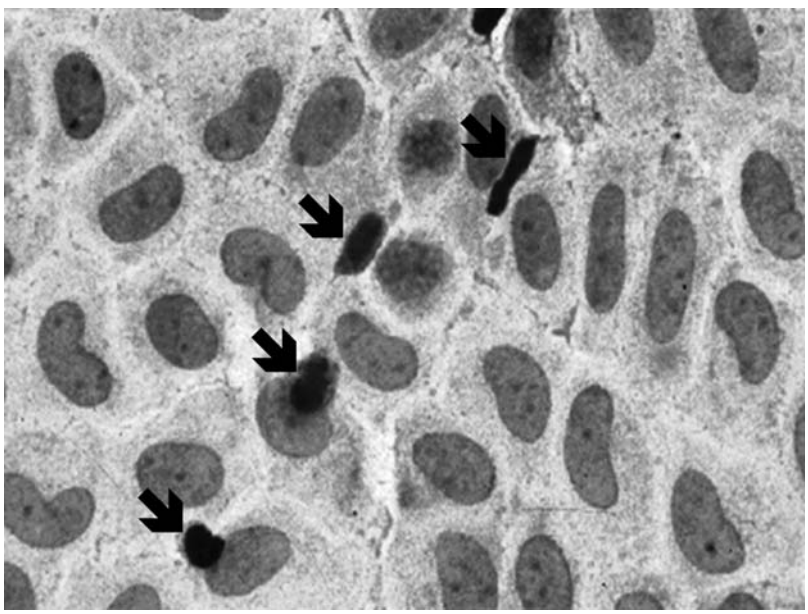

Fig. 5.46 Sample of a mesothelial imprint exfoliated from a rat after a 30 days exposure (one daily intraperitoneal injection) of 7.5% icodextrin dialysis solution. Notice the increased prevalenve of cells undergoing apoptosis (black arrow). (Hematoxylin-eosin; × 1,000)

Ultrastructure of Peritoneal Fluid Cells

Free-floating mesothelial cells are round or oval in shape and show a central, round nucleus (Fig. 5.47). Occasionally, binucleated mesothelial cells can be observed (Fig. 5.48). Nuclear chromatin is quite evenly distributed (Fig. 5.49, inset) and a small nucleolus may be observed. Numerous slender and sometimes branching microvilli emerge from the cytoplasmic membrane [379, 381, 393–395]. Branching microvilli, similar to those observed in human embryos [14], can be quite crowded in some cells, whereas in others they are scarce [381] (Fig. 5.49, inset). The glycocalyx covering the luminal aspect of the plasmalemma is endowed with electronegative fixed charges as shown in preparations exposed to the cationic tracer ruthenium red. Mitochondria, numerous cisternae of rough endoplasmic reticulum, and free ribosomes are mainly located in the outer part of the cytoplasm, and so are pinocytotic vesicles [379, 395]. The presence of intermediate-size filaments, perinuclear or irregularly scattered along the cytoplasm, has been documented in young free-floating mesothelial cells

Fig. 5.47 Effluent dialysate obtained from a non-infected uraemic patient, showing a floating mesothelial cell (star), as well as one macrophage. (*) (× 6,900)

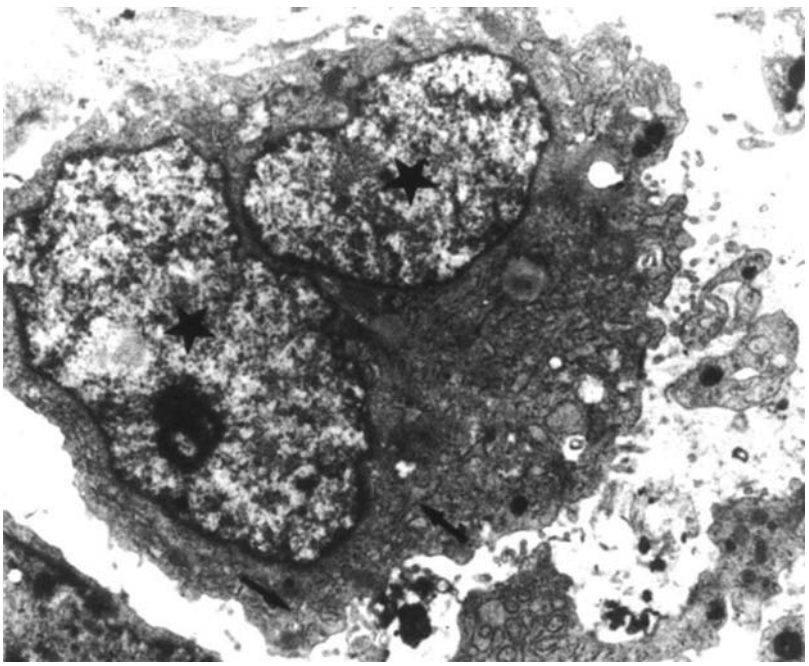

Fig. 5.48 Binucleated mesothelial cell observed in effluent fluid from a patient on CAPD. Note the abundance of rough endoplasmic reticulum (arrows) (stars: nuclei of mesothelial cell) (× 8,600)

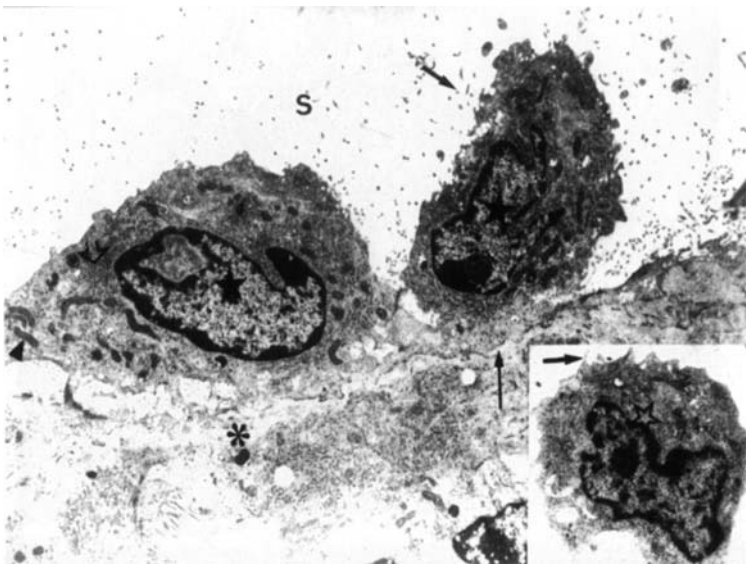

Fig. 5.49 Sample taken from the parietal peritoneum of a patient on CAPD. Two recently implanted young and active mesothelial cells (black stars), showing numerous mitochondria (arrowhead), rough endoplasmic reticulum (open arrow) and microvilli (short arrow). The cell on the right is forming its own basement membrane (long arrow) (*: submesothelial connective tissue; S: peritoneal space) (× 6,900).

Inset. Free-floating mesothelial cell (open star), seen in effluent dialysate of a CAPD patient (arrow: microvilli) (× 5,600)

[378, 380], as well as in those recently implanted on the peritoneal surface. These free-floating mesothelial cells should be distinguished from desquamated, degenerating mesothelial cells wandering in the peritoneal fluid (Fig. 5.48) [396].

Macrophages, which can be observed in large numbers, usually show an irregular and, at times, kidney-shaped nucleus with distorted masses of chromatin concentrated along the nuclear membrane (Figs. 5.42 and 5.47). The cytoplasmic outline of macrophages is irregular, with thin processes of variable length which, at times, engulf degenerated cells (Fig. 5.42) or take the form of signet-ring macrophages (Fig. 5.5, inset). Mitochondria, a small Golgi complex and phagolysosomes are more evident when the cell is involved in phagocytic activity (Fig. 5.42).

The ultrastructural aspect of inflammatory cells that eventually appear in the peritoneal fluid is similar to that classically described for other tissues.

The Origin of the New Mesothelial Cells

It has been experimentally shown that small and large mesothelial wounds heal at the same rate within 7–10 days after injury [397]. The basal, normally observed mitotic rate of mesothelial cells, as measured in the rat by ^{3}H-thymidine incorporation, ranges between 1 and 2% day (Fig. 5.50). This concept is supported by the fact that the steady state of the cell population is clearly defined by the following parameters: the proportion of cells passing through the G1 checkpoint, indicated by PCNA expression (proliferative cell nuclear antigen) that is also around 1–2%, as well as prevalence of non viable (Trypan Blue stained) senescent (positively stained with beta galactosidase at pH 6) (Fig. 5.45) and apoptotic mesothelial cells (Figs 5.46 and 5.51) that are within the same range [398, 399]. This rate of renewal is significantly increased during peritonitis, reaching maximal values of up to 19% between 1 and 3 days after injury, and returning to the basal activity on the 4th or 5th day [400]. It should be noted, however, that proliferations of fibroblasts, as well as mesothelial cell regeneration, are substantially inhibited in experimental uremic animals [400–402].

The origin of the new mesothelial cells repopulating denuded areas of injury is still controversial. Four different hypotheses have been proposed:

1. The repopulating cells originate from the bone marrow [102]. Other experimental studies showed, however, that whole-body irradiation sufficient to depress peripheral white blood cell count as well as cell replacement by the bone marrow did not prevent mesothelial healing [403]. Therefore, the existence of a circulating mesothelial precursor originating from the bone marrow seems unlikely.
2. Free-floating cells of the serosal cavity settle on the injured areas and gradually differentiate into new mesothelial cells [283, 404–406], (Fig. 5.49). Research done in order to settle this proposal, exposed evidence indicating that, after injury, free floating mesothelial cells, exfoliated from noninjured areas or from omental milky spots (12), settle on the injured areas, being instrumental to the healing of the monolayer [399, 407, 408]. Even though some investigators have not accepted this hypothesis [401, 406, 409], this approach finds support in other studies demonstrating the feasibility of mesothelial cells transplantation in humans, rabbits and rats as reported by several investigators [410, 411], as well as by our group (Fig. 5.52a).

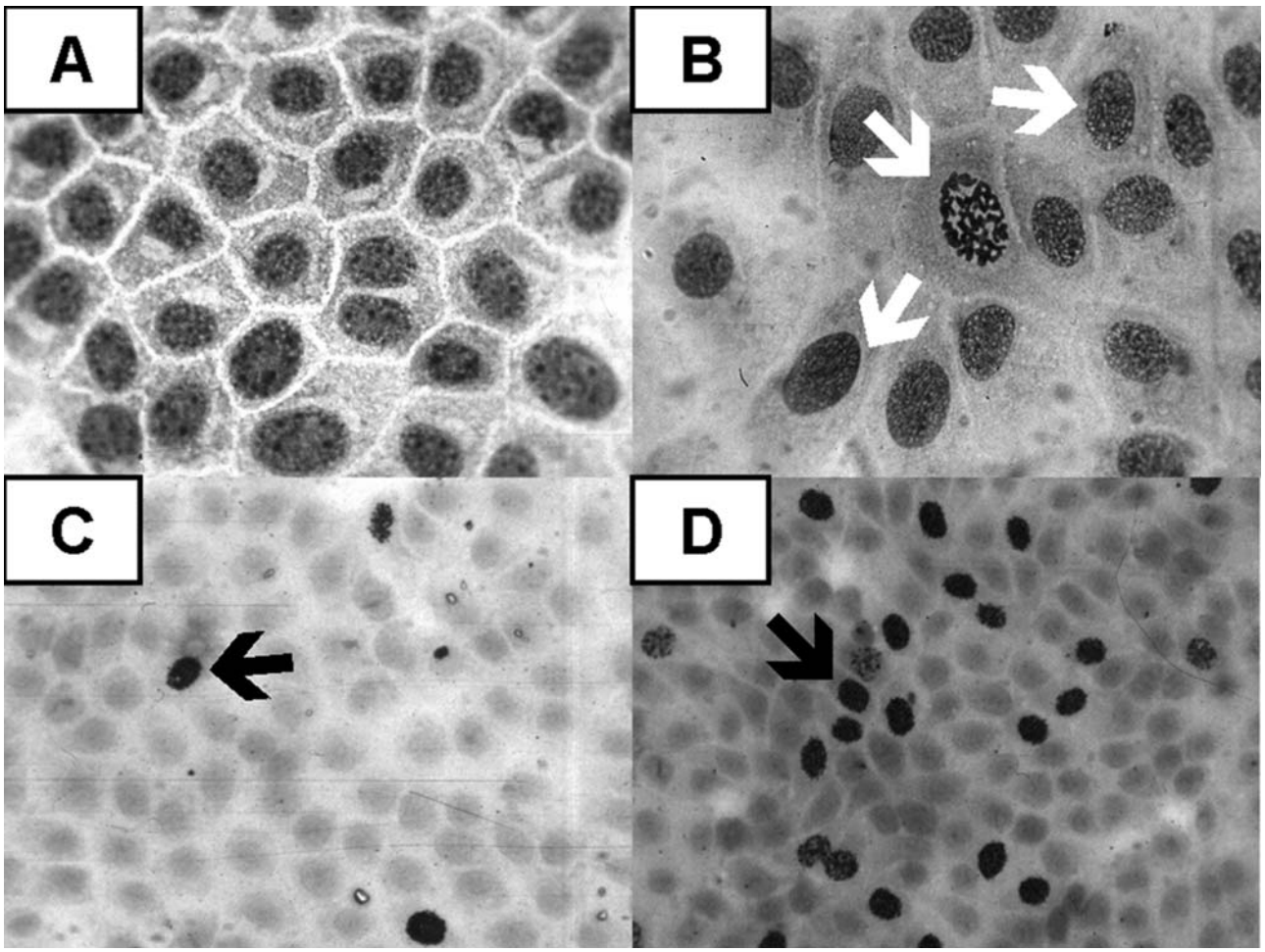

Fig. 5.50 **(A)** Intact unexposed mesothelium. Notice the normal density distribution of the cell population. (Hematoxylin-eosin; × 1,000). **(B)** Sample of the monolayer recovered from a mouse after a 2 h exposure to a 4.25% glucose, lactated dialysis solution. Notice the increased prevalence of cells undergoing mitosis (white arrows). Compare with precedent microphotograph. (Hematoxylin-eosin. × 1,000). **(C)** Again, intact unexposed mesothelium showing a few cells in S phase, incorporating tritriated thymidin (black arrows). (Autoradiography with tritriated thymidin and hematoxylin-eosin; × 400). **(D)** Imprint taken from a mouse after a 2 h exposure to the same high glucose concentration dialysis solution used in Inset B. Many cells are incorporating thymidin (black arrows), testifying for a remarkable acceleration of the cell cycle. In addition, this micro photograph, indicates that counts of cells in mitosis underestimate the mitotic activity, if compared with the information obtained by evaluation of cells incorporating thymidin. (Autoradiography with tritriated thymidin and hematoxylin-eosin; × 400)

3. Other studies [393, 401, 412] suggested the sequence of a two-stage process; during the first 24 h, macrophages forming the first line of defense [413] and coming from the peritoneal fluid, repopulate the wound surface (Fig. 5.5, inset). Later, during the second stage, new mesothelial cells, arising from metaplasia of mesenchymal precursors located in the interstitial tissue well below the site of injury, migrate to the surface and differentiate into mature mesothelial cells (Fig. 5.53). This hypothesis has not been universally accepted [25, 283, 399, 404, 414]. It has also been suggested that the early implanted macrophages are gradually transformed into mesothelial cells [414]. However, Raftery [415], after labeling peritoneal macrophages with polystyrene spheres, presented strong evidence against the hypothesis that peritoneal macrophages could be transformed into mesothelial cells.

   On the other hand, elongated, fish-like mesothelial cell precursors coming up from the submesothelial connective tissue were also observed under the damaged areas. The nuclear and cytoplasmic aspects of these cells were identical to that shown by new mesothelial cells already implanted on the peritoneal surface (Fig. 5.52b).
4. Mature mesothelial cells from adjacent areas migrate and proliferate to repopulate a depopulated area [407, 416]. This approach is supported by in vitro studies [417, 418] showing early migration and increased bromodeoxyuridine (BrdU) incorporation 24 h after injury, the latter showing values ranging between 20 and 26% of the observed cells. It should be noticed that these figures, representing the proportion of cells in S phase, imply an underestimation

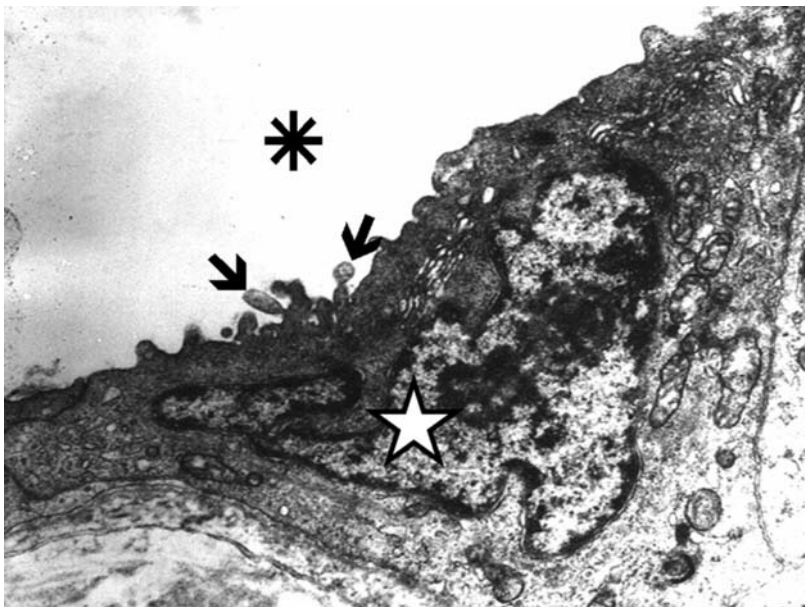

Fig. 5.51 Sample of parietal peritoneum taken from a patient undergoing peritoneal dialysis during a period of 16 months. Arrows point at areas of blebbing in the plasma membrane. Notice the absence of microvilli. Both elements define the situation of a cell at a relatively early stage of apoptosis. (Asterisk: peritoneal space; white arrow: nucleous of mesothelial cell; × 41,500).

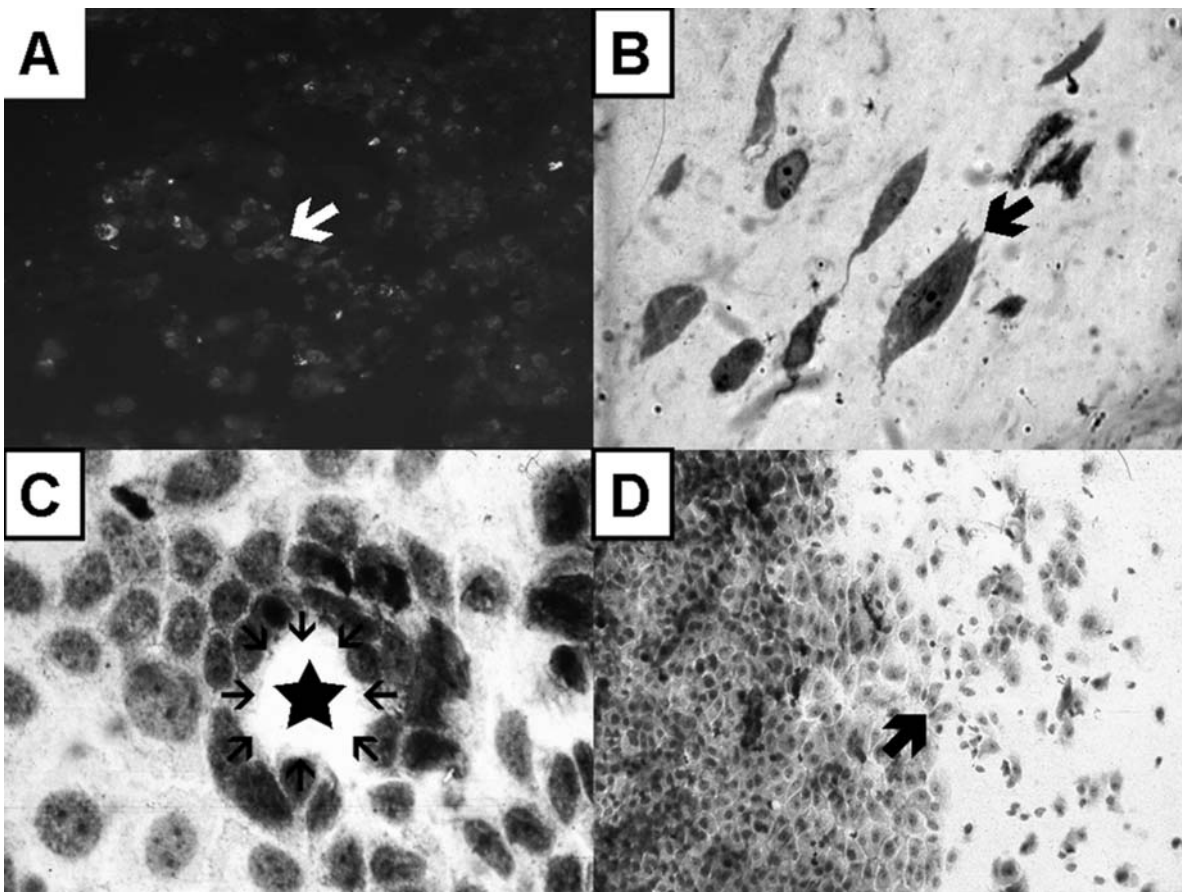

Fig. 5.52 (a) Imprint taken from a rat 24 h after autologous transplantation of mesothelial cells. White arrow points at cells already engrafted on the peritoneal surface. (PKH 26; × 400). **(b)** Peritoneal biopsy taken from a patient on peritoneal dialysis. Microphotograph shows elongated, fish like mesothelial cells migrating towards the cavitary aspect of the peritoneal membrane (arrow). (Toluidine blue; × 1,000). **(c)** Sample of the monolayer recovered 5 days after experimental, localized exfoliation of the mesothelial dressing. Young mesothelial cells that circumscribe an area of depopulated mesothelium (star), appear as moving centripetally in order to fill the gap in the monolayer. (Hematoxylin-eosin; × 1,000). **(d)** This imprint was taken from a rat 5 days after the experimental exfoliation. New mesothelial (arrow) redress the denude area through replication and centripetal migration. (Hematoxylin-eosin; × 160)

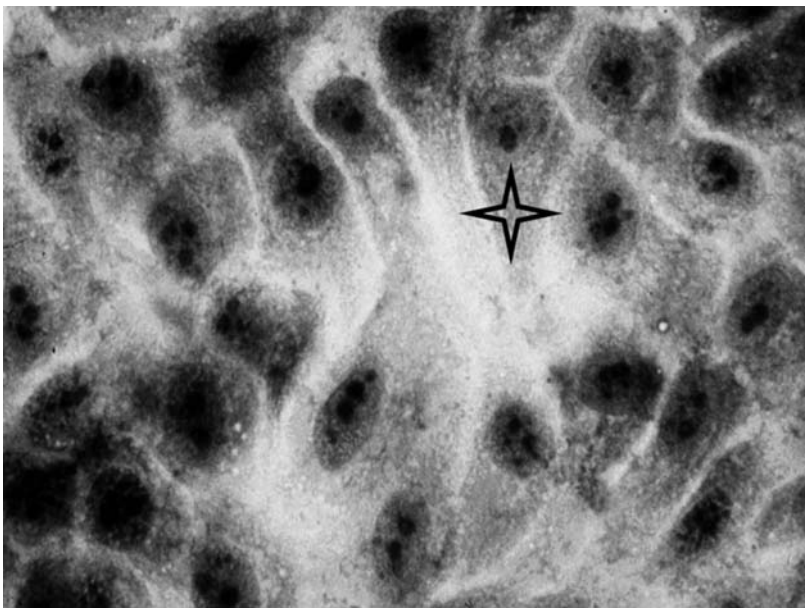

Fig. 5.53 Sample of mesothelium taken from a control animal, 10 days after the experimental exfoliation. Most of the peritoneal cavitary surface area has been repopulated. Yet, some elongated, fish like cells (four pointed star) are present, indicating that the regenerative process is still going on. (Hematoxylin-eosin. × 1,000)

of the actual number of cells undergoing mitosis. Indeed, the proportion of cells that passed the G1 checkpoint and supposed to reach S phase after some 10 h may well be similar, or even higher, than that observed during incorporation of BrdU. In addition, in vivo studies have been performed evaluating sequentially the dynamics of mesothelial repopulation, after a local mechanical exfoliation creating a doughnut-like area of undressed peritoneal surface [419]. This study demonstrated that repopulation also takes place by replication and centripetal migration of mature mesothelial cells located in in the monolayer bordering the injured area. (Figs 5.52c and 5.52d, Figs 5.53 and 5.54). Here again, the prevalence of cells undergoing mitosis is several times higher than that observed in intact, unexposed mesothelium.

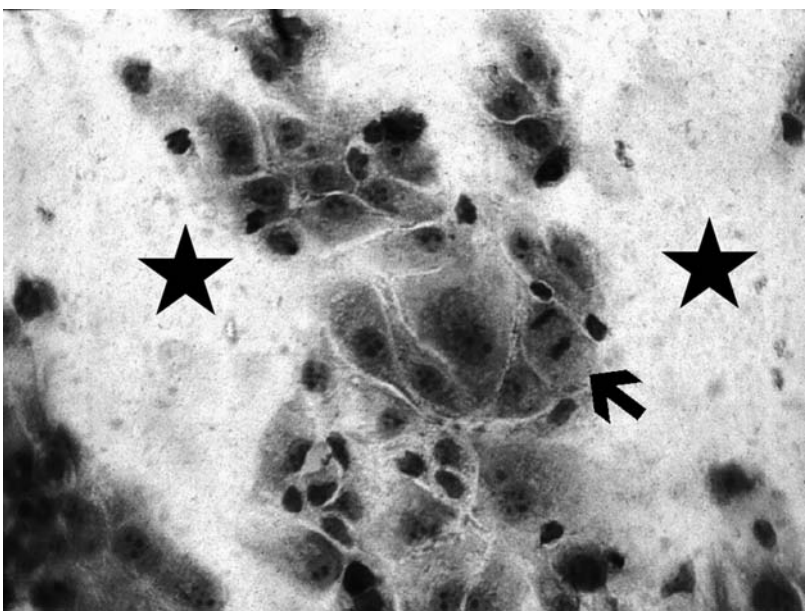

Fig. 5.54 Specimen obtained from a rat 2 days after experimental, localized, exfoliation of the monolayer. Mesothelial cells appear migrating, building up a bridge in order to repopulate undressed domains of the peritoneal cavitary surface of the liver (stars). Some cells are undergoing mitosis (arrow). (Hematoxylin-eosin; × 400)

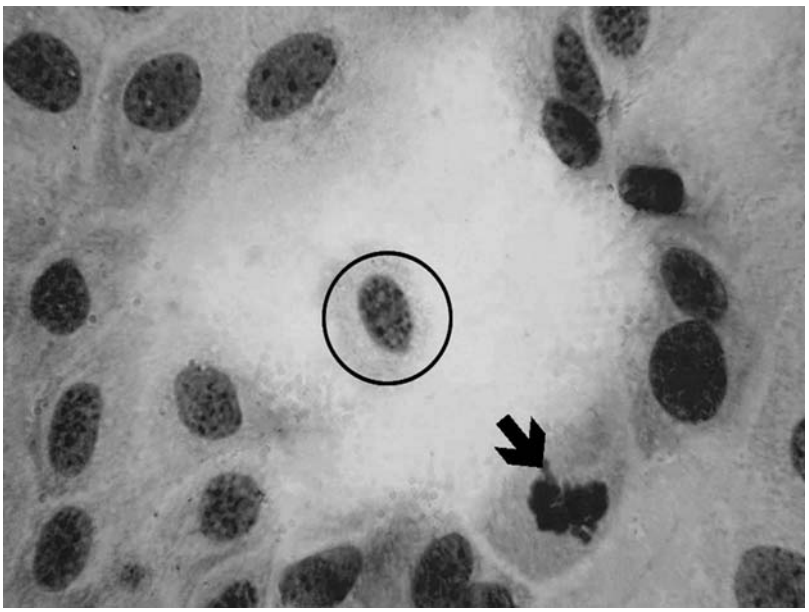

Fig. 5.55 Another sample of the monolayer recovered from a rat 5 days after the experimental exfoliation. One mesothelial cell is located in the middle of a depopulated area. (black circle), surrounded by young cells, one of them undergoing midosis (arrow). This image illustrates about the complexity of identifying the origin of new, repopulating cells. This specific cell could have reached the peritoneal surface migrating from the bordering area or from the submesothelial tisuue, or just be a free-floating mesothelial cell, recently implanted on the cavitary aspect of the peritoneum. (Hematoxylin-eosin; × 1,000)

All this evidence suggests that, most likely, mesothelial cell regeneration takes place through three different processes occurring simultaneously: implantation of young wandering mesothelial cells, migration of mesothelial cell precursors coming from the underlying connective tissue, and mitosis and migration of mature mesothelial cells bordering the injured area. The individual contribution of each mechanism cannot still be evaluated, as suggested by the presence of isolated new mesothelial cells repopulating denuded areas of the peritoneal surface (Fig. 5.55). These cells could eventually derive from by any of the already mentioned pathways of regeneration. According to studies done using the doughnut model of mesothelial regeneration, complete repopulation of the monolayer occurs after a recovery period of 15 days (Fig. 5.56).

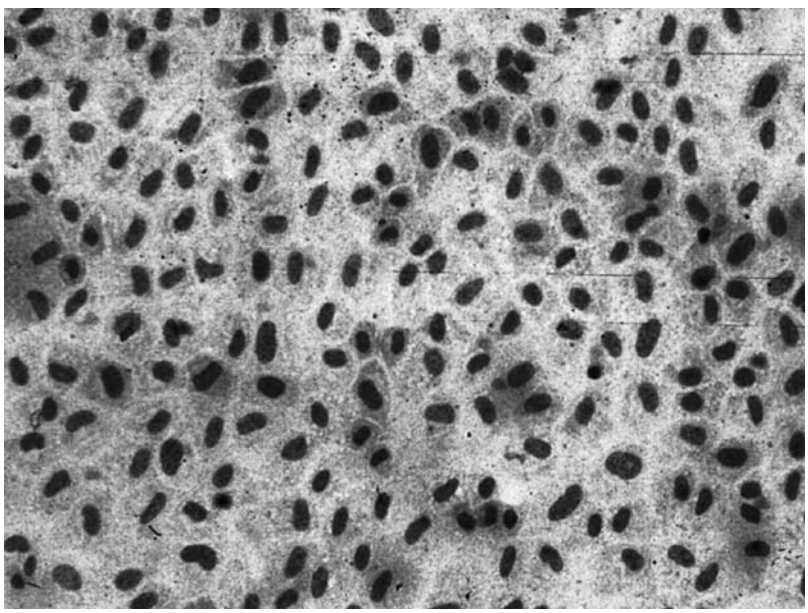

Fig. 5.56 Imprint recovered from a control rat, 15 days after performing a localized, doughnut shaped exfoliation of the monolayer dressing the anterior liver surface. The injured area appears completely repopulated. (Hematoxylin-eosin; × 400)

The Price of a Failing Regeneration

The normal density population of mesothelial cells dressing the cavitary aspect of the peritoneum is around 300,000/cm^2 in mice and rats [31, 420].

This number remains basically unchanged in the intact, unexposed animal, showing a minimal and non significant variability between samples of the same animal, as well as between those obtained from different mice or rats. This situation of no numerical change results from a continuous replacement of dying cells by means of cell replication. This mechanism has also been detected in peritoneal biopsies taken from human patients on long-term peritoneal dialysis [421], suggesting that the therapeutic procedure induced a situation of continuous mesothelial injury, coupled to an also continuous process of regeneration. This working hypothesis found support in the original observation of Di Paolo et al. [26] regarding the absence of mesothelial microvilli in peritoneal biopsies taken from patients on CAPD, later on identified as a sign of impending apoptosis [422] (Fig. 5.51).

A tight regulation of the rates of cell growth and cell death is critical for maintaining a normally populated monolayer. In this sense, a decreased rate of mesothelial cells growth, an increased proportion of dying cells, or both could eventually lead to a depopulated monolayer that, in turn, would result in repair by means of connective tissue [399, 423, 424], the thickness of which can be as high as 100 μ.

So far, during the situation of steady state, new mesothelial cells continuously replace the dying ones [425]. This steady state is broken when: a) the magnitude of cell injury overwhelms the regenerating capabilities of the monolayer; b) the cell cycle of the mesothelial cells is blocked or departs from its normal course; and c) both developments occurring simultaneously. When the balance between regeneration and injury is broken, proliferative mechanisms are required to relieve the structural alterations represented by a depopulated monolayer. This process of repopulation and regeneration is dependent on the presence of a resilient cell population that has retained the potential for proliferation and differentiation. Failure of this mechanism leads to repair by means of connective tissue, which, in turn, becomes the first step toward peritoneal fibrosis and sclerosis [425] (Fig. 5.57). At this point it is pertinent to remind that submesothelial peritoneal sclerosis is an extremely frequent complication of long term peritoneal dialysis. It has been detected in about one half of dialyzed patients during the first year on peritoneal dialysis [426], whereas its prevalence reaches an 80% level after only 2 years on the aforementioned technique of renal replacement therapy [427, 428]. Actually, a variable degree of diffuse peritoneal fibrosis has been documented in all patients who have been on long-term peritoneal dialysis [429]. And, in turn, this development paves the way to membrane failure [430], a situation in which, at least from the point of view of its dialytic capabilities, the peritoneum is no more peritoneum.

Mesothelial cells are extremely vulnerable to minor injury. Mild drying or wetting of rat cecal peritoneum for 5 min induced mesothelial cell degeneration and detachment, and severe interstitial edema [393, 394]. This fragility of the monolayer is somehow compensated by the remarkable regenerative capabilities mentioned before. Evidence of this property is brought to light by the almost complete repopulation of the mesothelium 15 days after its massive exfoliation resulting from exposure to a 0.125 mg% Trypsin solution during a period of 10 min [431] (Fig. 5.58). This enzyme is commonly used in order to harvest mesothelial cells from human omentum or from experimental animals [432].

However, as stated in the title of this section, exfoliation always demands a price. Meticulous observation of peritoneal biopsies showed, in the same animals, small domains were depopulation was repaired by connective tissue, launching at the local level the mechanisms involved in peritoneal sclerosis (Fig. 5.58). Recently published investigations have shown that new fibroblastic cells can develop from native mesothelial cells by a mechanism of epithelial-to-mesenchymal transition, launched by injury resulting from the use of poorly biocompatible dialysis solutions [433]. So far, these findings coincide with previously reported observations [420, 425] postulating that the mesothelial cell plays a key role in the preservation of the peritoneum as an effective dialysis membrane, as well as in its structural break down and final functional failure. In addition, it has been postulated that submesothelial myofibroblasts, actively involved in the reaction to the persistent tissue injury derived from exposure to PD solutions, take part in the inflammatory response leading to extracellular matrix accumulation and angiogenesis. Probably, these cells may also arise from mesothelial cells through epithelial to mesenchymal transition [433].

Peritoneal sclerosis goes along with a marked increase in the density of microvessels of neoformation. This phenomenon of neoangiogenesis has been detected in peritoneal biopsies of patients in long term peritoneal dialysis [433–436], as well as in rats after experimental induction of the fibrous reaction [431]. Those studies showed that the thicker the peritoneal tissue, the higher the number of vessels/surface area unit.

Besides, analysis of the microvascular alterations seen in humans on long-term peritoneal dialysis led Williams et al. [436] to systemize and define four sequential degrees of pathology, that go from presence of subendothelial hyaline material with thickness lower than 7 μm (degree 1); same changes but with thickness over 7 μm (degree 2); additional

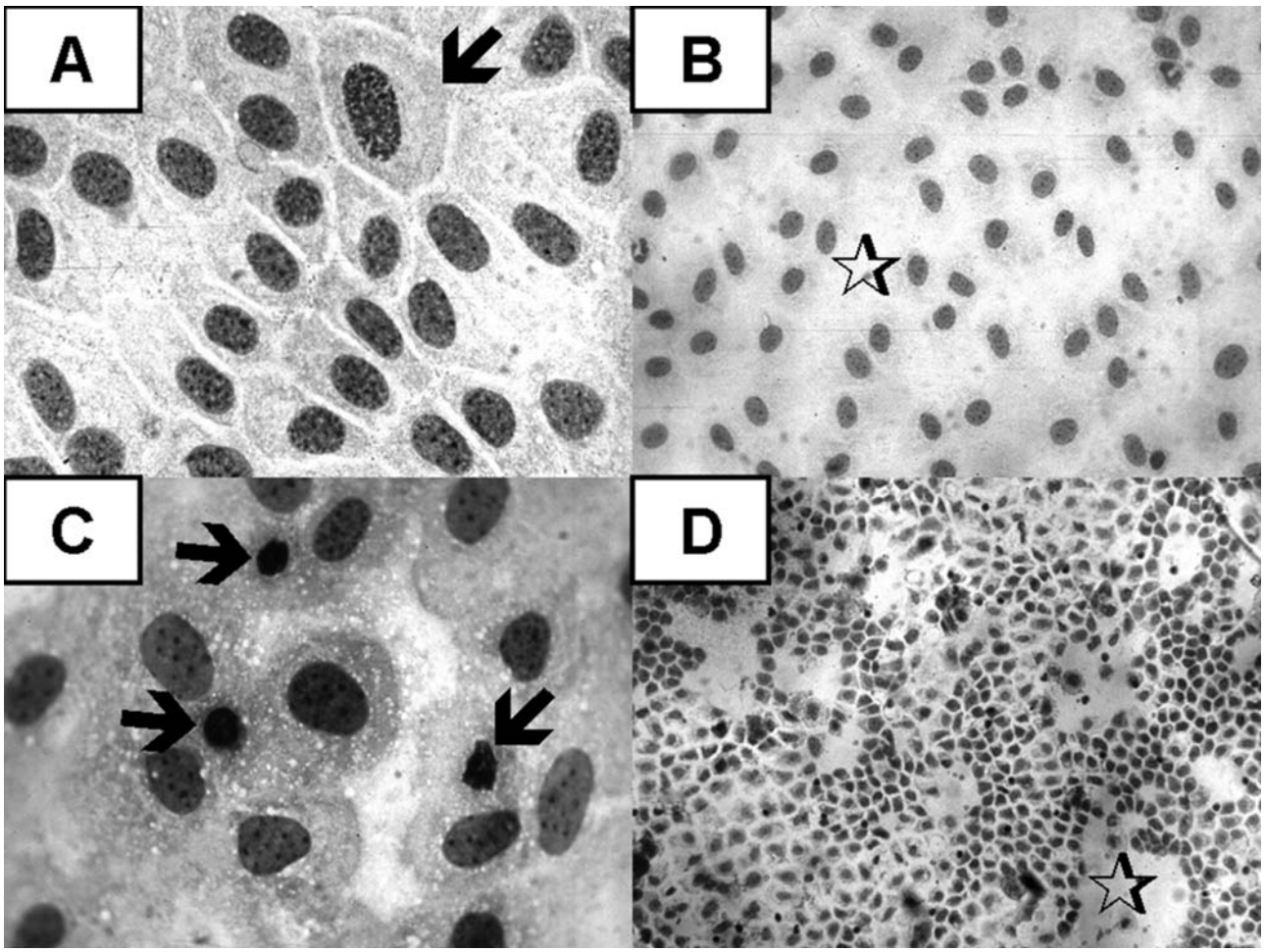

Fig. 5.57 **(a)** Mesothelial sample exfoliated from an intact, unexposed mouse. Arrow points at one cell in methaphase, (Hematoxylin-eosin; × 1,000). **(b)** Imprint obtained from a rat after being treated with one daily intraperitoneal injection of a 4.25% glucose, lactated dialysis solution. Open star denotes one of the many undressed domains of the liver surface. (Hematoxylin-eosin; × 400). **(c)** Same sample of Inset B at larger magnification. Notice the presence of unusual number of phagocytized apoptotic bodies (arrows). (Hematoxylin-eosin; ×1,000). **(d)** Specimen recovered from a rat treated during 30 days with one daily injection of 7.5% icodextrin dialysis fluid. Open star calls attention to the presence of large domains of undressed peritoneal liver surface. (Hematoxylin-eosin; × 160)

luminal distortion or narrowing (degree 3); and luminal obliteration (degree 4). It is interesting to remark that in this same study [436], 87% of patients treated with PD for periods of 6 years, exhibited clear signs of microvasculopathy, and that in 66% of them, changes reached degree 4. Therefore, two thirds of microvessels appeared closed. From this information it may be deduced that, in the long range, development of neovascularization does not automatically imply increase of blood flow. Indeed, having such a high proportion of occluded microvessels, not few areas of the peritoneal tissue become, with time, underperfused. This point should be taken into consideration in order to analyze the pathophysiology of permeability changes commonly detected in cases of membrane failure. This, in addition to the increased thickness of the peritoneal membrane that, per se, will substantially affect the transit time of solute's molecules between the still permeable capillaries and the peritoneal cavity.

All osmotic agents present in commercially available solutions for peritoneal dialysis share, regarding the long-term exposed monolayer, at least three basic effects: a substantial reduction of the cell population density of around 50%, a mitotic index near zero, and a significantly increased prevalence of nonviable cells [423].

This information suggested that the monolayer became depopulated under the influence of dialysis solutions (Figs. 5.59 and 5.60). But, going from bad to worse, the regenerative capabilities of the mesothelial cells still dressing the cavitary surface of the peritoneum appeared substantially reduced. In addition, the mechanisms leading to regeneration are substantially restrained, at least in experimental grounds, by the continuous exposure to the commonly used osmotic agents. This concept finds support in experimental observations done in rats using the "Doughnut" model of mesothelial regeneration in the rat [419]. After a ring of the monolayer was exfoliated, animals were exposed to either

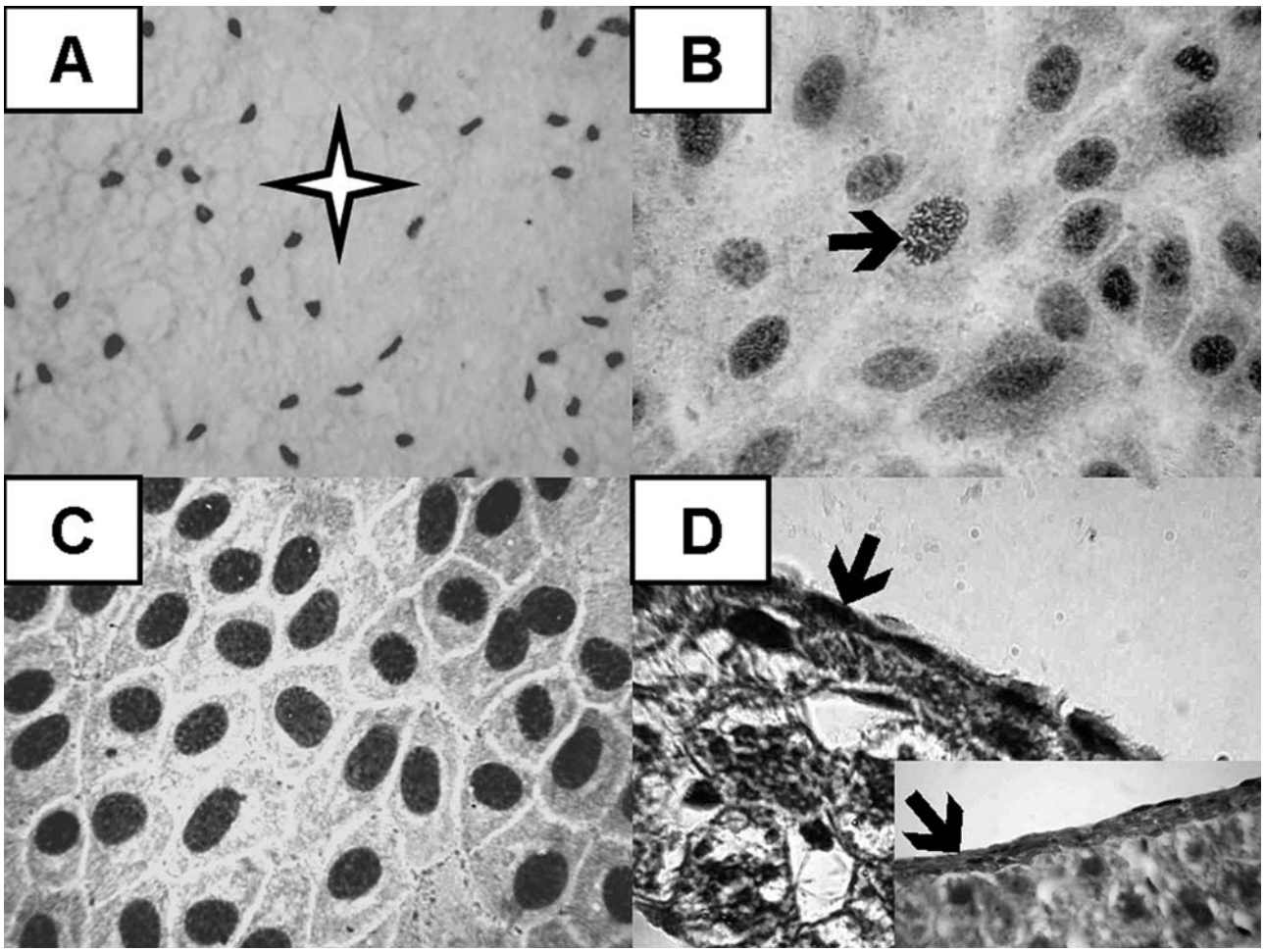

Fig. 5.58 **(a)** This sample was taken from a mouse after a 15-min exposure to 0.125% Trypsin solution. Notice the substantially decreased density of the cell population and the consequent presence of large depopulated areas (four-pointed star). (Hematoxylin-eosin; × 160). **(b)** Imprint exfoliated from a mouse 2 days after the 15-min exposure to the 0.125% Trypsin solution. Increased density as well as mitosis (arrow), point at the undergoing process of repopulation. (Hematoxylin-eosin; × 400). **(c)** Repopulated, normal monolayer seen after a recovery period of 30 days after the experimental intervention. (Hematoxylin-eosin; × 400). **(d)** Liver biopsy taken at the end of the 15-day recovery period. A normal monolayer is dressing the cavitary aspect of the liver surface (arrow). (Hematoxylin-eosin; × 400).

Inset. Other sector of the same biopsy showing that in spite of the repopulation, occasional areas of repair by means of fibrous tissue can be detected (arrow). (Hematoxilin–eosin; × 160)

4.25% glucose or 7.5 icodextrin dialysis solution for a period of 30 consecutive days. Macroscopic observation of the abdominal cavity at the end of the observation period showed that most animals developed scarring and fibrous adhesions at the level of the injured areas. Imprints and biopsies taken from the affected domains confirmed that not only repopulation failed, but that the missing mesothelial dressing was replaced by a thick layer of fibrous tissue, containing numerous microvessels of neoformation (Fig. 5.61). Consequently, these observations support the contention that both osmotic agents, 4.25% glucose and 7.5 icodextrin, substantially restrain the normal process of mesothelial repopulation expected to take place during and after the experimental exfoliation. This development launched the repair mechanisms leading to peritoneal sclerosis.

Several studies have shown evidence indicating that different cell types exposed to hydrogen peroxide display a reduced rate of proliferation, premature senescence, and, consequently, higher prevalence of apoptosis [437]. Within this context, additional experiments exposed to view the existence of a dose-related effect. Indeed, low levels of oxidants potentiate growth signals and enhance proliferation as long as the specific cell type can initiate new rounds of mitosis (Fig. 5.50), whereas higher concentrations of oxidants can block cell proliferation, which, in turn, derives in premature senescence and the consequent activation of the mechanisms leading to apoptotic cell death [438] (Figs. 5.45 and 5.46).

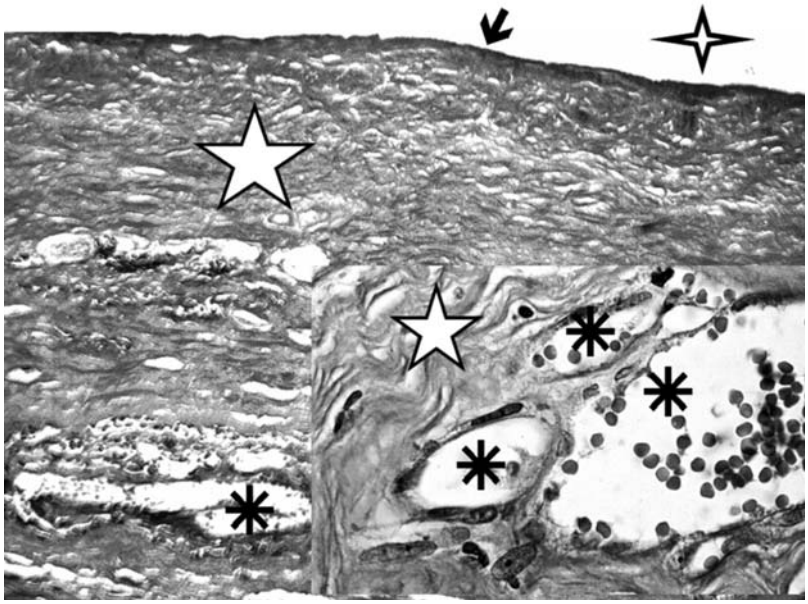

Fig. 5.59 Biopsy of parietal peritoneum taken from a patient with total membrane failure developed after being treated with CAPD for a period of 44 months. Notice the absence of mesothelial dressing (Arrow) on the peritoneal surface facing the abdominal cavity (four-pointed star). A thick layer of fibrous tissue (white star) replaced the missing monolayer. These images define the the situation of peritoneal sclerosis. (Asterisk: venule of neoformation). (Masson × 160).

Inset: Other section of the same biopsy showing a group of microvessels (asterisks) indicating the magnitude of neovascularization. (White star: fibrous tissue). (Masson × 400)

Higher degrees of oxidative injury lead to cell death by nonphysiological, necrotic pathways that, in turn, put in motion the local inflammatory reaction derived from extravasation of the cytoplasmic contents into the interstitial tissue [439] (Fig. 5.62). Both glucose-enriched solutions and icodextrin have the intrinsic capabilities of inducing different degrees of oxidative stress upon the exposed mesothelium. Glucose acts through products derived from its nonenzymatic degradation [440] and the irreversible formation of AGE products [441] by glucose autoxidation [442] and/or by oxidative mitochondrial DNA damage [443]. Icodextrin, in turn, induces substantial lipid peroxidation of mesothelial cell's membrane almost immediately after being infused into the abdominal cavity [444, 445].

This injury derives, at least in part, from the intra-abdominal formation of carbonyl compounds during the dwell time [446]. This phenomenon of carbonyl compounds liberation during the dwell time has been shown by the same group of investigators, using amino acid–based dialysis solutions.

Development of oxidative injury is facilitated by the demonstrated capability of mesothelial cells in culture to generate hydrogen peroxide [447]. This interpretation of the above-mentioned chain of events has been substantiated by a recent study, showing that acute and severe in vivo oxidative stress applied to the mesothelial monolayer results in

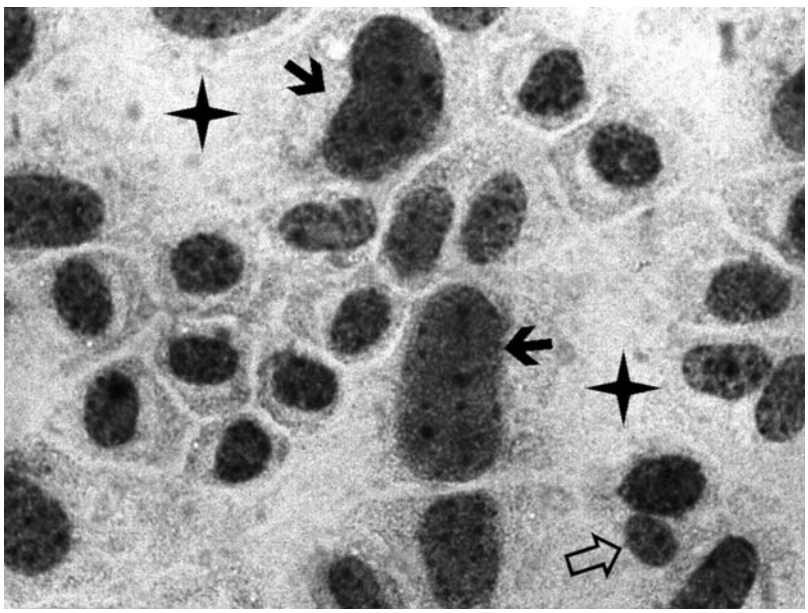

Fig. 5.60 Imprint of the mesothelial monolayer recovered from a mouse after being injected once a day, during 30 consecutive days with a 1.1% Aminoacids solution for peritoneal dialysis. Density of the mesothelium looks reduced as shown by the presence of depopulated areas (four-pointed stars). Black arrows indicate large, senescent cells. (Open arrow: Binucleated mesothelial cell with one micronucleus, the presence of which is suggestive of DNA damage). (Hematoxylin -eosin; × 1,000).

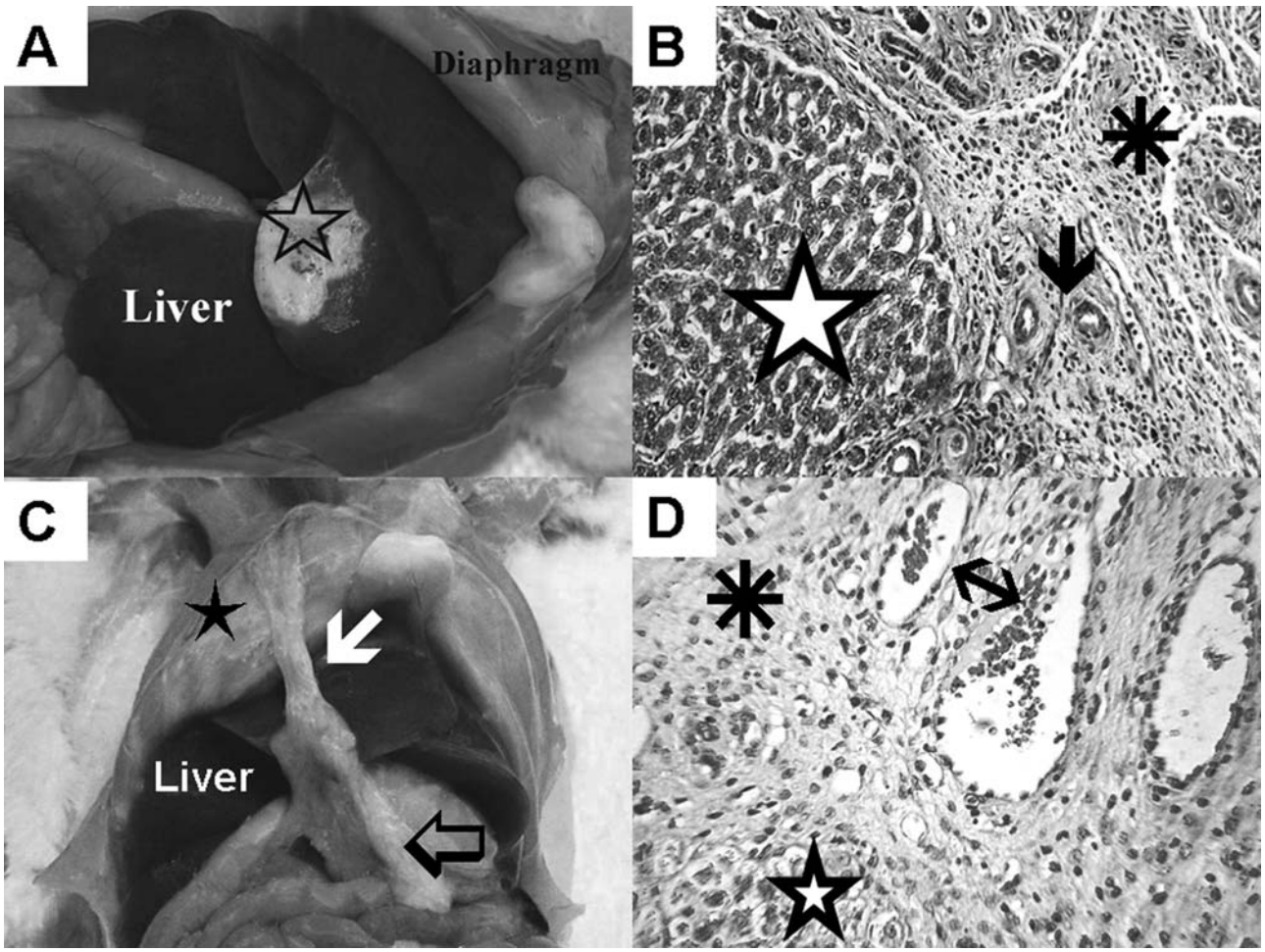

Fig. 5.61 **(A)** Photograph taken 15 days after focal exfoliation of an 8-mm diameter, doughnut-shaped area of mesothelium. The intervention was performed on the anterior liver surface of a rat that, after the procedure, was treated with one daily intraperitoneal injection of a 4.25% glucose, lactated dialysis solution. A failing repopulation derived in fibrous scarring of the exfoliated area (open star). **(B)** Sample of the liver taken from the same rat showing a thick layer of fibrous tissue (asterisk) that replaced the absent mesothelial dressing. (White star: liver tissue; black arrow: microvessels of neoformation). (Hematoxylin-eosin; × 160). **(C)** Open abdominal cavity of a rat that, after creation of a doughnut-like local exfoliation on the anterior liver surface, received one daily intraperitoneal injection of 7.5% icodextrin dialysis fluid, during 15 consecutive days. Notice the fibrous adhesion (white arrow) between an intestinal loop (open arrow), the experimentally injured liver surface and the diaphragm (black star). **(D)** This specimen belongs to the same rat of Inset C. A dense layer of fibrous tissue (asterisk) appears covering the subjacent liver tissue (five-pointed star). Double arrow points at two venules of neoformation. (Hematoxylin-eosin; × 160)

extensive fibrosis, adhesions, and permeability changes similar to those observed in clinical ultrafiltration failure [448] (Fig. 5.63).

Peritoneal sclerosis has been induced in rodents by in vivo exposing the membrane to a variety of experimental interventions: asbestos [449], 0.1% chlorexidine [450], iron dextran [451], glucose degradation products [452], AGE deposits derived from uremia per se [453], sodium hypochlorite [454], lipopolysaccharide [455], low pH of around 3.8 [456], pure water combining low pH and hypo-osmolarity [457], silica [458], and zymosan [459].

It should be noticed at this point of the analysis that, with a few exceptions (pure water, chloroxidine, and low pH), the other substances quoted as used to experimentally induce peritoneal sclerosis operate setting out different degrees of oxidative stress [460–471]. So far, after evaluating the aforementioned offered evidence, it may be concluded that addition of antioxidant agents to the currently used peritoneal dialysis solutions seems to be a quite rational and wanted development [472, 473].

We cannot complete this review without mentioning the enigmatic problem of sclerosing encapsulating peritonitis (SEP), currently also named encapsulating peritoneal sclerosis (EPS). This fearful syndrome leads to a situation in

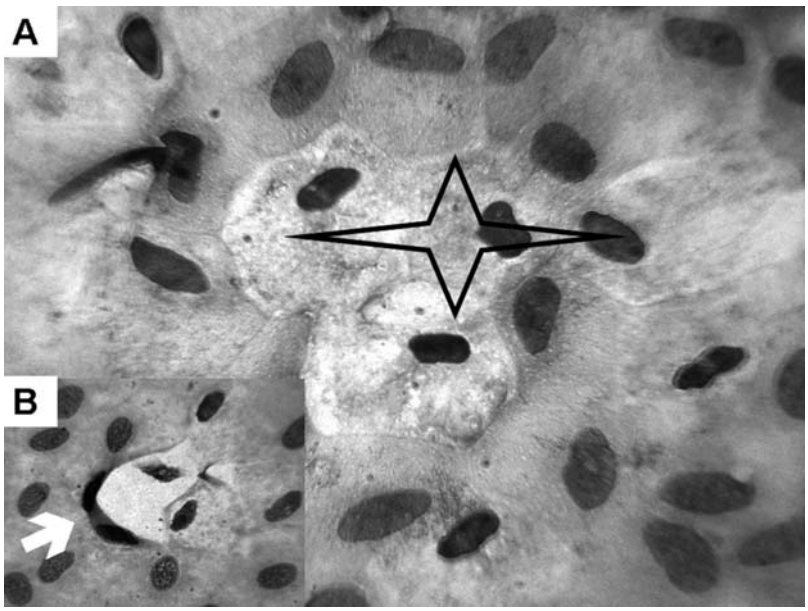

Fig. 5.62 **(A)** Imprint recovered from a rat 10 min after acute oxidative injury. Group of mesothelial cells undergoing picnotic changes (4 points star). (Hematoxylin-eosin; × 1,000). **(B)** Other aspect of the same specimen showing picnotic mesothelial cells exfoliating from the peritoneum dressing the anterior liver surface. (Hematoxylin-eosin; × 160)

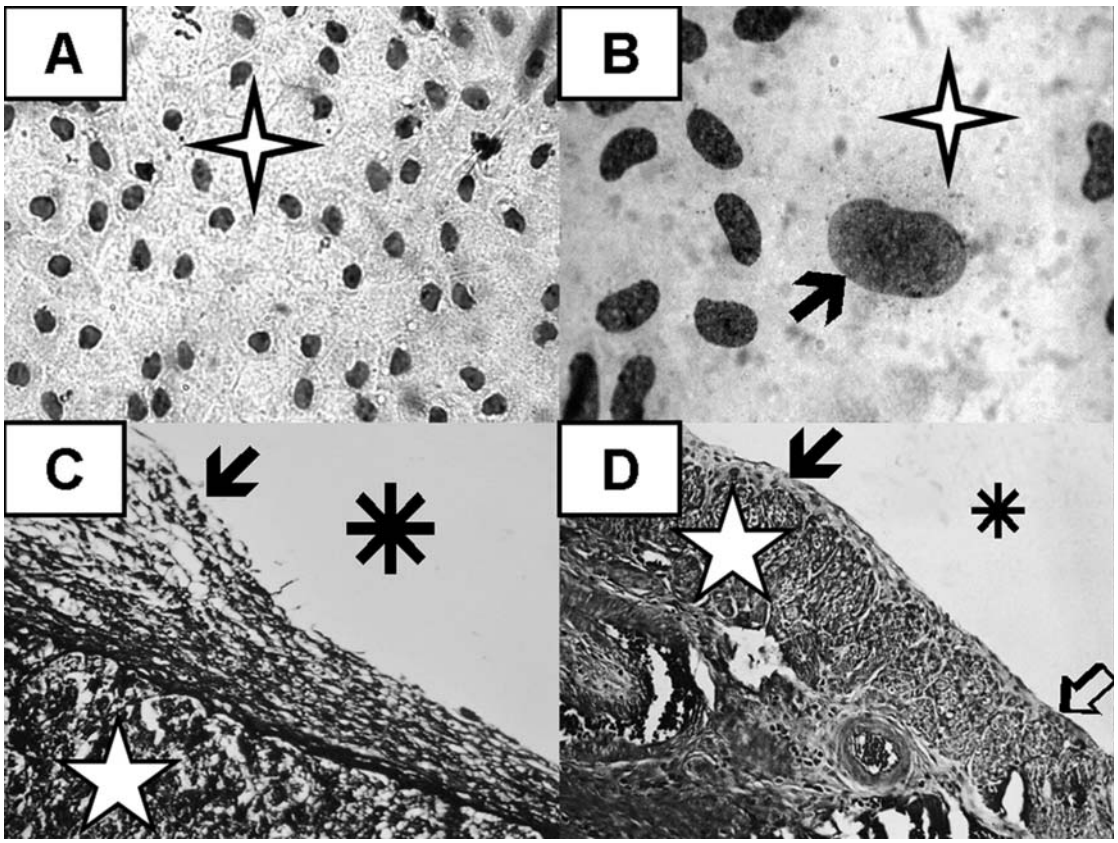

Fig. 5.63 **(A)** Imprint taken from the liver surface 10 min after experimental exfoliation by means of 5 mM/L deoxycholate solution. It is evident that most of the peritoneal surface is devoid of the normally seen mesothelial dressing (open star). (Hematoxylin-eosin; × 160). **(B)** After a recovery period of 15 days, mesothelial cells are still absent in large domains of the peritoneal surface (open star), suggesting that fibrous repair took place, instead of regeneration of the monolayer. Arrow points at a large senescent mesothelial cell. **(c)** Sample of a liver biopsy obtained from a rat, 15 days after the experimental intervention using deoxycholate. A thick layer (arrow) of fibrous tissue replaced the missing mesothelial monolayer. (Asterisk: peritoneal cavity; white star: liver tissue). (Hematoxylin-eosin; × 400). **(d)** Section of small intestine recovered from the same rat mentioned in Inset C. Some areas of the intestinal wall are covered by a wide coat of fibrous tissue (black arrow), whereas neighboring domains show a normal mesothelial dressing (open arrow). (Asterisk: peritoneal cavity; five-pointed white star: intestinal wall). (Hematoxylin-eosin; × 160)

which a thickened, fibrous sheet of tissue envelops the small intestine [474–477], liver, and stomach, as well as pelvic organs. This complication covers a wide range of morphological alterations starting from peritoneal opacification, passing through the tanned peritoneum syndrome, and finally reaching replacement of the serosal layer by fibrous tissue. Fibrous bands may be present compromising mesentery, gallbladder, spleen, liver, and stomach, as well as pelvic organs and even the cavitary aspect of the peritoneal tissue. The most affected areas configure, at times, a mass of fibrous tissue packaging abdominal viscera, conforming the cocoon that usually includes loops of small intestine as well as pockets of encapsulated ascites. Light microscopy reveals serosal fibrosis and total absence of the mesothelial monolayer, replaced by a thick layer of connective fibrous tissue, the thickness of which can reach 4 cm [478, 479] (Fig. 5.64). Neovascularization is also seen, even though these blood vessels show major structural alterations: sclerosis of the whole vascular wall, at times occlusion of the lumen, and even hyaline changes of the blocked microvessels (Fig. 5.65). Peritoneal calcifications and formation of bone and even bone marrow have been detected. All this may be combined with wide areas of inflammatory infiltrates [480, 481].

Changes detected in patients with SEP/EPS appear far away from those described in the commonly observed peritoneal sclerosis. Besides, its prevalence in patients on peritoneal dialysis is, fortunately, extremely low, whereas the impact of each condition is absolutely different. SEP/EPS carries a quite poor prognosis, with a mortality rate ranging between 26 and 93% [480], whereas simple peritoneal sclerosis basically leads patients to switch to other ways of renal replacement therapy, usually hemodialysis. These differences support the concept postulated by Di Paolo and Garosi [478, 479], who concluded that both conditions represent different nosological entities. In patients on peritoneal dialysis, the origin of this complication is still ill-defined. Many possible factors have been invoked (acetate, hyperosmolarity, recurrent peritonitis, glucose, antiseptics, intraperitoneal antibiotics, bacterial endotoxins), even though there is no available evidence clearly demonstrating specific relevance for any of them [474, 482]. Besides, at least one case has been reported on a chronic uremic patient having renal replacement therapy by means of only hemodialysis [483].

It should be noticed that sclerosing peritonitis has been reported in not few clinical situations unrelated to both, chronic uremia and peritoneal dialysis as: idiopathic [484, 485], associated with the use of some β-blockers such as practolol [486], propranolol [487], or timolol [488], as well as to metoprolol [489], oxprenolol [490], and intraperitoneally administered antibiotics such as tetracycline [491]. Besides, the literature mentions cases of sclerosing peritonitis associated to intra-abdominal tumors like gastric carcinoma, carcinoma of pancreas, familial polyposis of colon, renal carcinoma, lymphoma, ovarian teratoma or thecoma, and even in patients affected by liver cirrhosis as well as after liver transplantation [492–502]. So far, our understanding of SEP/EPS is still blurred as a result of the complexity of the problem, and namely, by its multiple ethiopathogenesis.

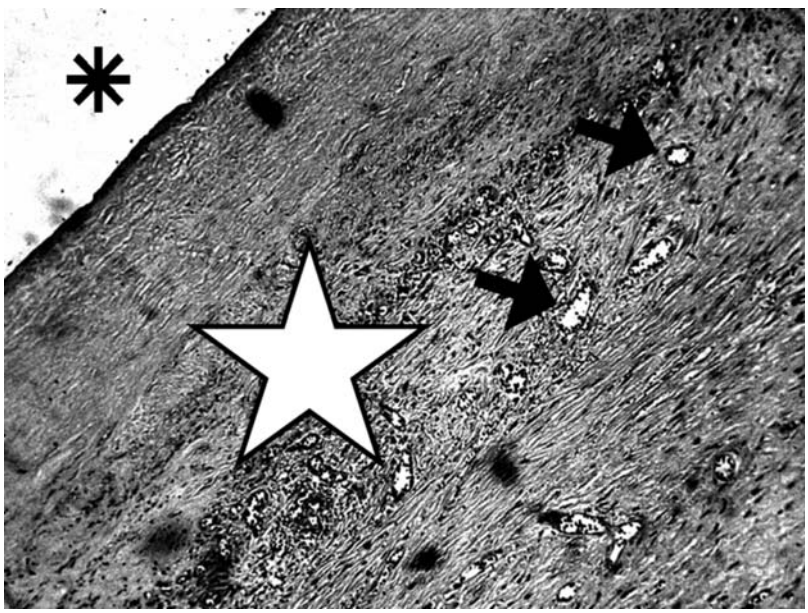

Fig. 5.64 Biopsy of parietal peritoneum recovered from a patient with sclerosing peritonitis. A thick layer of around 2,500 microns (white star) is covering the peritoneal surface. (Asterisk: peritoneal space; arrows: blood vessels of neoformation). (Hematoxylin-eosin; × 100)

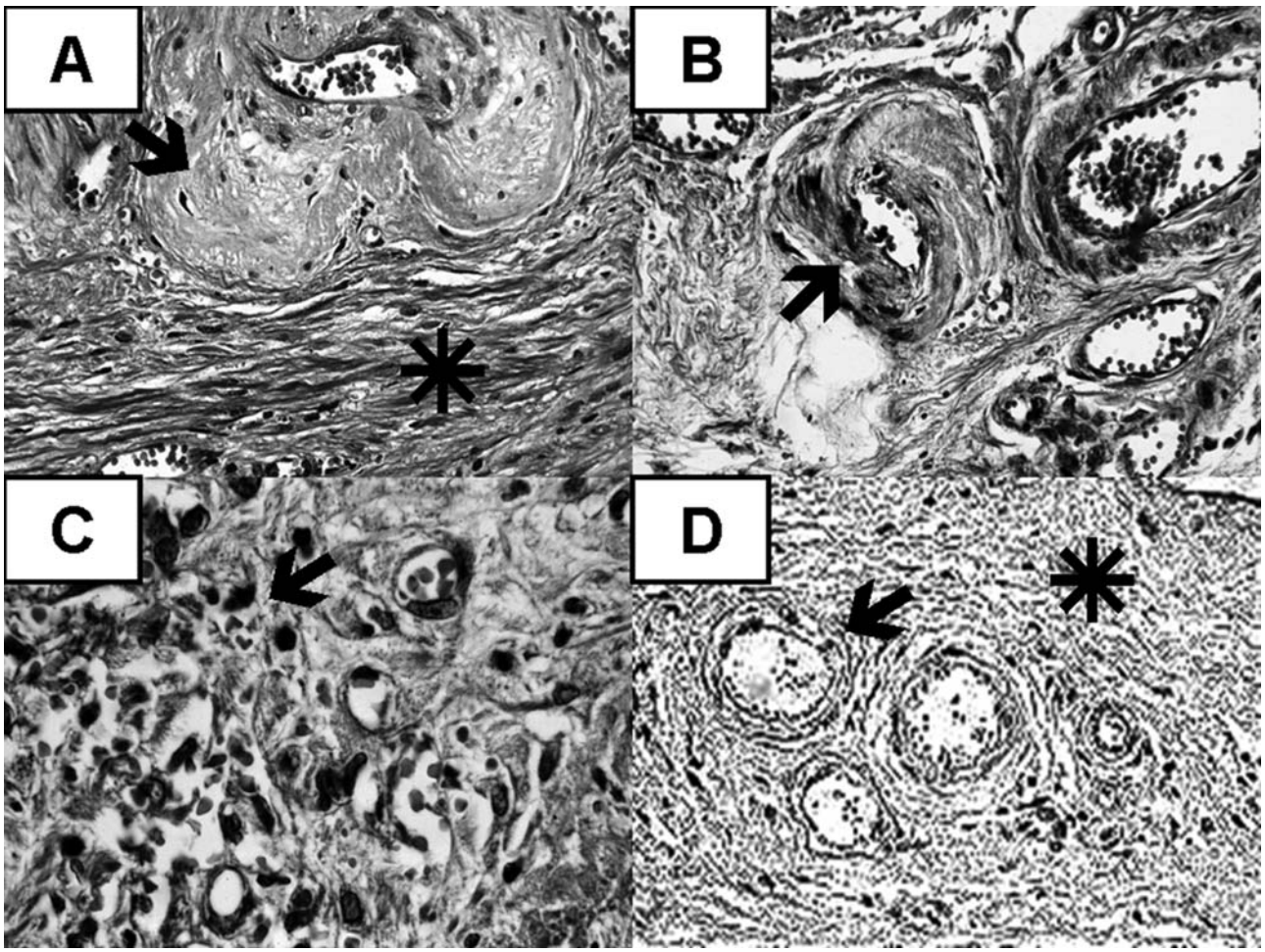

Fig. 5.65 **(A)** Dense hyaline deposits (arrow) located in the thickened wall of an almost obstructed blood vessel of neoformation, embedded in a mass of fibrous tissue (asterisk). (Masson; × 160). **(B)** Microvessels of neoformation showing thickened sclerotic wall (arrow). (Masson; × 160). **(C)** Mononuclear cells (black arrow) infiltrating the fibrous tissue surrounding blood vessels of neoformation (open arrow). (Masson; × 400). **(D)** Perivascular fibrosis in blood vessels (arrow) embedded into a densely packed interstitial mass of fibrous tissue. (Hematoxylin-eosin; × 400)

The Potential Use of the Mesothelium as a Source of Mesenchymal Stem Cells

As stated in the previous paragraphs, the existence of pluripotent mesenchymal cells as precursors of the mesothelium has been already proposed. Even though a mesothelial stem cell has not yet been definitely identified, the existence of pluripotent mesenchymal cells in the mesothelial monolayer as well as in the submesothelial connective tissue, has been repeatedly considered in the literature [401], opening the way in order to consider their use, as an actual option, in regenerating therapies [503].

Some observations performed in human pathology as well as in animal experimentally induced tissue reactions lend strong support to this contention. As a living proof, it may be mentioned that differentiation towards cartilage and bone has been described in a primary tumour of pleura, suggesting that mesothelial cells are pluripotent. In this sense, being mesenchyma, they may well retain the potential to differentiate along embryonic developmental lines, including cartilage and bone [504, 505].

Besides, cartilaginous differentiation of the peritoneum not associated with intra-abdominal malignancy has been already detected [506], whereas bone and cartilaginous formation has been reported in both, human patients and experimentally induced mesothelioma [507, 508]. Bone formation was also seen in four cases of sclerosing peritonitis observed in patients treated by means of peritoneal dialysis, whereas in two of them, islands of bone marrow were also detected [481].

Interestingly, glomerular-like structures in fibrous tissue of biopsies of visceral peritoneum have been detected in biopsies taken from rats with experimentally induced peritoneal sclerosis [505] (Fig. 5.66). This information emphasizes the capability of the mesothelium to differentiate in other cell lines in response to injury [504].

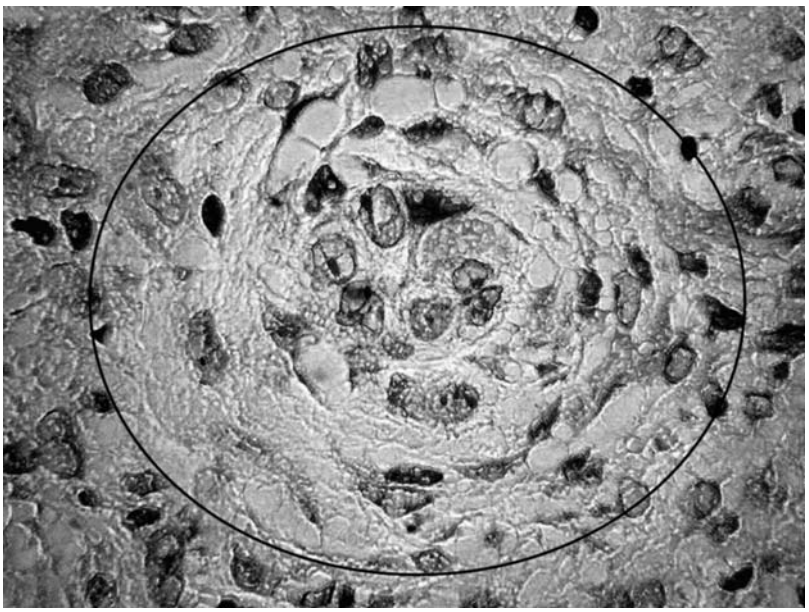

Fig. 5.66 Glomerular-like structure detected in fibrous tissue covering the cavitary aspect of the liver. The specimen was taken from a rat with experimentally induced peritoneal sclerosis. (Hematoxylin-eosin; × 400).

Additional research identified mesenchymal cells in the adult human synovial membrane. These cells showed the capability to differentiate in chondrocytes and osteocytes [509, 510]. Synovium, also of mesenchymal origin, is considered one more type of serous membrane like peritoneum, pericardium and pleura [511]. Therefore, this common embryological origin opens the possibility of eventual therapeutic interventions in the course of joint diseases that could be performed using peritoneal mesothelial cells [505].

Recent published evidence exposed to view the fact that, when placed under the appropriate biophysical and/or biochemical conditions mesothelial cells demonstrate a remarkable degree of plasticity. This property supports the concept, that mesothelial cell progenitors are endowed with the capability to switch between different cell types, according to the conditions of their microenvironment [504]. Within this context, it is illustrating to remind the observed myofibroblastic conversion of human adult mesothelial cells in culture, under the influence of transforming growth factor (TGF)-β-1 [512, 513].

The relationship between blood cells and mesothelium represents one more exciting aspect of this topic. As mentioned before, a proposed mechanism of mesothelial healing postulated that progenitor cells, originally located in the bone marrow, migrate and convert into mesothelial cells [380]. Although additional research concluded that this hypothesis looks unlikely [403], a link between both cell lines seems to be possible. A quite strong point is that hemangioblasts, a proposed progenitor of the endothelial and hematopoietic cell lineages, derive from the embryonic splanchnic mesothelium. This structure, in turn, has been proposed as the embryonic source of the endothelium-lined vascular system, pointing at a specialization of the phylogenetically older celomic cavities. Within this context, the origin of the hematopoietic cells might be related to differentiation of celomocytes derived from the celomic epithelium. So far, endothelial and blood cells appear to derive from a common mesothelial-derived progenitor [514].

In addition, morphological and immunohistochemical evidence for a translocation of cells from the celomic mesothelium to the ventral wall has been observed during development of the quail embryos. Consequently, the concurrence of translocation of mesothelial cells and the appearance of aortic smooth muscle cell progenitors point at a link between the former and the latter cells lineages [515].

This ontogenetic relationship between mesothelium, blood, and blood vessels is substantiated by two excellent studies performed applying the tools of tissue bioengineering. Donna et al. [516] presented evidence demonstrating that cultured adult human mesothelial cells have the capabilities to generate hematopoietic cells, similar to those of the bone marrow. This conversion was confirmed by morphological analysis as well as by cell immunoreactivity toward specific antibodies directed to antigens of the hematopoietic cell lines, at various stages of differentiation. The experiment was performed culturing mesothelial cells in collagen sponges. This is one more suggestion of the remarkable plasticity of the mesothelium, as well as of the relevance of the microenvironment hosting the cultured cells. Regarding blood vessels, a key study is that reported by Campbell et al. [517], who succeeded in creating an artificial blood conduct by inserting a Silastic tubing into the peritoneal cavity of rats. Two weeks after the surgical intervention, a new laparotomy showed that the implanted

silicon rubber tubing was covered by several layers of fibroblasts, collagen matrix, and a single layer of mesothelium. This new "blood vessel" was everted and successfully grafted by end-to-end anastomosis, in arteries of the same animal in which it was grown. These observations have been confirmed by Moldovan and Haveman [518], as well as by our group [505].

So far, it seems evident that peritoneal mesothelial cells are endowed with a degree of plasticity that shapes their capability of generating other cell lines, if placed in the appropriate micro-environment. Investigative steps will have to define the best conditions that will eventually lead to the use of mesothelium in stem cell therapy as well as in tissue engineering, taking also in account that harvesting of large numbers of cells from patients having an unexposed monolayer, may well be unlimited.

Final Remarks

It was not the purpose of the author merely to deliver a cold and tedious description of anatomical structures. On the contrary, the goal has been to offer the reader a comprehensive and balanced analytical approach of structure and function covering, at least in part, their interactions. It is evident that the function of the peritoneum as a dialysis membrane cannot be evaluated only within the frame of passive diffusion through water-filled, cylindrical pores [204] and/or mathematical models [519], based on assumptions that, at times, lose sight of the formidable barrier of the living cell membrane as well as the structural organization of the tissues.

Research during the last two decades provided enough evidence to characterize the peritoneum not as an inert dialyzing sheet, but as a living and reusable membrane for dialysis [271], as predicted more than 25 years ago [520].

It becomes evident that the mesothelial monolayer continuously exposed to dialysis solutions in vivo is structurally and functionally different, at least from the histochemical point of view, from that observed in unexposed–intact cells, or in those growing in the in vitro set-up of culture and later exposed to experimental incubation [521]. Therefore, I have the feeling that a good deal of creative thinking is required to integrate data obtained during 50 years of physiological studies and mathematical models, with the realities of tissue structure and cell biology.

Introduction of peritoneal dialysis as a therapeutic tool to fight chronic uremia shaped a kind of chain reaction that went well beyond the expectations of the early years. Actually, observations made in clinical settings showed the way to a new window open to the fascinating world of cell biology. Within this specific field, there are still more questions than answers.

It is the author's hope that this chapter will serve to stimulate the imagination of young scientists as a catalytic element for further research.

References

1. Robinson B. The Peritoneum. Chicago, IL: WT Keener, 1897, p. 13.
2. Ganter G. Uber die Beseitigung giftiger Stoffe aus dem Blute durch dialyse. Munchen Med Wochenschr 1923; 70: 1478–1480.
3. Boen ST. Peritoneal Dialysis in Clinical Medicine. Springfield, IL: Charles C. Thomas, 1964.
4. Tenckhoff H, Schechter H. A bacteriologically safe peritoneal access device for repeated dialysis. Trans Am Soc Artif Intern Organs 1968; 14: 181–187.
5. Popovich RP, Moncrief JW, Decherd JF, Bomar JB, Pyle WK. Preliminary verification of the low dialysis clearance hypothesis via a novel equilibrium peritoneal dialysis technique. Absts Am Soc Artif Intern Organs 1976; 5: 64.
6. Nolph KD, Sorkin M, Rubin J, Arfania D, Prowant B, Fruto L, Kennedy D. Continuous ambulatory peritoneal dialysis: three-year experience at one center. Ann Intern Med 1980; 92: 609–613.
7. Luschka H. Die Structure der serosen haute des menschen. Tubingen, 1851.
8. Putiloff PV. Materials for the study of the laws of growth of the human body in relation to the surface areas of different systems: the trial on Russian subjects of planigraphic anatomy as a mean of exact anthropometry. Presented at the Siberian branch of the Russian Geographic Society, Omsk, 1886.
9. Wegner G. Chirurgische bemerkingen uber die peritoneal Hole, mit Besonderer Berucksichtigung der ovariotomie. Arch Klin Chir 1877; 20: 51–59.
10. Esperanca MJ, Collins DL. Peritoneal dialysis efficiency in relation to body weight. J Pediatr Surg 1966; 1: 162–169.
11. Krediet RT, Zemel D, Imholz AL, Struijk DG. Impact of surface area and permeability on solute clearances. Perit Dial Int 1994; 14 (suppl. 3): S70–S77.
12. Chagnac A, Herskovitz P, Weinstein T, Elyashiv S, Hirsh J, Hammel I, Gafter U. The peritoneal membrane in peritoneal dialysis patients: estimation of its functional surface area by applying stereologic methods to computerized tomography. J Am Soc Nephrol 1999; 10: 342–346.
13. Flessner M. Small-solute transport across specific peritoneal tissue surfaces in the rat. J Am. Soc Nephrol 1996; 7: 225–233.
14. Gotloib L, Digenis GE, Rabinovich S, Medline A, Oreopolous DG. Ultrastructure of normal rabbit mesentery. Nephron 1983; 34: 248–255.
15. Gosselin RE, Berndt WO. Diffusional transport of solutes through mesentery and peritoneum. J Theor Biol 1962; 3: 487.

16. Haar JL, Ackerman GA. A phase and electron microscopic study of vasculogenesis and erythropoiesis in the yolk sac of the mouse. Anat Rec 1971; 170: 199–224.
17. Ukeshima A, Hayashi Y, Fujimore T. Surface morphology of the human yolk sac: endoderm and mesothelium. Arch Histol Jpn 1986; 49: 483–494.
18. Puulmala RM. Morphologic comparison of parietal and visceral peritoneal epithelium in fetus and adult. Anat Rec 1937; 68: 327–330.
19. Robertson JD. Molecular structure of biological membranes. In: Lima de Faria A, ed. Handbook of Molecular Cytology. Amsterdam: North Holland, 1969, p. 1404.
20. Kolossow A. Weber die struktur des endothels der pleuroperitoneal hole der blut und lymphgefasse. Biol Centralbl Bd 1892; 12: S87–S94.
21. Odor L. Observations of the rat mesothelium with the electron and phase microscopes. Am J Anat 1954; 95: 433–465.
22. Felix DM, Dalton AJ. A comparison of mesothelial cells and macrophages in mice after the intraperitoneal inoculation of melanine granules. J Biophys Biochem Cytol 1956; 2 (suppl. part 2): 109–117.
23. Baradi AF, Hope J. Observations on ultrastructure of rabbit mesothelium. Exp Cell Res 1964; 34: 33–34.
24. Baradi AF, Crae SN. A scanning electron microscope study of mouse peritoneal mesothelium. Tissue Cell 1976; 8: 159.
25. Whitaker D, Papadimitriou JM, Walters MNI. The mesothelium and its reactions: a review. CRC Crit Rev Toxicol 1982; 10: 81–144.
26. Di Paolo N, Sacchi G, De-Mia M et al. Morphology of the peritoneal membrane during continuous ambulatory peritoneal dialysis. Nephron 1986; 44: 204–211.
27. Kondo T, Takeuchi K, Doi Y, Yonemura S, Nagata S, Tsukita S. ERM (ezrin–radixin/moesin)-based molecular mechanism of microvillar breakdown at an early stage of apoptosis. J Cell Biol 1997; 139: 749–758.
28. Bonelli G, Sacchi MC, Barbiero G et al. Apoptosis of L929 cells by etoposide: a quantitative and kinetic approach. Exp Cell Res 1996; 228: 292–305.
29. Boe R, Gjertsen BT, Doskeland SO, Vintermyr OK. 8-Chloro-cAMP induces apoptotic cell death in a human mammary carcinoma cell (MCF–7) line. Br J Cancer 1995; 72: 1151–1159.
30. Efskind L. Experimentelle Untersuchungen uber die Biologie des Peritoneums. 1. Die morphologische reaktion des peritoneums auf riexze. Oslo: Det Norske Videnk aps Academii, 1940.
31. Gotloib L, Wajsbrut V, Shostak A, Kushnier R. Acute and long-term changes observed in imprints of mouse mesothelium exposed to glucose-enriched, lactated, buffered dialysis solutions. Nephron 1995; 70: 466–477.
32. Fukata H. Electron microscopic study on normal rat peritoneal mesothelium and its changes in adsorption of particulate iron dextran complex. Acta Pathol Jpn 1963; 13: 309–325.
33. Lieberman-Meffet D, White H. The Greater Omentum: Anatomy, Physiology, Pathology, Surgery with an Historical Survey. Berlin: Springer-Verlag, 1983, p. 6.
34. Madison LD, Bergstrom MU, Porter B, Torres R, Shelton E. Regulation of surface topography of mouse peritoneal cells. J Cell Biol 1979; 82: 783.
35. Gotloib L, Shostak A. Ultrastructural morphology of the peritoneum: new findings and speculations on transfer of solutes and water during peritoneal dialysis. Perit Dial Bull 1987; 7: 119–129.
36. Gotloib L. Anatomical basis for peritoneal permeability. In: La Greca G, Chiaramonte S, Fabris A, Feriani M, Ronco G, eds. Peritoneal Dialysis. Milan: Wichtig Ed, 1986, pp. 3–10.
37. Gotloib L, Shostak A, Jaichenko J. Ruthenium red stained anionic charges of rat and mice mesothelial cells and basal lamina: the peritoneum is a negatively charged dialyzing membrane. Nephron 1988; 48: 65–70.
38. Luft JH. Fine structure of capillary and endocapillary layer as revealed by ruthenium red. Fed Proc 1966; 25: 1173–1183.
39. Gotloib L, Bar-Sella P, Jaichenko J, Shostak A. Ruthenium red stained polyanionic fixed charges in peritoneal microvessels. Nephron 1987; 47: 22–28.
40. Curry FE, Michel CC. A fiber matrix model of capillary permeability. Microvasc Res 1980; 20: 96–99.
41. Morris RG, Hargreaves AD, Duvall E. Wyllie AH. Hormone-induced cell death. 2. Surface changes in thymocytes undergoing apoptosis. Am J Pathol 1984; 115: 426–436.
42. Moog F. The lining of the small intestine. Sci Am 1981; 2455: 116–125.
43. Gotloib L. Anatomy of the peritoneal membrane. In: La Greca G, Biasoli G, Ronco G, eds. Peritoneal dialysis. Proceedings of the First Int Course. Vicenza, Italy. Milan: Wichtig Ed., 1982, pp. 17–30.
44. Leak LV. Distribution of cell surface charges on mesothelium and lymphatic endothelium. Microvasc Res 1986; 31: 18–30.
45. Lewis WH. Pinocytosis. Bull Johns Hopkins Hosp 1931; 49: 17–23.
46. Casley-Smith JR. The dimensions and numbers of small vesicles in cells, endothelial and mesothelial and the significance of these for endothelial permeability. J Microsc 1969; 90: 251–269.
47. Casley-Smith JR, Chin JC. The passage of cytoplasmic vesicles across endothelial and mesothelial cells. J Microsc 1971; 93: 167–189.
48. Fedorko ME, Hirsch JG, Fried B. Studies on transport of macromolecules and small particles across mesothelial cells of the mouse omentum. Exp Cell Res 1971; 63: 313–323.
49. Simionescu N, Simionescu M, Palade GE. Structural basis of permeability in sequential segments of the microvasculature. II. Pathways followed by microperoxidase across the endothelium. Microvasc Res 1978; 15: 17–36.
50. Palade GE, Simionescu M, Simionescu N. Structural aspects of the permeability of the microvascular endothelium. Acta Physiol Scand Suppl 1979; 463: 11–32.
51. Palade GE. Fine structure of blood capillaries. J Appl Phys 1953; 24: 1424.
52. Florey HW. The transport of materials across the capillary wall. Q J Exp Physiol 1964; 49: 117–128.
53. Pappenheimer JR, Renkin EM, Borrero LM. Filtration, diffusion and molecular sieving through peripheral capillary membranes. A contribution to the pore theory of capillary permeability. Am J Physiol 1951; 167: 13–46.
54. Frokjaer-Jensen J. The plasmalemmal vesicular system in capillary endothelium. Prog Appl Microcirc 1983; 1: 17–34.
55. Wagner RC, Robinson CS. High voltage electron microscopy of capillary endothelial vesicles. Microvasc Res 1984; 28: 197–205.
56. Smart EJ, Foster DC, Ying YS, Kamen BA, Anderson RGW. Protein kinase G activators inhibit receptor-mediated potocytosis by preventing internalization of caveolae. J Cell Biol 1994; 124: 307–313.

57. Lisanti MP, Scherer PE, Vidugiriene J et al. Characterization of caveolin-rich membrane domains isolated from an endothelial-rich source: implications for human disease. J Cell Biol 1994; 126: 111–126.
58. Moldovan NI, Heltianu G, Simionescu N, Simionescu M. Ultrastructural evidence of differential solubility in Triton X–100 of endothelial vesicles and plasma membrane. Exp Cell Res 1995; 219: 309–313.
59. Shasby DM, Roberts RL. Transendothelial transfer of macromolecules *in vivo*. Fed Proc 1987; 46: 2506–2510.
60. Shasby DM, Shasby SS. Active transendothelial transport of albumin. Interstitium to lumen. Circ Res 1985; 57: 903–908.
61. Milici AJ, Watrous NE, Stukenbrok M, Palade GE. Transcytosis of albumin in capillary endothelium. J Cell Biol 1987; 105: 2603–2612.
62. Ghitescu L, Bendayan M. Transendothelial transport of serum albumin: a quantitative immunocytochemical study. J Cell Biol 1992; 17: 747–755.
63. Schnitzer JE, Oh P. Albondin-mediated capillary permeability to albumin. Differential role of receptors in endothelial transcytosis and endocytosis of native and modified albumins. J Biol Chem 1994; 269: 6072–6082.
64. Ghitescu L, Galis Z, Simionescu M, Simionescu N. Differentiated uptake and transcytosis of albumin in successive vascular segments. J Submicrosc Cytol Pathol 1988; 20: 657–669.
65. Williams SK, Devenny JJ, Bitensky MW. Micropinocytic ingestion of glycosylated albumin by isolated microvessels: possible role in pathogenesis of diabetic microangiopathy. Proc Natl Acad Sci U S A 1981; 78: 2393–2397.
66. Ghilescu L, Fixman A, Simionescu M, Simionescu N. Specific binding sites for albumin restricted to plasmalemmal vesicles of continuous capillary endothelium: receptor-mediated transcytosis. J Cell Biol 1986; 102: 1304–1311.
67. Predescu D, Simionescu M, Simionescu N, Palade GE. Binding and transcytosis of glycoalbumin by the microvascular endothelium of the murine myocardium: evidence that glycoalbumin behaves as a bifunctional ligand. J Cell Biol 1988; 107: 1729–1738.
68. Dehouck B, Fenart L, Dehouck MP, Pierce A, Torpier G, Cecchelli R. A new function for the LDL receptor: transcytosis of LDL across the blood–brain barrier. J Cell Biol 1997; 138: 877–889.
69. Simionescu N, Simionescu M. Interactions of endogenous lipoproteins with capillary endothelium in spontaneously hyperlipoproteinemic rats. Microvasc Res. 1985; 30: 314–332.
70. Snelting-Havinga I, Mommaas M, Van-Hinsbergh VW, Daha MR, Daems WT, Vermeer BJ. Immunoelectron microscopic visualization of the transcytosis of low density lipoproteins in perfused rat arteries. Eur J Cell Biol 1989; 48: 27–36.
71. Vasile E, Simionescu M, Simionescu N. Visualization of the binding, endocytosis, and transcytosis of low-density lipoprotein in the arterial endothelium *in situ*. J Cell Biol 1983; 96: 1677–1689.
72. Ghinea N, Hai MTV, Groyer-Picard MT, Milgrom E. How protein hormones reach their target cells. Receptor mediated transcytosis of hCG through endothelial cells. J Cell Biol 1994; 125: 87–97.
73. Bendayan M, Rasio EA. Transport of insulin and albumin by the microvascular endothelium of the rete mirabile. J Cell Sci 1996; 109: 1857–1864.
74. Schmidt AM, Vianna M, Gerlach M et al. Isolation and characterization of two binding proteins for advanced glycosylation end products from bovine lung which are present on the endothelial cell surface. J Biol Chem 1992; 267: 14987–14997.
75. Predescu D, Predescu S, McQuistan T, Palade GE. Transcytosis of alpha 1-acidic glycoprotein in the continuous microvascular endothelium. Proc Natl Acad Sci U S A 1998; 95: 6175–6180.
76. Pappenheimer JR. Passage of molecules through capillary walls. Physiol Rev 1953; 33: 387–423.
77. Grotte G. Passage of dextran molecules across the blood–lymph barrier. Acta Chir Scand 1956; (suppl. 211): 1–84.
78. Nolph KD. The peritoneal dialysis system. Contrib Nephrol 1979; 17: 44–49.
79. Gotloib L, Shostak A. Endocytosis and transcytosis of albumin–gold through mice peritoneal mesothelium. Kidney Int 1995; 47: 1274–84.
80. Schnitzer JE, Allard J, Oh P. NEM inhibits transcytosis, endocytosis and capillary permeability: implication of caveolae fusion in endothelia. Am J Physiol 1995; 168: H48–H55.
81. Schnitzer JE, Oh P, Pinney E, Allard J. Filipin-sensitive caveolae-mediated transport in endothelium: reduced transcytosis, scavenger endocytosis, and capillary permeability of select macromolecules. J Cell Biol 1994; 127: 1217–1232.
82. Tiruppathi G, Song W, Bergenfeldt M, Sass P, Malik AB. Gp60 activation mediates albumin transcytosis in endothelial cells by tyrosine kinase-dependent pathway. J Biol Chem 1997; 272: 25968–25975.
83. Schnitzer JE, Oh P, Jacobson BS, Dvorak AM. Caveolae from luminal plasmalemma of rat lung endothelium: microdomains enriched in caveolin, Ca (2 +)-ATPase, and inositol triphos–phate receptor. Proc Natl Acad Sci U S A 1995; 92: 1759–1763.
84. Glenney JR, Soppet D. Sequence and expression of caveolin, a protein component of caveolae plasma membrane domains phosphorylated on tyrosine in Rous sarcoma virus-transformed fibroblasts. Proc Natl Acad Sci U S A 1992; 89: 10517–10521.
85. Bush KT, Stuart RO, Li SH et al. Epithelial inositol 1,4,5-triphosphate receptors. Multiplicity of localization, solubility, and isoforms. J Biol Chem 1994; 269: 23694–23699.
86. Brown D, Lydon J, McLaughlin M, Stuart-Tilley A, Tyszkowski R, Alper S. Antigen retrieval in cryostat tissue sections and cultured cells by treatment with sodium dodecyl sulfate (SDS). Histochem Cell Biol 1996; 105: 261–267.
87. Breton S, Lisante MP, Tyszkowski R, McLaughlin M, Brown D. Basolateral distribution of caveolin-1 in the kidney. Absence from ATPase-coated endocytic vesicles in intercalated cells. J Histochem Cytochem 1998; 46: 205–214.
88. Schmid SL. Clathrin-coated vesicle formation and protein sorting: an integrated process. Annu Rev Biochem 1997; 66: 511–548.
89. Pfeffer SR, Drubin DG, Kelly RB. Identification of three coated vesicle components as alpha- and beta-tubulin linked to a phosphorylated 50,000-dalton polypeptide. J Cell Biol 1983; 97: 40–47.
90. Pearse BMF. Clathrin: a unique protein associated with intracellular transfer of membrane by coated vesicles. Proc Natl Acad Sci U S A 1976; 73: 1255–1259.
91. Lin HC, Duncan JA, Kozasa T, Gilman AG. Sequestration of the G protein beta gamma subunit complex inhibits receptor-mediated endocytosis. Proc Natl Acad Sci U S A 1998; 95: 505–560.
92. Damke H. Dynamin and receptor-mediated endocytosis. FEBS Lett 1996; 389: 48–51.
93. Sweitzer SM, Hinsshaw JE. Dynamin undergoes a GTP dependent conformational change causing vesiculation. Cell 1998; 93: 1021–1029.
94. Henley JR, Krueger EW, Oswald BJ, McNiven MA. Dynamin-mediated internalization of caveolae. J Cell Biol 1998; 141: 85–99.

95. Oh P, McIntosh DP, Schnitzer JE. Dynamin at the neck of caveolae mediates their budding to form transport vesicles by GTP-driven fission from the plasma membrane of endothelium. J Cell Biol 1998; 141: 101–114.
96. Chambers R, Zweifach BW. Capillary cement in relation to permeability. J Cell Comp Physiol 1940; 15: 255–272.
97. Rippe B. A three-pore model of peritoneal transport. Perit Dial Int 1993; 13 (suppl. 2): S35–S38.
98. Simionescu N, Simionescu M, Palade GE. Differentiated microdomains on the luminal surface of capillary endothelium. I. Preferential distribution of anionic sites. J Cell Biol 1981; 90: 605–613.
99. Steinman RM, Mellman IS, Muller WA, Cohn ZA. Endocytosis and the recycling of plasma membrane. J Cell Biol 1983; 96: 1–27.
100. Shea SM, Karnovsky MJ. Brownian motion: a theoretical explanation for the movement of vesicles across the endothelium. Nature (Lond) 1966; 212: 353–354.
101. Simionescu M, Simionescu N, Palade GE. Morphometric data on the endothelium of blood capillaries. J Cell Biol 1974; 60: 128–152.
102. Wagner JC, Johnson NF, Brown DG, Wagner MMF. Histology and ultrastructure of serially transplanted rat mesotheliomas. Br J Cancer 1982; 46: 294–299.
103. Petersen OW, Van Deurs B. Serial section analysis of coated pits and vesicles involved in adsorptive pinocytosis in cultured fibroblasts. J Cell Biol 1983; 96: 277–281.
104. Peters KR, Carley WW, Palade GE. Endothelial plasmalemmal vesicles have a characteristic stripped bipolar surface structure. J Cell Biol 1985; 101: 2233–2238.
105. Fishchereder M, Schryppel B, Wiese P, Fink M, Banas B, Schmidbauer S, Schlyndorff D. Regulation of glucose transporters in human peritoneal mesothelial cells. J Nephrol 2003; 16: 103–109.
106. Sands JM. Regulation of urea transporter proteins in kidney and liver. Mount Sinai J Med 2000;67: 112–119.
107. Takahashi H, Hasegawa H, Kamijo T et al. Regulation and localization of peritoneal water channels in rats. Perit Dial Int 1998; 18 (suppl. 2): S70.
108. Henle FGH. Splacnologie, Vol. II, pp. 175, 1875.
109. Simionescu M, Simionescu N, Silbert J, Palade GE. Differentiated microdomains on the luminal surface of the capillary endothelium. II. Partial characterization of their anionic sites. J Cell Biol 1981; 90: 614–621.
110. Simionescu M, Simionescu N. Organization of cell junctions in the peritoneal mesothelium. J Cell Biol 1977; 74: 98.
111. Von Recklinghausen FD. Zur Fettresorption. Arch Pathol Anat Physiol 1863; Bd 26: S172–S208.
112. Bizzozero G, Salvioli G. Sulla suttura della membrana serosa e particolarmente del peritoneo diaphragmatico. Giorn R Acad Med Torino 1876; 19: 466–470.
113. Allen L. The peritoneal stomata. Anat Rec 1937; 67: 89–103.
114. French JE, Florey HW, Morris B. The adsorption of particles by the lymphatics of the diaphragm. Q J Exp Physiol 1959; 45: 88–102.
115. Tourneux F, Herman G. Recherches sur quelques epitheliums plats dans la serie animale (Deuxieme partie). J Anat Physiol 1876; 12: 386–424.
116. Kolossow A. Uber die struktur des pleuroperitoneal und gefassepithels (endothels). Arch Mikr Anat 1893; 42: 318–383.
117. Simer PM. The passage of particulate matter from the peritoneal cavity into the lymph vessels of the diaphragm. Anat Rec 1948; 101: 333–351.
118. Leak LW, Just EE. Permeability of peritoneal mesothelium. J Cell Biol 1976; 70: 423a.
119. Tsilibarry EC, Wissig SL. Absorption from the peritoneal surface of the muscular portion of the diaphragm. Am J Anat 1977; 149: 127–133.
120. Abu-Hijleh MF, Scothorne RJ. Studies on haemolymph nodes. IV. Comparison of the route of entry of carbon particles into parathymic nodes after intravenous and intraperitoneal injection. J Anat 1996; 188: 565–573.
121. Hashimoto B, Filly RA, Callen PW, Parer JT. Absorption of fetal intraperitoneal blood after intrauterine transfusion. J Ultrasound Med 1987; 6: 421–423.
122. Smedsrood B, Aminoff D. Studies on the sequestration of chemically and enzymatically modified erythrocytes. Am J Hematol 1983; 15: 123–133.
123. Fowler JM, Knight R, Patel KM. Intraperitoneal blood transfusion in African adults with hookworm anaemia. Br Med J 1968; 3: 200–201.
124. Chandler K, Fitzpatrik J, Mellor D, Milne M, Fishwick G. Intraperitoneal administration of whole blood as a treatment for anaemia in lambs. Vet Rec 1998; 142: 175–176.
125. Aba MA, Pissani AA, Alzola RH, Videla-Dorna I, Ghezzi MS, Marcilese NA. Evaluation of intraperitoneal route for the transfusion of erythrocytes using rats and dogs. Acta Physiol Pharmacol Ther Latinoam 1991; 41: 387–395.
126. Remmele W, Richter IE, Wildenhof H. Experimental investigations on cell resorption from the peritoneal cavity by use of the scanning electron microscope. Klin Wochenschr 1975; 53: 913–922.
127. Dumont AE, Maas WK, Iliescu H, Shin RD. Increased survival from peritonitis after blockade of transdiaphragmatic absorption of bacteria. Surg Gynecol Obstet 1986; 162: 248–252.
128. Leak LV. Permeability of peritoneal mesothelium: a TEM and SEM study. J Cell Biol 1976; 70: 423–433.
129. Leak LV. Polycationic ferritin binding to diaphragmatic mesothelial and lymphatic endothelial cells. J Cell Biol 1982; 95: 103–111.
130. Ettarh RR, Carr KE. Ultrastructural observations on the peritoneum in the mouse. J Anat 1996; 188: 211–215.
131. Wassilev M, Wedel T, Michailova K, Kuhnel W. A scanning electron microscopy study of peritoneal stomata in different peritoneal regions. Anat Anz 1998; 180: 137–143.
132. Li J, Zhou J, Gao Y. The ultrastructure and computer imaging of the lymphatic stomata in the human pelvic peritoneum. Anat Anz 1997; 179: 215–220.
133. Yoffey JM, Courtice FC. Lymphatics, Lymph and Lymphoid Tissue. London: Edward Arnold, 1956, p. 176.
134. Andrews PM, Porter KR. The ultrastructural morphology and possible functional significance of mesothelial microvilli. Anat Rec 1973; 177: 409–414.
135. Ghadially FN. Ultrastructural Pathology of the Cell. London: Butterworths, 1978, p. 403.
136. Todd RB, Bowman W. The Physiological Anatomy and Physiology of Man, Vols I and II, London, 1845 and 1846.
137. Baron MA. Structure of the intestinal peritoneum in man. Am J Anat 1941; 69: 439–496.

138. Maximow A. Bindgewebe und blutbildende gewebe. Handbuch der mikroskopischen Anatomie des menschen. von Mollendorf 1927; Bd 2 T 1: S232–S583.
139. Kanwar YS, Farquhar MG. Anionic sites in the glomerular basement membrane. *In vivo* and *in vitro* localization to the laminae rarae by cationic probes. J Cell Biol 1979; 81: 137–153.
140. Rohrbach R. Reduced content and abnormal distribution of anionic sites (acid proteoglycans) in the diabetic glomerular basement membrane. Virchows Arch B Cell Pathol Incl Mol Pathol 1986; 51: 127–135.
141. Ghinea N, Simionescu N. Anionized and cationized hemeundecapeptides as probes for cell surface charge and permeability studies: differentiated labeling of endothelial plasmalemmal vesicles. J Cell Biol 1985; 100: 606–612.
142. Gotloib L, Shostak A, Jaichenko J. Loss of mesothelial electronegative fixed charges during murine septic peritonitis. Nephron 1989; 51: 77–83.
143. Shostak A, Gotloib L. Increased peritoneal permeability to albumin in streptozotocin diabetic rats. Kidney Int 1996; 49: 705–714.
144. Gotloib L, Shostak A, Bar-Sella P, Eiali V. Reduplicated skin and peritoneal blood capillaries and mesothelial basement membrane in aged non-diabetic chronic uremic patients. Perit Dial Bull 1984; 4: S28.
145. Di Paolo N, Sacchi G. Peritoneal vascular changes in continuous ambulatory peritoneal dialysis (CAPD): an *in-vivo* model for the study of diabetic microangiopathy. Perit Dial Int 1989; 9: 41–45.
146. Gersh I, Catchpole HR. The organization of ground substances and basement membrane and its significance in tissue injury, disease and growth. Am J Anat 1949; 85: 457–522.
147. Williamson JT, Vogler NJ, Kilo CH. Regional variations in the width of the basement membrane of muscle capillaries in man and giraffe. Am J Pathol 1971; 63: 359–367.
148. Vracko R. Skeletal muscle capillaries in non-diabetics. A quantitative analysis. Circulation 1970; 16: 285–297.
149. Parthasarathy N, Spiro RG. Effect of diabetes on the glycosaminoglycan component of the human glomerular basement membrane. Diabetes 1982; 31: 738–741.
150. Vracko R. Basal lamina scaffold – anatomy and significance for maintenance of orderly tissue structure. A review. Am J Pathol 1974; 77: 313–346.
151. Vracko R, Pecoraro RE, Carter WB. Basal lamina of epidermis, muscle fibers, muscle capillaries, and renal tubules: changes with aging and diabetes mellitus. Ultrastruct Pathol 1980; 1: 559–574.
152. Hruza Z. Connective tissue. In: Kaley G, Altura BM, eds. Microcirculation, Vol. I, Baltimore, MD: University Park Press, 1977, pp. 167–83.
153. Comper WD, Laurent TC. Physiological function of connective tissue polysaccharides. Physiol Rev 1978; 58: 255–315.
154. Flessner MF. The importance of the interstitium in peritoneal transport. Perit Dial Int 1996; 16 (suppl. 1): S76–S79.
155. Parker JC, Gilchrist S, Cartledge JT. Plasma–lymph exchange and interstitial distribution volumes of charged macromolecules in the lung. J Appl Physiol 1985; 59: 1128–1136.
156. Lai-Fook SJ, Brown LV. Effects of electric charge on hydraulic conductivity of pulmonary interstitium. J Appl Physiol 1991; 70: 1928–1932.
157. Gilchrist SA, Parker JC. Exclusion of charged macromolecules in the pulmonary interstitium. Microvasc Res 1985; 30: 88–98.
158. Haljamae H. Anatomy of the interstitial tissue. Lymphology 1978; 11: 128–32.
159. Guyton AC. A concept of negative interstitial pressure based on pressures in implanted perforated capsules. Circ Res 963; 12: 399–414.
160. Scholander PF, Hargens AR, Miller SL. Negative pressure in the interstitial fluid of animals. Fluid tensions are spectacular in plants; in animals they are elusively small, but just as vital. Science 1968; 161: 321–328.
161. Aukland K, Reed PK. Interstitial–lymphatic mechanisms in the control of extracellular fluid volume. Physiol Rev 1993; 73: 1–78.
162. Rutili G, Arfors KE. Protein concentration in interstitial and lymphatic fluids from the subcutaneous tissue. Acta Physiol Scand 1977; 99: 1–8.
163. Rutili G, Kvietys P, Martin D, Parker JC, Taylor AE. Increased pulmonary microvascular permeability induced by alpha-naphthylthiourea. J Appl Physiol 1982; 52: 1316–1323.
164. Flessner MF. Peritoneal transport physiology: insights from basic research. J Am Soc Nephrol 1991; 2: 122–135.
165. Gotloib L, Mines M, Garmizo AL, Varka I. Hemodynamic effects of increasing intra-abdominal pressure in peritoneal dialysis. Perit Dial Bull 1981; 1: 41–42.
166. Flessner MF, Schwab A. Pressure threshold for fluid loss from the peritoneal cavity. Am J Physiol 1996; 270: F377–F390.
167. Simionescu N. Cellular aspects of transcapillary exchange. Physiol Rev 1983; 63: 1536–1579.
168. Wolff JR. Ultrastructure of the terminal vascular bed as related to function. In: Kaley G, Altura BM, eds. Microcirculation, Vol. I, Baltimore, MD: University Park Press, 1977, pp. 95–130.
169. Majno G. Ultrastructure of the vascular membrane. Handbook of Physiology. Section II – Circulation, Vol. III. Washington, DC: Am Physiol Soc, 1965, pp. 2293–2375.
170. Gotloib L, Shostak A, Jaichenko J. Fenestrated capillaries in mice submesothelial mesenteric microvasculature. Int J Artif Organs 1989; 12: 20–24.
171. Gotloib L, Shostak A. In search of a role for submesothelial fenestrated capillaries. Perit Dial Int 1993; 13: 98–102.
172. Gotloib L, Shostak A, Bar-Sella P, Eiali V. Fenestrated capillaries in human parietal and rabbit diaphragmatic peritoneum. Nephron 1985; 41: 200–202.
173. Friederici HHR. The tridimensional ultrastructure of fenestrated capillaries. J Ultrastruct Res 1968; 23: 444–456.
174. Clough G, Smaje LH. Exchange area and surface properties of the microvasculature of the rabbit submandibular gland following duct ligation. J Physiol 1984; 354: 445–456.
175. Gotloib L, Shostak A, Jaichenko J, Galdi P, Fudin R. Anionic fixed charges in the fenestrated capillaries of the mouse mesentery. Nephron 1990; 55: 419–422.
176. Rhodin JAG. The diaphragm of capillary endothelial fenestrations. J Ultrastruc Res 1962; 6: 171–185.
177. Gotloib L, Shostak A, Bar-Sella P, Eiali V. Heterogeneous density and ultrastructure of rabbit's peritoneal microvasculature. Int J Artif Organs 1984; 7: 123–125.

178. Rhodin YAG. Ultrastructure of mammalian venous capillaries, venules and small collecting veins. J Ultrastruct Res 1968; 25: 452–500.
179. Gotloib L, Shostak A, Jaichenko J. Loss of mesothelial and microvascular fixed anionic charges during murine experimentally induced septic peritonitis. In: Avram M, Giordano G, eds. Ambulatory Peritoneal Dialysis. New York: Plenum, 1990, pp. 63–66.
180. Simionescu M, Simionescu N, Palade GE. Differentiated microdomains on the luminal surface of capillary endothelium: distribution of lectin receptors. J Cell Biol 1982; 94: 406–413.
181. Schneeberger EE, Hamelin M. Interactions of serum proteins with lung endothelial glycocalyx: its effect on endothelial permeability. Am J Physiol 1984; 247: H206–H217.
182. Bundgaard M, Frokjaer-Jensen J. Functional aspects of the ultrastructure of terminal blood vessels: a quantitative study on consecutive segments of the frog mesenteric microvasculature. Microvasc Res 1982; 23: 1–30.
183. Palade GE. Transport in quanta across the endothelium of blood capillaries. Anat Rec 1960; 116: 254.
184. Milici AJ, L'Hernault N, Palade GE. Surface densities of diaphragmed fenestrae and transendothelial channels in different murine capillary beds. Circ Res 1985; 56: 709–717.
185. Lombardi T, Montesano R, Furie MB, Silverstein SC, Orci L. *In-vitro* modulation of endothelial fenestrae: opposing effects of retinoic acid and transforming growth factor beta. J Cell Sci 1988; 91: 313–318.
186. Kitchens CS, Weiss L. Ultrastructural changes of endothelium associated with thrombocytopenia. Blood 1975; 46: 567–578.
187. Horiuchi T, Weller PF. Expression of vascular endothelial growth factor by human eosinophils: upregulation by granulocyte macrophage colony-stimulating factor and interleukin-5. Am J Respir Cell Mol Biol 1997; 17: 70–77.
188. Collins PD, Connolly DT, Williams TJ. Characterization of the increase in vascular permeability induced by vascular permeability factor *in vivo*. Br J Pharmacol 1993; 109: 195–199.
189. Yeo KT, Wang HH, Nagy JA, Sioussat TM et al. Vascular permeability factor (vascular endothelial growth factor) in guinea pig and human tumor inflammatory effusions. Cancer Res 1993; 53: 2912–2918.
190. Taichman NS, Young S, Cruchley AT, Taylor P, Paleolog E. Human neutrophils secrete vascular endothelial growth factor. J Leukoc Biol 1997; 62: 397–400.
191. Roberts WG, Palade GE. Increased microvascular permeability and endothelial fenestration induced by vascular endothelial growth factor. J Cell Sci 1995; 108: 2369–2370.
192. Roberts WG, Palade GE. Neovasculature induced by vascular endothelial growth factor is fenestrated. Cancer Res 1997; 57: 765–772.
193. Simionescu M, Simionescu N, Palade GE. Sulfated glycosaminoglycans are major components of the anionic sites of fenestral diaphragms in capillary endothelium. J Cell Biol 1979; 83: 78a.
194. Milici AJ, L'Hernault N. Variation in the number of fenestrations and channels between fenestrated capillary beds. J Cell Biol 1983; 97: 336.
195. Peters KR, Milici AJ. High resolution scanning electron microscopy of the luminal surface of a fenestrated capillary endothelium. J Cell Biol 1983; 97: 336a.
196. Bankston PW, Milici AJ. A survey of the binding of polycationic ferritin in several fenestrated capillary beds: indication of heterogeneity in the luminal glycocalyx of fenestral diaphragms. Microvasc Res 1983; 26: 36–49.
197. Levick JR, Smaje LH. An analysis of the permeability of a fenestra. Microvasc Res 1987; 33: 233–256.
198. Wayland H, Silberberg A. Blood to lymph transport. Microvasc Res 1978; 15: 367–374.
199. Bearer EL, Orci L. Endothelial fenestral diaphragms: a quick freeze, deep-etch study. J Cell Biol 1985; 100: 418–428.
200. Simionescu M, Simionescu N, Palade GE. Preferential distribution of anionic sites on the basement membrane and the abluminal aspect of the endothelium in fenestrated capillaries. J Cell Biol 1982; 95: 425–434.
201. Deen WN, Satvat B. Determinants of the glomerular filtration of proteins. Am J Physiol 1981; 241: F162–F170.
202. Deen WM, Bohrer MP, Robertson CR, Brenner BM. Determinants of the transglomerular passage of macromolecules. Fed Proc 1977; 36: 2614–2618.
203. Kanwar YS, Linker A, Farquhar MG. Characterization of anionic sites in the glomerular basement membrane: *in vitro* and *in vivo* localization to the lamina rarae by cationic probes. J Cell Biol 1980; 86: 688–693.
204. Renkin EM. Multiple pathways of capillary permeability. Circ Res 1977; 41: 735–743.
205. Charonis AS, Wissig SL. Anionic sites in basement membranes. Differences in their electrostatic properties in continuous and fenestrated capillaries. Microvasc Res 1983; 25: 265–285.
206. Renkin EM. Cellular and intercellular transport pathways in exchange vessels. Am Rev Respir Dis 1992; 146: S28–S31.
207. Farquhar MG, Palade GE. Junctional complexes in various epithelia. J Cell Biol 1963; 17: 375–442.
208. Simionescu M, Simionescu N, Palade GE. Segmental differentiations of cell junctions in the vascular endothelium. J Cell Biol 1975; 67: 863–885.
209. Thorgeirsson G, Robertson AL Jr. The vascular endothelium. Pathobiologic significance. Am J Pathol 1978; 95: 801–848.
210. Gumbiner B. Breaking through the tight junction barrier. J Cell Biol 1993; 123: 1631–1633.
211. Gumbiner B. Structure, biochemistry, and assembly of epithelial tight junctions. Am J Physiol 1987; 253: C749–C758.
212. Furuse M, Hirase T, Itoh M et al. Occludin: a novel integral membrane protein localized at tight junctions. J Cell Biol 1993; 123: 1777–1788.
213. Furuse M, Itoh M, Hirase T et al. Direct association of occludin with ZO-1 and its possible involvement in the localization of occludin at tight junctions. J Cell Biol 1994; 127: 1617–1626.
214. Hirase T, Staddon JM, Saitou M et al. Occludin as a possible determinant of tight junction permeability in endothelial cells. J Cell Sci 1997; 110: 1603–1613.
215. Balda MS, Anderson JM. Two classes of tight junctions are revealed by ZO-1 isoforms. Am J Physiol 1993; 264: C918–C924.
216. Mitic LL, Anderson JM. Molecular architecture of tight junctions. Annu Rev Physiol 1998; 60: 121–142.
217. Navarro P, Caveda L, Breviario F, Mandoteanu I, Lampugnani MG, Dejana E. Catenin-dependent and independent functions of vascular endothelial cadherin. J Biol Chem 1995; 270: 30965–30972.
218. Leach L, Firth JA. Structure and permeability of human placental microvasculature. Microsc Res Tech 1997; 38: 137–44.

219. Alexander JS, Blaschuk OW, Haselton FR. An N-cadherinlike protein contributes to solute barrier maintenance in cultured endothelium. J Cell Physiol 1993; 156: 610–618.
220. Bundgaard M. The three dimensional organization of tight junctions in capillary endothelium revealed by serial-section electron microscopy. J Ultrastrucl Res 1984; 88: 1–17.
221. Zand T, Underwood JM, Nunnari JJ, Majno G, Joris I. Endothelium and 'silver lines'. An electron microscopic study. Virchows Arch Pathol Anat 1982; 395: 133–144.
222. Anderson JM, Van-Itallie CM. Tight junctions and the molecular basis for regulation of paracellular permeability. Am J Physiol 1995; 269: G467–G475.
223. Robinson PJ, Rapoport SI. Size selectivity of blood–brain barrier permeability at various times after osmotic opening. Am J Physiol 1987; 253: R459–R466.
224. Blum MS, Toninelli E, Anderson JM et al. Cytoskeletal rearrangement mediates human microvascular endothelial tight junction modulation by cytokines. Am J Physiol 1997; 273: H286–H294.
225. Schneeberger EE, Lynch RD. Structure, function and regulation of cellular tight junctions. Am J Physiol 1992; 262: L647–L661.
226. Burns AR, Walker DC, Brown ES et al. Neutrophil transendothelial migration is independent of tight junctions and occurs preferentially at tricellular corners. J Immunol 1997; 159: 2893–2903.
227. Rohrbach DH, Hassell JR, Klechman HK, Martin GR. Alterations in basement membrane (heparan sulfate) proteoglycan in diabetic mice. Diabetes 1982; 31: 185–188.
228. Chakrabarti S, Ma N, Sima AAF. Anionic sites in diabetic basement membranes and their possible role in diffusion barrier abnormalities in the BB-rat. Diabetologia 1991; 34: 301–306.
229. Shimomura H, Spiro RG. Studies on macromolecular components of human glomerular basement membrane and alterations in diabetes. Decreased levels of heparan sulfate, proteoglycan and laminin. Diabetes 1987; 36: 374–381.
230. Abrahamson DR. Recent studies on the structure and pathology of basement membranes. J Pathol 1986; 149: 257–278.
231. Hasslacher G, Reichenbacher R, Getcher F, Timpl R. Glomerular basement membrane synthesis and serum concentration of type IV collagen in streptozotocin-diabetic rats. Diabetologia 1984; 26: 150–154.
232. Li W, Shen S, Khatami M, Rockey JH. Stimulation of retinal capillary pericyte protein and collagen synthesis in culture by high glucose concentration. Diabetes 1984; 33: 785–789.
233. Cagliero E, Maiello M, Boeri D, Roy S, Lorenzi M. Increased expression of basement membrane components in human endothelial cells cultured in high glucose. J Clin Invest 1988; 82: 735–738.
234. Ashworth CT, Erdmann RR, Arnold NJ. Age changes in the renal basement membrane of rats. Am J Pathol 1960; 36: 165–179.
235. Pino RM, Essner E, Pino LC. Location and chemical composition of anionic sites in Bruch's membrane of the rat. J Histochem Cytochem 1982; 30: 245–252.
236. Kanwar YS, Rosenzweig LJ, Kerjaschki DI. Glycosaminoglycans of the glomerular basement membrane in normal and nephrotic states. Ren Physiol 1981; 4: 121–130.
237. Kitano Y, Yoshikawa N, Nakamura H. Glomerular anionic sites in minimal change nephrotic syndrome and focal segmental glomerulosclerosis. Clin Nephrol 1993; 40: 199–204.
238. Torihara K, Suganuma T, Ide S, Morimitsu T. Anionic sites in blood capillaries of the mouse cochlear duct. Hear Res 1994; 77: 69–74.
239. Lawrenson JG, Reid AR, Allt G. Molecular characterization of anionic sites on the luminal front of endoneural capillaries in sciatic nerve. J Neurocytol 1994; 23: 29–37.
240. Lawrenson JG, Reid AR, Allt G. Molecular characteristics of pial microvessels of the rat optic nerve. Can pial microvessels be used as a model for the blood–brain barrier? Cell Tissue Res 1997; 288: 259–265.
241. Vorbrodt AW. Ultracytochemical characterization of anionic sites in the wall of brain capillaries. J Neurocytol 1989; 18: 359–368.
242. Dos-Santos WL, Rahman J, Klein N, Male DK. Distribution and analysis of surface charge on brain endothelium *in vitro* and *in situ*. Acta Neuropathol (Berl) 1995; 90: 305–311.
243. Ohtsuka A, Yamana S, Murakami T. Localization of membrane associated sialomucin on the free surface of mesothelial cells of the pleura, pericardium, and peritoneum. Histochem Cell Biol 1997; 107: 441–447.
244. Meirelles MN, Souto-Padron T, De-Souza W. Participation of cell surface anionic sites in the interaction between *Trypanosoma cruzi* and macrophages. J Submicrosc Cytol 1984; 16: 533–545.
245. Danon D, Marikovsky Y. The aging of the red blood cell. A multifactor process. Blood Cells 1988; 14: 7–18.
246. Lupu G, Calb M. Changes in the platelet surface charge in rabbits with experimental hypercholesterolemia. Atherosclerosis 1988; 72: 77–82.
247. Curry FE. Determinants of capillary permeability: a review of mechanisms based on single capillary studies in the frog. Circ Res 1986; 59: 367–380.
248. Haraldsson B. Physiological studies of macromolecular transport across capillary walls. Acta Physiol Scand 1986; 128 (suppl. 553): 1–40.
249. Hardebo JE, Kahrstrom J. Endothelial negative surface charge areas and blood–brain barrier function. Acta Physiol Scand 1985; 125: 495–499.
250. Brenner BM, Hostelter TH, Humes HD. Glomerular permeability: barrier function based on discrimination of molecular size and charge. Am J Physiol 1978; 234: F455–F460.
251. Bray J, Robinson GB. Influence of charge on filtration across renal basement membrane films *in vitro*. Kidney Int 1984; 25: 527–533.
252. Skutelsky E, Danon D. Redistribution of surface anionic sites on the luminal front of blood vessel endothelium after interaction with polycationic ligand. J Cell Biol 1976; 71: 232–241.
253. Reeves WH, Kanwar YS, Farquhar MG. Assembly of the glomerular filtration surface. Differentiation of anionic sites in glomerular capillaries of newborn rat kidney. J Cell Biol 1980; 85: 735–753.
254. Adamson RH, Huxley VH, Curry FE. Single capillary permeability to proteins having similar size but different charge. Am J Physiol 1988; 254: H304–H312.
255. Nakao T, Ogura M, Takahashi H, Okada T. Charge-affected transperitoneal movement of amino acids in CAPD. Perit Dial Int 1996; 16 (suppl. 1): S88–S90.
256. Leypoldt JK, Henderson LW. Molecular charge influences transperitoneal macromolecule transport. Kidney Int 1933; 43: 837–844.

257. Myers BD, Guasch A. Selectivity of the glomerular filtration barrier in healthy and nephrotic humans. Am J Nephrol 1993; 13: 311–317.
258. Krediet RT, Koomen GC, Koopman MG et al. The peritoneal transport of serum proteins and neutral dextran in CAPD patients. Kidney Int 1989; 35: 1064–1072.
259. Vernier RL, Steffes MW, Sisson-Ross S, Mauer SM. Heparan sulfate proteoglycan in the glomerular basement membrane in type 1 diabetes mellitus. Kidney Int 1992; 41: 1070–1080.
260. Vernier RL, Klein DJ, Sisson SP, Mahan JD, Oegema TR, Brown DM. Heparan sulfate-rich anionic sites in the human glomerular basement membrane. N Engl J Med 1983; 309: 1001–1009.
261. Van-den-Heuvel LP, Van-den-Born J, Jalanko H et al. The glycosaminoglycan content of renal basement membranes in the congenital nephrotic syndrome of the Finnish type. Pediatr Nephrol 1992; 6: 10–15.
262. Washizawa K, Kasai S, Mori T, Komiyama A, Shigematsu H. Ultrastructural alteration of glomerular anionic sites in nephrotic patients. Pediatr Nephrol 1993; 7: 1–5.
263. Ramjee G, Coovadia HM, Adhikari M. Direct and indirect tests of pore size and charge selectivity in nephrotic syndrome. J Lab Clin Med 1996; 127: 195–199.
264. Rosenzweig LJ, Kanwar YS. Removal of sulfated (heparan sulfate) or nonsulfated (hyaluronic acid) glycosaminoglycans results in increased permeability of the glomerular basement membrane to ^{125}I–bovine serum albumin. Lab Invest 1982; 47: 177–184.
265. Wu VY, Wilson B, Cohen MP. Disturbances in glomerular basement membrane glycosaminoglycans in experimental diabetes. Diabetes 1987; 36: 679–683.
266. Van-den-Born J, Van-Kraats AA, Bakker MA et al. Reduction of heparan sulphate-associated anionic sites in the glomerular basement membrane of rats with streptozotocin induced diabetic nephropathy. Diabetologia 1995; 38: 1169–1175.
267. Galdi P, Shostak A, Jaichenko J, Fudin R, Gotloib L. Protamine sulfate induces enhanced peritoneal permeability to proteins. Nephron 1991; 57: 45–51.
268. Arfors KE, Rutili G, Svensjo E. Microvascular transport of macromolecules in normal and inflammatory conditions. Acta Physiol Scand Suppl 1979; 463: 93–103.
269. Gotloib L, Shostak A, Jaichenko J, Galdi P. Decreased density distribution of mesenteric and diaphragmatic microvascular anionic charges during murine abdominal sepsis. Resuscitation 1988; 16: 179–192.
270. Gotloib L, Shostak A, Galdi P, Jaichenko J, Fudin R. Loss of microvascular negative charges accompanied by interstitial edema in septic rats' heart. Circ Shock 1992; 36: 45–46.
271. Golloib L, Shostak A. Lessons from peritoneal ultrastructure: from an inert dialyzing sheet to a living membrane. Contrib Nephrol 1992; 100: 207–235.
272. Shostak A, Gotloib L. Increased mesenteric, diaphragmatic, and pancreatic interstitial albumin content in rats with acute abdominal sepsis. Shock 1998; 9: 135–137.
273. Gotloib L, Barzilay E, Shostak A, Lev A. Sequential hemofiltration in monoliguric high capillary permeability pulmonary edema of severe sepsis: preliminary report. Crit Care Med 1984; 12: 997–1000.
274. Gotloib L, Barzilay E, Shostak A, Wais Z, Jaichenko J, Lev A. Hemofiltration in septic ARDS. The artificial kidney as an artificial endocrine lung. Resuscitation 1986; 13: 123–132.
275. Klein NJ, Shennan GI, Heyderman RS, Levin M. Alteration in glycosaminoglycan metabolism and surface charge on human umbilical vein endothelial cells induced by cytokines, endotoxin and neutrophils. J Cell Sci 1992; 102: 821–832.
276. Bone RC. The pathogenesis of sepsis. Ann Intern Med 1991; 115: 457–469.
277. Bone RS. Immunologic dissonance: a continuing evolution in our understanding of the systemic inflammatory response syndrome (SIRS) and the multiple organ dysfunction syndrome (MODS). Ann Intern Med 1996; 125: 680–687.
278. Gotloib L, Wajsbrot V, Shostak A, Kushnier R. Population analysis of mesothelium *in situ* and *in vivo* exposed to bicarbonate-buffered peritoneal dialysis fluid. Nephron 1996; 73: 219–227.
279. Sirois MG, Edelman ER. VEGF effect on vascular permeability is mediated by synthesis of platelet-activating factor. Am J Physiol 1997; 272: H2746–H2756.
280. Ryan GB, Grobety J, Majno G. Mesothelial injury and recovery. Am J Pathol 1973; 71: 93–112.
281. Gabbiani G, Badonnel MC, Majno G. Intra-arterial injections of histamine, serotonin, or bradykinin: a topographic study of vascular leakage. Proc Soc Exp Biol Med 1970; 135: 447–452.
282. Ryan GB, Majno G. Acute inflammation. A review. Am J Pathol 1977; 86: 183–276.
283. Joris I, Majno G, Corey EJ, Lewis RA. The mechanism of vascular leakage induced by leukotriene E4. Endothelial contraction. Am J Pathol 1987; 126: 19–24.
284. Gardner TW, Lesher T, Khin S, Vu G, Barber AJ, Brennan WA Jr. Histamine reduces ZO-1 tight-junction protein expression in cultured retinal microvascular endothelial cells. Biochem J 1996; 320: 717–721.
285. Kevil CG, Payne DK, Mire E, Alexander JS. Vascular permeability factor/vascular endothelial cell growth factor mediated permeability occurs through disorganization of endothelial junctional proteins. J Biol Chem 1998; 273: 15099–15103.
286. Predescu D, Palade GE. Plasmalemmal vesicles represent the large pore system of continuous microvascular endothelium. Am J Physiol 1993; 265: H725–H733.
287. Esser S, Wolburg K, Wolburg H, Breier G, Kurzchalia T, Risau W. Vascular endothelial growth factor induces endothelial fenestrations *in vitro*. J Cell Biol 1998; 140: 947–959.
288. Feng D, Nagy JA, Hipp J, Pyne K, Dvorak AM. Reinterpretation of endothelial cell gaps induced by vasoactive mediators in guinea-pig, mouse and rat: many are transcellular pores. J Physiol (Lond) 1997; 504: 747–761.
289. Carlsson O, Nielsen S, Zakaria-el R, Rippe B. *In vivo* inhibition of transcellular water channels (aquaporin-1) during acute peritoneal dialysis in rats. Am J Physiol 1996; 271: H2254–H2262.
290. Panekeet MM, Mulder JB, Weening JJ, Struijk DG, Zweers MM, Krediet RT. Demonstration of aquaporin-CHIP in peritoneal tissue of uremic and CAPD patients. Perit Dial Int 1996; 16 (suppl. 1): S54–S57.
291. Schnitzer JE, Oh P. Aquaporin-1 in plasma membrane and caveolae provides mercury-sensitive water channels across lung endothelium. Am J Physiol 1996; 270: H416–H422.

292. Nielsen S, Smith BL, Christensen EL, Agre P. Distribution of the aquaporin CHIP in secretory and resorptive epithelia and capillary endothelia. Proc Natl Acad Sci U S A 1993; 90: 7275–7279.
293. Wintour EM. Water channels and urea transporters. Clin Exp Pharmacol Physiol 1997; 24: 1–9.
294. Ikomi F, Hunt J, Hanna G, Schmid-Schonbein GW. Interstitial fluid, plasma protein, colloid, and leukocyte uptake into initial lymphatics. J Appl Physiol 1996; 81: 2060–2067.
295. Rutili G, Parker JC, Taylor AE. Fluid balance in ANTU-injured lungs during crystalloid and colloid infusions. J Appl Physiol 1984; 56: 993–998.
296. Drake RE, Gabel JC. Abdominal lymph flow response to intraperitoneal fluid in awake sheep. Lymphology 1991; 24: 77–81.
297. Ottaviani G, Azzali G. Ultrastructure of lymphatic vessels in some functional conditions. In: Comel M, Laszt L, eds. Morphology and Histochemistry of the Vascular Wall. Basel: Karger, 1966, pp. 325.
298. Foldi M, Csanda E, Simon M et al. Lymphogenic haemangiopathy. 'Prelymphatic' pathways in the wall of cerebral and cervical blood vessels. Angiologica 1968; 5: 250–262.
299. Hauck G. The connective tissue space in view of the lymphology. Experientia 1982; 38: 1121–1122.
300. Crone G. Exchange of molecules between plasma, interstitial tissue and lymph. Pflugers Arch 1972; (suppl.): 65–79.
301. Casley-Smith JR. Lymph and lymphatics. In: Kaley G, Altura BM, eds. Microcirculation, Vol. 4. Baltimore, MD: University Park Press, 1981, pp. 423.
302. Schmid-Schonbein GW. Mechanisms causing initial lymphatics to expand and compress to promote lymph flow. Arch Histol Cytol 1990; 53 (suppl. 1): 107–114.
303. Rhodin JA, Sue SL. Combined intravital microscopy and electron microscopy of the blind beginnings of the mesenteric lymphatic capillaries of the rat mesentery. A preliminary report. Acta Physiol Scand Suppl 1979; 463: 51–58.
304. Jones WR, O'Morchoe CC, Jarosz HM, O'Morchoe PJ. Distribution of charged sites on lymphatic endothelium. Lymphology 1986; 19: 5–14.
305. Schmid-Schonbein GW. Microlymphatics and lymph flow. Physiol Rev 1990; 70: 987–1028.
306. Leak LV, Burke JF. Fine structure of the lymphatic capillary and the adjoining connective tissue area. Am J Anat 1966; 118: 785–809.
307. Leak LV, Burke JF. Electron microscopic study of lymphatic capillaries in the removal of connective tissue fluids and particulate substances. Lymphology 1968; 1: 39–52.
308. Gerli R, Ibba L, Fruschelli G. Ultrastructural cytochemistry of anchoring filaments of human lymphatic capillaries and their relation to elastic fibers. Lymphology 1991; 24: 105–112.
309. Taylor AE. The lymphatic edema safety factor: the role of edema dependent lymphatic factors (EDLF). Lymphology 1990; 23: 111–123.
310. Hogan RD, Unthank JL. The initial lymphatics as sensors of interstitial fluid volume. Microvasc Res 1986; 31: 317–324.
311. Leak V. Electron microscopic observations on lymphatic capillaries and the structural components of the connective tissue–lymph interface. Microvasc Res 1970; 2: 361–391.
312. Leak LV. The structure of lymphatic capillaries in lymph formation. Fed Proc 1976; 35: 1863–1871.
313. Shinohara H, Nakatani T, Matsuda T. Postnatal development of the ovarian bursa of the golden hamster (*Mesocricetus auratus*): its complete closure and morphogenesis of lymphatic stomata. Am J Anat 1987; 179: 385–402.
314. Hauck G. Capillary permeability and micro-lymph drainage. Vasa 1994; 23: 93–97.
315. McCallum WG. On the mechanisms of absorption of granular material from the peritoneum. Bull Johns Hopkins Hosp 1903; 14: 105–115.
316. Tsilibary EC, Wissig SL. Absorption from the peritoneal cavity. SEM study of the mesothelium covering the peritoneal surface of the muscular portion of the diaphragm. Am J Anat 1977; 149: 127–133.
317. Leak LV, Rahil K. Permeability of the diaphragmatic mesothelium. The ultrastructural basis for stomata. Am J Anat 1978; 151: 557–592.
318. Leak LV. Lymphatic endothelial–interstitial interface. Lymphology 1987; 20: 196–204.
319. Simer PM. Omental lymphatics in man. Anat Rec 1935; 63: 253–262.
320. Vajda J. Innervation of lymph vessels. Acta Morphol Acad Sci Hung 1966; 14: 197–208.
321. Hargens AR, Zweifach BW. Contractile stimuli in collecting lymph vessels. Am J Physiol 1977; 233: H57–H65.
322. Gnepp DR, Green FH. Scanning electron microscopic study of canine lymphatic vessels and their valves. Lymphology 1980; 13: 91–99.
323. Ohtani O. Structure of lymphatics in rat cecum with special reference to submucosal collecting lymphatics endowed with smooth muscle cells and valves. I. A scanning electron microscopic study. Arch Histol Cytol 1992; 55: 429–436.
324. Moller R. Arrangement and fine structure of lymphatic vessels in the human spermatic cord. Andrologia 1980; 12: 564–576.
325. Zweifach BW, Prather JW. Micromanipulation of pressure in terminal lymphatics in the mesentery. Am J Physiol 1975; 228: 1326–1335.
326. Horstmann E. Anatomie und Physiologie des lymphgefa B systems im bauchraum. In: Bartelheimer H, Heising N, eds. Actuelle Gastroenterologie. Stuttgart: Verh, Thieme, 1968, p. 1.
327. Ohhashi T, Azuma T, Sakaguchi M. Active and passive mechanical characteristics of bovine mesenteric lymphatics. Am J Physiol 1980; 239: H88–H95.
328. Watanabe N, Kawai Y, Ohhashi T. Demonstration of both B1 and B2 adrenoreceptors mediating negative chronotropic effects on spontaneous activity in isolated bovine mesenteric lymphatics. Microvasc Res 1990; 39: 50–59.
329. Ohhashi T, Azuma T. Sympathetic effects on spontaneous activity in bovine mesenteric lymphatics (retracted by Ohhashi T, Azuma T. In: Am J Physiol 1986; 251: H226). Am J Physiol 1984; 247: H610–H615.
330. Ohhashi T, Azuma T. Pre and postjunctional alpha-adrenoceptors at the sympathetic neuroeffector junction in bovine mesenteric lymphatics. Microvac Res 1986; 31: 31–40.
331. Watanabe N, Kawai Y, Ohhashi T. Dual effects of histamine on spontaneous activity in isolated bovine mesenteric lymphatics. Microvasc Res 1988; 36: 239–249.
332. Ferguson MK, Shahinian HK, Michelassi F. Lymphatic smooth muscle responses to leukotrienes, histamine and platelet activating factor. J Surg Res 1988; 44: 172–177.

333. Ohhashi T, Kawai Y, Azuma T. The response of lymphatic smooth muscles to vasoactive substances. Pflugers Arch 1978; 375: 183–188.
334. Azuma T, Ohhashi T, Roddie IC. Bradykinin-induced contractions of bovine mesenteric lymphatics. J Physiol (Lond) 1983; 342: 217–227.
335. Ohhashi T, Olschowka JA, Jacobowitz DM. Vasoactive intestinal peptide inhibitory innervation in bovine mesenteric lymphatics. A histochemical and pharmacological study. Circ Res 1983; 53: 535–538.
336. Abu-Hiljeh MF, Habbai OA, Moqattash ST. The role of the diaphragm in lymphatic absorption from the peritoneal cavity. J Anat 1995; 186: 453–467.
337. Fruschelli G, Gerli R, Alessandrini G, Sacchi G. II controllo neurohumorale dalla contratilita dei vasi linfatici. In: Atti dalla Societa Italiana di Anatomia. 39th Convegno Nazaionale, 19/21 September. Firenze: I Sedicesimo, 1983, p. 2.
338. Starling EH, Tubby A. On absorption from and secretion into the serous cavities. J Physiol (Lond) 1894; 16: 140–155.
339. Starling EH. On the absorption of fluid from the connective tissue spaces. J Physiol (Lond) 1896; 19: 312–321.
340. Drinker CF, Field ME. The protein of mammalian lymph and the relation of lymph to tissue fluid. Am J Physiol 1931; 97: 32–45.
341. Allen L, Vogt E. Mechanisms of lymphatic absorption from serous cavities. Am J Physiol 1937; 119: 776–782.
342. Brace RA, Guyton AC. Interstitial fluid pressure: capsule, free fluid, gel fluid and gel absorption pressure in subcutaneous tissue. Microvasc Res 1979; 18: 217–228.
343. Guyton AC, Granger HJ, Taylor AE. Interstitial fluid pressure. Physiol Rev 1971; 51: 527–563.
344. Guyton AC, Taylor AE, Granger HJ, Gibson WH. Regulation of interstitial fluid volume and pressure. Adv Exp Med Biol 1972; 33: 111–118.
345. Guyton AC, Taylor AE, Brace RA. A synthesis of interstitial fluid regulation and lymph formation. Fed Proc 1976; 35: 1881–1885.
346. Zink J, Greenway CV. Intraperitoneal pressure in formation and reabsorption of ascites in cats. Am J Physiol 1977; 233: H185–H190.
347. Zink J, Greenway CV. Control of ascites absorption in anesthetized cats: effects of intraperitoneal pressure, protein, and furosemide diuresis. Gastroenterology 1977; 73: 119–124.
348. Imholz AL, Koomen GC, Struijk DG, Arisz L, Krediet RT. Effect of an increased intraperitoneal pressure on fluid and solute transport during CAPD. Kidney Int 1993; 44: 1078–1085.
349. Durand PY, Chanliau J, Gamberoni J, Hestin D, Kessler M. Intraperitoneal pressure, peritoneal permeability and volume of ultrafiltration in CAPD. Adv Perit Dial 1992; 8: 22–25.
350. Gotloib L, Garmizo AL, Varka I, Mines M. Reduction of vital capacity due to increased intra-abdominal pressure during peritoneal dialysis. Perit Dial Bull 1981; 1: 63–64.
351. Flessner MF. Net ultrafiltration in peritoneal dialysis: role of direct fluid absorption into peritoneal tissue. Blood Purif 1992; 10: 136–147.
352. Flessner MF, Parker RJ, Sieber SM. Peritoneal lymphatic uptake of fibrinogen and erythrocytes in the rat. Am J Physiol 1983; 244: H89–H96.
353. Silk YN, Goumas WM, Douglass HO Jr, Huben RP. Chylous ascites and lymphocyst management by peritoneovenous shunt. Surgery 1991; 110: 561–565.
354. Casley Smith JR. A fine structural study of variations in protein concentration in lacteals during compression and relaxation. Lymphology 1979; 12: 59–65.
355. O'Morchoe CC, Jones WR 3d, Jarosz HM, O'Morchoe PJ, Fox LM. Temperature dependence of protein transport across lymphatic endothelium *in vitro*. J Cell Biol 1984; 98: 629–640.
356. Dobbins WO, Rollins EL. Intestinal mucosal lymphatic permeability: an electron microscopic study of endothelial vesicles and cell junctions. J Ultrastruct Res 1970; 33: 29–59.
357. Shasby DM, Peterson MW. Effects of albumin concentration on endothelial albumin transport *in vitro*. Am J Physiol 1987; 253: H654–H661.
358. Albertini KH, O'Morchoe CC. Renal lymphatic ultrastructure and translymphatic transport. Microvasc Res 1980; 19: 338–351.
359. Von Recklinghausen F. Über Eiter-Bindegewebskörperchen. Virchows Arch Pathol Anat 1863; 28: 157–166.
360. Seifert E. Zur Biologie des menschlichen grossen Netzes. Arch Klin Chir 1921; 116: 510–517.
361. Koten JW, Den Otter W. Are omental milky spots an intestinal thymus? Lancet 1991; 338: 1189–1190.
362. Garosi G, Di Paolo N. Recent advances in peritoneal morphology: the milky spots in peritoneal dialysis. Adv Perit Dial 2001; 17: 25–28.
363. Di Paolo N, Sacchi G, Garosi G, Sansoni E, Bargagli L, Ponzo P, Tanganelli P, Gaggiotti E. Omental milky spots. Review and personal experience. Perit Dial Int 2005; 25: 48–57.
364. Haller A. Primae linae physiologiae in usum Praelectionum Academicarum avetae et emendato. Gottingae, Capit 25, 1751, p. 41.
365. Furness JB. Arrangement of blood vessels and their relation with adrenergic nerves in the rat mesentery. J Anat 1973; 115: 347–364.
366. Beattie JM. The cells of inflammatory exudations: an experimental research as to their function and density, and also as to the origin of the mononucleated cells. J Pathol Bacteriol 1903; 8: 130–177.
367. Durham HE. The mechanism of reaction to peritoneal infection. J Pathol Bacteriol 1897; 4: 338–382.
368. Josey AL. Studies in the physiology of the eosinophil. V. The role of the eosinophil in inflammation. Folia Haematol 1934; 51: 80–95.
369. Webb RL. Changes in the number of cells within the peritoneal fluid of the white rat, between birth and sexual maturity. Folia Haematol 1934; 51: 445–451.
370. Padawer J, Gordon AS. Cellular elements in the peritoneal fluid of some mammals. Anat Rec 1956; 124: 209–222.
371. Fruhman GJ. Neutrophil mobilization into peritoneal fluid. Blood 1960; 16: 1753–1761.
372. Seeley SF, Higgins GM, Mann FC. The cytologic response of the peritoneal fluid to certain substances. Surgery 1937; 2: 862–876.
373. Bercovici B, Gallily R. The cytology of the human peritoneal fluid. Cytology 1978; 22: 124.
374. Becker S, Halme J, Haskill S. Heterogeneity of human peritoneal macrophages: cytochemical and flow cytometric studies. J Reticuloendothel Soc 1983; (ES) 33: 127–138.
375. De Brux JA, Dupre-Froment J, Mintz M. Cytology of the peritoneal fluids sampled by coelioscopy or by cul de sac puncture. Its value in gynecology. Acta Cytol 1968; 12: 395–403.

376. Mahoney CA, Sherwood N, Yap EH, Singleton TP, Whitney DJ, Cornbleet PJ. Ciliated cell remnants in peritoneal dialysis fluid. Arch Pathol Lab Med 1993; 117: 211–213.
377. Fruhmann GJ. Adrenal steroids and neutrophil mobilization. Blood 1962; 20: 335–363.
378. Spriggs AI, Boddington MM. The Cytology of Effusions, 2nd edn. New York: Grune & Straton, 1968, pp. 5–17.
379. Domagala W, Woyke S. Transmission and scanning electron microscopic studies of cells in effusions. Acta Cytol 1975; 19: 214–224.
380. Efrati P, Nir E. Morphological and cytochemical investigation of human mesothelial cells from pleural and peritoneal effusions. A light and electron microscopy study. Isr J Med Sci 1976; 12: 662–673.
381. Bewtra Ch, Greer KP. Ultrastructural studies of cells in body cavity effusions. Acta Cytol 1985; 29: 226–238.
382. Chapman JS, Reynolds RC. Eosinophilic response to intraperitoneal blood. J Lab Clin Med 1958; 51: 516–520.
383. Northover BJ. The effect of various anti-inflammatory drugs on the accumulation of leucocytes in the peritoneal cavity of mice. J Pathol Bacteriol 1964; 88: 332–335.
384. Hurley JV, Ryan GB, Friedman A. The mononuclear response to intrapleural injection in the rat. J Pathol Bacteriol 1966; 91: 575–587.
385. Rubin J, Rogers WA, Taylor HM et al. Peritonitis during continuous ambulatory peritoneal dialysis. Ann Intern Med 1980; 92: 7–13.
386. Cichoki T, Hanicki Z, Sulowicz W, Smolenski O, Kopec J, Zembala M. Output of peritoneal cells into peritoneal dialysate. Cytochemical and functional studies. Nephron 1983; 35: 175–182.
387. Strippoli P, Coviello F, Orbello G et al. First exchange neutrophilia is not always an index of peritonitis during CAPD. Adv Perit Dial 1989; 4: 121–123.
388. Kubicka U, Olszewski WL, Maldyk J, Wierzbicki Z, Orkiszewska A. Normal human immune peritoneal cells: phenotypic characteristics. Immunobiology 1989; 180: 80–92.
389. Gotloib L, Mines M, Garmizo AL, Rodoy Y. Peritoneal dialysis using the subcutaneous intraperitoneal prosthesis. Dial Transplant 1979; 8: 217–220.
390. Hoeltermann W, Schlotmann-Hoelledr E, Winkelmann M, Pfitzer P. Lavage fluid from continuous ambulatory peritoneal dialysis. A model for mesothelial cell changes. Acta Cytol 1989; 33: 591–594.
391. Chan MK, Chow L, Lam SS, Jones B. Peritoneal eosinophilia in patients on continuous ambulatory peritoneal dialysis: a prospective study. Am J Kidney Dis 1988; 11: 180–183.
392. Gokal R, Ramos JM, Ward MK, Kerr DN. 'Eosinophilic' peritonitis in continuous ambulatory peritoneal dialysis (CAPD). Clin Nephrol 1981; 15: 328–330.
393. Leak LV. Interaction of mesothelium to intraperitoneal stimulation. Lab Invest 1983; 48: 479–490.
394. Raftery AT. Regeneration of parietal and visceral peritoneum: an electron microscopical study. J Anat 1973; 115: 375–392.
395. Raftery AT. Mesothelial cells in peritoneal fluid. J Anat 1973; 115: 237–253.
396. Koss LG. Diagnostic Cytology and Its Histopathologic Bases, 3rd edn. Philadelphia, PA: Lippincot, 1979, chs 16–25.
397. Whitaker D, Papadimitriou J. Mesothelial healing: morphological and kinetic investigations. J Pathol Bacteriol 1957; 73: 1–10.
398. Gotloib L, Shostak A, Wajsbrot V, Kushnier R. High glucose induces a hypertrophic, senescent mesothelial cell phenotype after long in-vivo exposure. Nephron 1999; 82: 164/173.
399. Shostak A, Wajsbrot V, Gotloib L. High glucose accelerates the life cycle of the in-vivo exposed mesothelium". Kidney Int 2000; 58: 2044–2052.
400. Renvall SY. Peritoneal metabolism and intrabdominal adhesion formation during experimental peritonitis. Acta Chir Scand Suppl 1980; 503: 1–48.
401. Ellis H, Harrison W, Hugh TB. The healing of peritoneum under normal and pathological conditions. Br J Surg 1965; 52: 471–476.
402. Ellis H. The cause and prevention of postoperative intraperitoneal adhesions. Surg Gynecol Obstet 1971; 133: 497–511.
403. Whitaker D, Papadimitriou J. Mesothelial healing: morphological and kinetic investigations. J Pathol 1985; 145: 159–175.
404. Ryan GB, Grobety J, Majno G. Postoperative peritoneal adhesions: a study of the mechanisms. Am J Pathol 1971; 65: 117–148.
405. Walters WB, Buck RC. Mitotic activity of peritoneum in contact with a regenerative area of peritoneum. Virchows Arch B Zellpathol 1973; 13: 48–52.
406. Johnson FR, Whitting HW. Repair of parietal peritoneum. Br J Surg 1962; 49: 653–660.
407. Watters WB, Buck RC. Scanning electron microscopy of mesothelial regeneration in the rat. Lab Invest 1972; 26: 604–609.
408. Cameron GR, Hassan SM, De SN. Repair of Glisson's capsule after tangential wounds on the liver. J Pathol Bacteriol 1957; 73: 1–10.
409. Eskeland G. Regeneration of parietal peritoneum in rats. A light microscopical study. Acta Pathol Microbiol Scand 1966; 68: 355–378.
410. Di Paolo N, Vanni L, Sacchi G. Autologous implant of peritoneal mesothelium in rabbits and man. Clin Nephrol 1991; 57: 323–331.
411. Foley-Comer AJ, Herrick SA, Al-Mishlab T, Prele CM, Laurent GJ, Mutsaers SE. Evidence for incorporation of free-floating mesothelial cells as a mechanism of serosal healing. J Cell Sci 2002; 115: 1383–1389.
412. Williams DC. The peritoneum. A plea for a change in attitude towards this membrane. Br J Surg 1955; 42: 401–405.
413. Shaldon S. Peritoneal macrophage: the first line of defense. In: La Greca G, Chiaramonte S, Fabris A, Feriani M, Ronco G, eds. Peritoneal Dialysis. Milan: Wichtig. Ed, 1986, p. 201.
414. Eskeland G, Kjaerheim A. Regeneration of parietal peritoneum in rats. 2. An electron microscopical study. Acta Pathol Microbiol Scand 1966; 68: 379–395.
415. Raftery AT. Regeneration of parietal and visceral peritoneum. A light microscopical study. Br J Surg 1973; 60: 293–299.
416. Yung S, Thomas GJ, Davies M. Induction of hyaluronan metabolism after mechanical injury of peritoneal cells in vitro. Kidney Int 2000; 58: 1953–1962.
417. Yung S, Davies M. Response of human peritoneal cell to injury: an in vitro model of peritoneal wound healing. Kidney Int 1998; 54: 2160–2169.
418. Horiuchi T, Miyamoto K, Miyamoto S, Fujita M, Sano N et al. Image analysis of remesothelialization following chemical wounding of cultured human peritoneal cells: the role of hyaluronan synthesis. Kidney Int 2003; 64: 2280–2290.
419. Gotloib l, Wajsbrot V, Shostak A, Khrizman V. Repopulation of the mesothelial monolayer during long-term experimental peritoneal dialysis. Contrib Nephrol 2006; 150: 54–61.
420. Gotloib L, Wajsbrot V, Shostak A. Acute oxidative stress induces peritoneal hypermeability, mesothelial loss and fibrosis. Perit Dial Int 2002; 22 (suppl. 1): S9.

421. Gotloib L, Shostak A, Bar Sella P, Kohen R. Continuous mesothelial injury and regeneration during long-term peritoneal dialysis. Perit Dial Bull 1987; 7: 148–155.
422. Kawamoto K, Okada T, Kannan Y, Ushio H, Matsumoto M, Matsuda H. Nerve growth factor prevents apoptosis of rat peritoneal masts cells through the trk proto-oncogene receptor. Blood 1995; 15: 4638–4644.
423. Gotloib L, Shostak A, Wajsbrot V. Detrimental effects of peritoneal dialysis solutions upon in vitro and in situ exposed mesothelium. Perit Dial Int 1997; 17 (suppl. 2): S13–S16.
424. Gotloib L, Wajsbrot V, Shostak A, Kushnier R. Effects of hyperosmolarity upon the mesothelial monolayer exposed in-vivo and in-situ to a mannitol enriched dialysis solution. Nephron 1999; 81: 301–309.
425. Gotloib L, Wajsbrot V, Shostak A. Ecology of the peritoneum: a substantial role for the osmotic agents resulting in apoptosis of mesothelial cells. Contrib Nephrol 2003; 140: 10–17.
426. Schneble F, Bonzel KE, Waldherr R, Bachman S, Roth H, Scharer K. Peritoneal morphology in children treated by continuous ambulatory peritoneal dialysis. Pediatr Nephrol 1992; 6: 542–546.
427. Garossi G, Di Paolo N. Pathophysiology and morphological clinical correlation in experimental and peritoneal dialysis-induced peritoneal sclerosis. Adv Perit Dial 2000; 16: 204–207.
428. Garossi G, Di Paolo N. Morphological aspects of peritoneal sclerosis. J Nephrol 2001; 14 (suppl. 4): 30–38.
429. Mactier RA. The spectrum of peritoneal fibrosing syndromes in peritoneal dialysis. Adv Perit Dial 2000; 16: 223–228.
430. Flessner MF. The effect of fibrosis on peritoneal transport. Contrib Nephrol 2006; 150: 174–180.
431. Gotloib L, Wajsbrot V, Shostak A. A short review of experimental peritoneal sclerosis: from mice to men". Int J Artif Organs 2005; 28: 97–104.
432. Yung S, Li FK, Chan TM. Peritoneal mesothelial cell culture and biology. Perit Dial Int 2006; 26: 162–173.
433. Aroeira LS, Aguilera A, Sanchez-Tomero JA, Bajo MA, Del Peso G, Jimenez-Heffernan JA, Selgas R, Lopez-Cabrera M. Epithelial to mesenchymal transition and peritoneal membrane failure in peritoneal dialysis patients: pathologic significance and potential therapeutic interventions. J Am Soc Nephrol 2007; 18: 2004–2013.
434. Garosi G, Di Paolo N. Peritoneal sclerosis. An overview. Adv Perit Dial 1999; 15: 85–192.
435. Mateijsen MAM, Van der Wal AC, Hendricks PMEM, Zweers MM, Mulder J, Strujik DG, Krediet RT. Vascular and interstitial changes in the peritoneum of CAPD patients with peritoneal sclerosis. Perit Dial Int 1999; 19: 517–525.
436. Williams JD, Craig KJ, Topley N, Von Ruhland C, Fallon M, Newman GR, Mackenzie RK, Williams GT. Morphological changes in the peritoneal membrane of patients with renal disease. J Am Soc Nephrol 2002; 13: 470–479.
437. Bladier G, Wolvetang EJ, Mutchinson P, de-Haan JB, Kola I. Response of a primary human fibroblast cell line to H2O2: senescence-like growth arrest or apoptosis? Cell Growth Differ 1997; 8: 588–598.
438. Dypbuki JM, Ankarcrona M, Burkitt M, Sjoholm A, Strom K, Orrenius S, Nicotera P. Different pro-oxidant levels stimulate growth, trigger apoptosis or produce necrosis of insulin-secreting RINm5F cells. The role of intracellular polyamines. J Biol Chem 1994; 269: 30553–30560.
439. Ryter SW, Kim HP, Hoetzel A, Park JW, Nakahira K, Wang X, Choi AMK. Mechanisms of cell death in oxidative stress. Antioxid Redox Signal 2007; 9: 49–89.
440. Nilsson-Thorell CB, Nuscalu N, Andren AH, Kjellstrand PT, Wieslander AP. Heat sterilization of fluids for peritoneal dialysis gives rise to aldehydes. Perit Dial Int 1993; 13: 208–213.
441. Miyata T, Horie K, Ueda Y, Fujita Y, Izuhara Y, Hirano H, Uchida K, Saito A, Van Ypersele de Strihou C, Kurokawa K. Advanced glycation and lipoxidation of the peritoneal membrane: respective roles of serum and peritoneal fluid reactive carbonyl compounds. Kidney Int 2000; 58: 425–435.
442. Santini SA, Cotroneo P, Marra G, Manto A, Giardina B, Mordent A, Greco AV, Martorana GE, Magnani P, Ghirlanda G. Na/K ATPase impairement and experimental glycation: the role of autoxidation. Free Radic Res 1996; 24: 381–389.
443. Ishibashi Y, Sugimoto T, Ichikawa Y, Akatsuka A, Miyata T, Nangaku M, Tagawa H, Kurokawa K. Glucose dialysate induces mitochondrial DNA damage in peritoneal mesothelial cells. Perit Dial Int 2002; 22: 11–21.
444. Gotloib L, Wajsbrot V, Shostak A. Mesothelial dysplastic changes and lipid peroxidation induced by 7.5% Icodextrin. Nephron 2002; 92: 142–155.
445. Gotloib L, Wajsbrot V, Shostak A. Icodextrin induced lipid peroxidation disrupts the mesothelial cell cycle engine. Free Radic Biol Med 2003; 34: 419–428.
446. Ueda Y, Miyata T, Goffin E, Yoshino A, Inagi R, Ishibashi Y, Izuhara Y, Saito A, Kurokawa K, Van Ypersele de Strihou C. Effect of dwell time on carbonyl stress using Icodextrin and aminoacid peritoneal dialysis fluids. Kidney Int 2000; 58: 2529–2534.
447. Shostak A, Pivnik C, Gotloib L. Cultured rat mesothelial cells generate hydrogen peroxide: a new player in peritoneal defense?" J Am Soc Nephrol 1996; 7: 2371–2378.
448. Gotloib L, Wajsbrot V, Cuperman Y, Shostak A. Acute oxidative stress induces peritoneal hyperpermeability, mesothelial loss and fibrosis. J Lab Clin Med 2004; 143: 31–40.
449. Friemann J, Muller KM, Pott F. Mesothelial proliferation due to asbestos and man-made fibres. Experimental studies on rat omentum. Pathol Res Pract 1990; 186: 117–123.
450. Imai H, Nakamoto H, Ishida Y, Inone T, Kanno Y, Okada H, Suzuki S, Okano H, Suzuki H. Glucocorticoid restores the deterioration of water transport in the peritoneum through increment in aquaporin. Adv Perit Dial 2000; 16: 297–302.
451. Park SE, Twardowski ZJ, Moore HL, Khanna R, Nolph KD. Chronic administration of iron dextran into the peritoneal cavity of rats. Perit Dial Int 1997; 17: 179–185.
452. Zareie M, Hekking LHP, Welten AGA, Driesprong BAJ, Schadee-Eestermans IL, Faret D, Leyssens A, Schalkwijk CG, Beelen RMJ, Ter Wee PM, Van den Born J. Contribution of lactate buffer, glucose and glucose degradation products to peritoneal injury in vivo. Nephrol Dial Transplant 2003; 8: 2629–2637.
453. Combet S, Ferrier ML, Van Landschoot M, Stoenoiu M, Moulin P, Miyata T, Lameire N, Devuyst O. Chronic uremia induces permeability changes, increased mitric oxidative synthase expression and structural modifications of the peritoneum. J Am Soc Nephrol 2001; 12: 2146–2157.

454. Levine S, Saltzman A. Repeated toxic injury of the peritoneum: accumulation of toxicity and adaptation to injury. J Appl Toxicol 2000; 20: 431–434.
455. Margetts PJ, Kolb M, Yu L, Hoff CM, Gaultie J. A chronic inflammatory infusion of peritoneal dialysis in rats. Perit Dial Int 2001; 21 (suppl. 3): S368–S372.
456. Nakamoto H, Imai H, Ishida Y, Yamanouchi Y, Inoue T, Okada H, Suzuki H. New animal models for encapsulating peritoneal sclerosis. Role of acidic solution. Perit Dial Int 2001; 21 (suppl. 3): S349–S353.
457. Levine S, Saltzman A. Peritoneal toxicity to water: a model of chemical peritonitis caused by osmotic disequilibrium in rats. J Appl Toxicol 2001; 21: 303–306.
458. Fang CC, Lai MN, Chien CT, Hung KY, Tsai CC, Tsai TJ, Hsien BS. Effects of pentoxyfilline on peritoneal fibroblasts and silica-induced peritoneal fibrosis. Perit Dial Int 2003; 23: 228–236.
459. Van der Vliet A, Van der Poel KI, Bast A. Intestinal smooth muscle dysfunction after intraperitoneal injection of zymosan in the rat: are oxygen radicals involved? Gut 1992; 33: 336–341.
460. Panduri V, Weitzman SA, Chandel NS, Kamp DW. Mitochondrial-derived free radicals mediate asbestos-induced alveolar epithelial cell apoptosis. Am J Physiol Lung Cell Mol Physiol 2004; 286: L1220–L1127.
461. Oyama Y, Sakai H, Arata T, Okano Y, Akaide N, Sakal K, Noda K. Cytotoxic effects of methanol, formaldehyde and formate on dissociated rat thymocytes: a possibility of aspartame toxicity. Cell Biol Toxicol 2002; 18: 43–50.
462. Shangari N, O'Brien PJ. The cytotoxic mechanism of glyoxal involves oxidative stress. Biochem Pharmacol 2004; 68: 1433–1442.
463. Zavodnik IB, Lapshina EA, Zavodnik LB, Labieniec C, Bryszewska M, Reiter RJ. Hypochlorous acid-induced oxidative stress in Chinese hamster B14 cells: viability, DNA and protein damage and the protective effect of melatonin. Mutat Res 2004; 559: 39–48.
464. Galleano M, Aimo L, Puntarulo S. Ascorbyl radical/ascorbate ratio in plasma from iron overloaded rats as oxidative stress indicator. Toxicol Lett 2002; 133: 193–201.
465. Sulliman HB, Welty-Wolf KE, Carraway M, Tatro L, Piantadosi CA. Lipopolysaccharide induces oxidative cardiac mitochondrial damage and biogenesis. Cardiovasc Res 2004; 64: 279–288.
466. Fubini B, Hubbard A. Reactive oxygen species (ROS) and reactive nitrogen species (RNS) generation by silica in inflammation and fibrosis. Free Radic Biol Med 2003; 34: 1507–1516.
467. Aoshiba K, Yasuda K, Yasui S, Tamaoki J, Nagai A. Serine proteases increase oxidative stress in lung cells. Am J Physiol Lung Cell Mol Physiol 2001; 281: L556–L564.
468. Zhang Z, Dimitrieva NI, Park JH, Levine RL, Curg MB. High urea and NaCl carbonylate proteins in renal cells in culture and in vivo, and high urea causes 8-oxoguananine lesions in their DNA. Proc Natl Acad Sci U S A 2004; 101: 9491–9496.
469. Antolini F, Valente F, Ricciardi D, Fagugli RM. Normalization of oxidative stress parameters after kidney transplant is secondary to full recovery of renal function. Clin Nephrol 2004; 62: 131–137.
470. Sama R 2nd, Blaydes B, Warbritton A, Lomax LD, Bucci T, Delclos KB. Differences in the response to oxidative stress and mutant frequency in CD (Sprague-Dawley) and Fisher 344 rats due to an induced inflammatory response. Environ Mol Mutagen2000; 35: 336–342.
471. Tan RJ, Fattman CL, Watkins SC, Oury TD. Redistribution of pulmonary EC-SOD after exposure to asbestos. J Appl Physiol 2004; 97: 2006–2013.
472. Shostak A, Gotloib L, Kushnier R, Wajsbrot V. Protective effect of pyruvate upon cultured mesothelial cells exposed to 2 mM hydrogen peroxide. Nephron 2000; 84: 362–366.
473. Diaz-Buxo JA, Gotloib L. Agents that modulate peritoneal membrane structure and function. Perit Dial Int 2007; 27: 16–30.
474. Dobbie JW. Pathogenesis of peritoneal fibrosing syndromes (sclerosing peritonitis) in peritoneal dialysis. Perit Dial Int 1992; 12: 14–27.
475. Verger G, Celicout B, Larpent L, Goupil A. Encapsulating peritonitis during continuous ambulatory peritoneal dialysis. A physio-pathologic hypothesis. Presse Med 1986; 15: 1311–1314.
476. Gandhi VC, Humayun HM, Ing TS et al. Sclerotic thickening of the peritoneal membrane in maintenance peritoneal dialysis patients. Arch Intern Med 1980; 140: 1201–1203.
477. Slingeneyer A, Mion G, Mourad G, Canaud B, Faller B, Beraud JJ. Progressive sclerosing peritonitis: a late and severe complication of maintenance peritoneal dialysis. Trans Am Soc Artif Intern Organs 1983; 29: 633–640.
478. Di Paolo N, Garossi G. Peritoneal sclerosis. J Nephrol 1999; 12: 347–361.
479. Garosi G, Di Paolo N. Peritoneal sclerosis: one or two nosological entities? Semin Dial 2000; 13: 297–308.
480. Garosi G. Different aspects of peritoneal sclerosis. Contrib Nephrol 2006; 140: 18–29.
481. Di Paolo N, Sacchi G, Lorenzoni P, Sansoni E, Gaggiotti E. Ossification of the peritoneal membrane. Perit Dial Int 2004; 24: 471–477.
482. Di Paolo N, Di Paolo M, Tanganelli P, Brardi S, Bruci A. Technique Nefrologiche e Dialitici. Perugia: Bios Editore, 1988, p. 5.
483. Mc Laughling K, Butt G, Madi A, Mc Millan R, Mactier R. Sclerosing peritonitis occurring in a hemodialysis patient. Am J Kidney Dis 1996; 27: 729–732.
484. Foo KT, Ng-Kc, Rauff A, Foong WC, Sinniah R. Unusual small intestinal obstruction in adolescent girls: the abdominal cocoon. Br J Surg 1978; 65: 427–430.
485. Narayanan R, Kabra SG, Bhargava BN, Sangal BC. Idiopathic sclerosing encapsulating peritonitis. Lancet 1989; ii: 127–129.
486. Lee RE, Baddeley H, Marshall AJ, Read AE. Practolol peritonitis. Clin Radiol 1977; 28: 119–128.
487. Harty RF. Sclerosing peritonitis and propranolol. Arch Intern Med 1978; 138: 1424–1426.
488. Baxter-Smith DC, Monypenny IJ, Dorricott NJ. Sclerosing peritonitis in patient on timolol. Lancet 1978; 2: 149.
489. Clarck CV, Terris R. Sclerosing peritonitis associated with metoprolol. Lancet 1983; 1: 937.
490. Marigold JH, Pounder RE, Penberton J, Thompson RP. Propanolol, oxprenolol and sclerosing peritonitis. Brit Med J 1982; 284: 870.
491. Phillips RK, Dudley HA. The effect of tetracycline lavage and trauma on visceral and parietal peritoneal ultrastructure and adhesion formation. Br J Surg 1984; 71: 537–539.
492. Vorhauer W, Biere J, Passa PH, Charleux H, Chelloul N. Encapsulating peritonitis symptomatic of gastric carcinoma. Sem Hop 1976; 52: 1715–1718.

493. Marusawa H, Katsurada A, Takaya H, Kumegawa Y, Kajimura K, Yamashita Y. A case of encapsulating peritonitis associated with pancreatic ascites induced by carcinoma of pancreas. Lutheinized thecoma with sclerosing peritonitis. Arch Pathol Lab Med 1996; 120: 303–306.
494. Gold RS, Mucha SJ. Unique case of mesenteric fibrosis in multiple polyposis. Am J Surg 1975; 130: 366–369.
495. Sufrin G, Chason S, Golio A, Murphy J. Paraneoplastic and serologic syndrome of renal carcinoma. Semin Urol 1989; 7: 158–171.
496. Werness BA, Hansen RM, Komaki R, Hanson GA, Schleuter DP, Anderson T. Indolent diffuse histiocytic lymphoma with sclerosis and chylous effusions. Cancer 1983; 51: 2144–2146.
497. Stenram U. Sclerosing peritonitis in a case of benign ovarian teratoma: a case report. APMIS 1997; 105: 414–416.
498. Lin CH, Yu JC, Chen TW, Chan DC, Chen CJ, Hsieh CB. Sclerosing encapsulating peritonitis in a liver transplant patient: a case report. World J Gastroenterol 2005; 11: 5412–5413.
499. Cohen O, Abrahamson J, Ben-Ari J, Frajewicky V, Eldar S. Sclerosing encapsulating peritonitis. J Clin Gastroenterol 1996; 22: 45–47.
500. Greenlee HB, Stanley MM, Reinhardt GF, Chejfec G. Small bowel obstruction (SBO) from compression and kinking of intestine by thickened peritoneum in cirrhotics with ascites treated with Le Veen shunt (abstract). Gastroenterology 1979; 76: 1282.
501. Buhac I, Jarmolych J. Histology of the intestinal peritoneum in patients with cirrhosis of the liver and ascites. Dig Dis 1978; 23: 417–422.
502. Abul S, Al-Oazweni H, Zalat S, Al-Sumait B, Asfar S. Cocoon abdomen in a liver transplant transplant patient. J R Coll Surg Edinb 2002; 47: 579–581.
503. Raftery AT. Regeneration of parietal and visceral peritoneum: an electron microscopic study. Br J Surg 1973; 115: 375–392.
504. Herrick SE, Mutsaers SE. Mesothelial progenitor cells and their potential in tissue engineering. Int J Biochem Cell Biol 2004; 36: 621–642.
505. Gotloib L, Gotloib LC, Khrizman V. The use of peritoneal mesothelium as a potential source of adult stem cells. Int J Artif Organs 2007; 30: 501–512.
506. Donna A, Beteta PG. Differentiation towards cartilage and bone in a primary tumor of pleura. Further evidence in support of the concept of mesodermoma. Histopathology 1986; 10: 101–108.
507. Kyozuka Y, Miyazaki H, Yoshizawa K, Senzaki H, Yamamoto D, Inoue K. An autopsy case of malignant mesothelioma with osseous and cartilaginous differentiation: bone morphogenetic protein-2 in mesothelial cells and its tumor. Dig Dis Sci 1999; 44: 1626–1631.
508. Rittinghausen S, Ernst H, Muhle H, Mohr V. Atypical malignant mesotheliomas with osseous and cartilaginous differentiation after intraperitoneal injection of various types of mineral fibres in rats. Exp Toxicol Pathol 1992; 44: 55–58.
509. De Bari C, Dell'Accio F, Tylzanowski P, Luyten FP. Multipotent mesenchymal stem cells from adult humal synovial membrane. Arthritis Rheum 2001; 44: 1928–1942.
510. Vandenabeele F, De Basi C, Moreels M, Lambrichts I, Dell'Accio F, Lippens L, Luyten FP. Morphological and immunocytochemical characterization of cultured fibroblast-like cells derived from adult human synovial membrane. Arch Histol Cytol 2003; 66: 145–153.
511. Dobbie JW. Serositis: comparative analysis of histological findings and pathogenetic mechanisms in non bacterial serosal inflammation. Perit dial Int 1993; 13: 256–269.
512. Yang AH, Chen JY, Lin JK. Myofibroblastic conversion of mesothelial cells. Kidney Int 2003; 63: 1530–1539.
513. Lopez-Cabrera M, Aguilera A, Aroeira LS, Ramirez-Huesca M, Perez-Lozano ML, Jimenez-Heffernan JA, Bajo MA, Del Peso G, Sanchez-TomeroJA, Selgas R. Ex vivo analysis of dialysis effluent-derived mesothelial cells as an approach to unveiling the mechanism of peritoneal membrane failure. Perit Dial Int 2006; 26: 26–34.
514. Munoz-Chapuli R, Perez-Pomares JM, Macias D, Garcia-Garrido L, Carmona R, Gonzalez M. Differentiation of hemangioblasts from embryonic mesothelial cells. A model on the origin of the vertebrate cardiovascular system. Differentiation 1999; 64: 133–141.
515. Perez-Pomares JM, Macias-Lopez F, Garcia-Carrido M, Munoz-Chaguli R. Immunohistochemical evidence for a mesothelial contribution to ventral wall of the avian aorta. Histochem J 1999; 31: 771–779.
516. Donna A, Ribotta M, Betta PG, Libener R, Bellingeri D. The in-vitro hematopoietic capacity of the adult human mesothelial cell: a model of cell differentiation induced by the structure of the microenvironment. Ital J Anat Embryol 1993; 98: 269–275.
517. Campbell JH, Efendy JL, Campbell GR. Novel vascular graft grown within recipient's own peritoneal cavity. Circ Res 1999; 85: 1173–1178.
518. Moldovan NI, Haveman K. Transdifferentiation: a potential mechanism for covering vascular grafts grown within recipient's peritoneal cavity with endothelial-like cells. Circ Res 2002; 191: e1.
519. Leypoldt JK. Evaluation of peritoneal membrane pore models. Blood Purif 1992; 10: 227–238.
520. Gotloib L, Oreopoulos DG. Transfer across the peritoneum: passive or active? Nephron 1981; 29: 201–202.
521. Gotloib L. Large mesothelial cells in peritoneal dialysis: a sign of degeneration or adaptation? Perit Dial Int 1996; 16: 118–120.